e-ISSN 2088-6985
p-ISSN 2087-3379

Journal of Mechatronics, Electrical Power, and Vehicular Technology

Volume 10, Issue 2, 2019

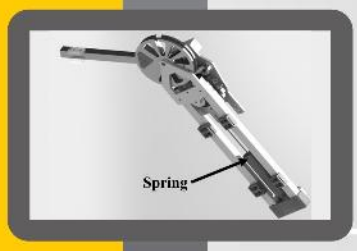

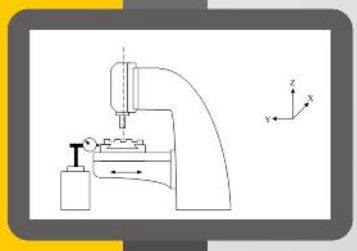

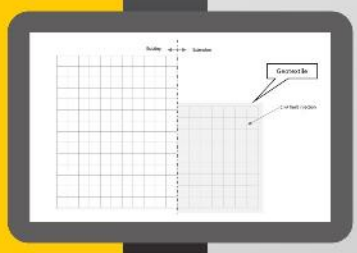

The effect of lightning impulse characteristics and line arrester to the lightning protection performance on 150 kV overhead lines: ATP-EMTP computational approach
F. Murdiya, Febrizal, C. Stevany, H. A. Sano, Firdaus

Design and development of the sEMG-based exoskeleton strength enhancer for the legs
M. Cenit, V. Gandhi

Smart Grid communication applications: measurement equipment and networks architecture for data and energy flow
T. D. Atmaja, D. Andriani, R. Darussalam

Safety assessment of high voltage substation earthing systems with synthetic geotextile membrane
M. Nazih

Three axis deviation analysis of CNC milling machine
D. G. Subagio, R. A. Subekti, H. M. Saputra, A. Rajani, K. H. Sanjaya

Published by:
Research Centre for Electrical Power and Mechatronics
Indonesian Institute of Sciences
LIPI

Front Cover

e-ISSN 2088-6985
p-ISSN 2087-3379

Journal of Mechatronics, Electrical Power, and Vehicular Technology

Volume 10, Issue 2, 2019

Aim and Scope

Journal of Mechatronics, Electrical Power, and Vehicular Technology (MEV) is an internationally peer-reviewed journal aims to provide authoritative global source of scientific information for researchers and engineers in academia, research institutions, government agencies, and industries. The Journal publishes original research papers, review articles and case studies focused on:

Mechatronics: including control system, robotic, CNC Machine, sensor, signal processing, electronics, actuator, and mechanical dynamics.

Electrical Power: including power generation, transmission system, new and renewable energy, turbine and generator design and analysis, grid system, and source assessment.

Vehicular Technology: including electric/hybrid vehicle design and analysis, vehicle on grid, fuel efficiency, and safety analysis.

Selected Applications: including all implementations or implications related to mechatronics, electrical power, or vehicular technology.

MEV's vision is to become an international platform with high scientific contribution for the global community. MEV's mission is presenting important results of work, whether in the form of research, development, application, or design.

Imprint

MEV is published by Research Centre for Electrical Power and Mechatronics - Indonesian Institute of Sciences (RCEPM-LIPI).

ISSN print: 2087-3379
ISSN electronics: 2088-6985

Electronics edition is available at: http://www.mevjournal.com

All published article are embedded with DOI number affiliated with Crossref DOI prefix 10.14203

Publication Frequency

MEV is managed to be issued twice in every year. The first issue should be in the mid of the year (July) and the second issue is at the end of the year (December).

Peer Review Policy

MEV reviewing policies are:

Every submitted paper will be reviewed by at least two peer-reviewers.

Reviewers are unaware of the identity of the authors, and authors are also unaware of the identity of reviewers (double blind review method).

Reviewing process will consider novelty, objectivity, method, scientific impact, conclusion, and references.

Accreditation

MEV has been certificated as an Indonesian Scientific Journal by Indonesian Institute of Sciences (LIPI). MEV has also been certificated by Ministry of Research, Technology and Higher Education (RTHE) as an online scientific journal.

LIPI Accreditation:

Accreditation Number:
633/AU/P2MI-LIPI/03/2015

Acc date: 15 April 2015
Valid thru: 15 April 2020.

RISTEKDIKTI Accreditation:

Accreditation Number:
1/E/KPT/2015

Acc date: 15 September 2015
Valid thru: 21 September 2020.

Postal Address

MEV Journal Secretariat:

Research Centre for Electrical Power and Mechatronics, Indonesian Institute of Sciences (RCEPM - LIPI)

Komp LIPI Jl. Sangkuriang, Building 20, 2nd Floor, R209
Bandung, West Java, 40135
Indonesia

Tel: +62-022-2503055 (ext. 215)
Tel: +62-022-2504770 (ext. 203)
Fax: +62-22-2504773

Business hour: Monday to Friday 08:00 to 16:00 GMT+7

e-mail:
sekretariat@mevjournal.com

e-ISSN 2088-6985
p-ISSN 2087-3379

Journal of Mechatronics, Electrical Power, and Vehicular Technology

Volume 10, Issue 2, 2019

Online Submissions

If you already have a Username/Password for Journal of Mechatronics, Electrical Power, and Vehicular Technology?
Go to login at:
http://mevjournal.com/index.php/mev/login

Need a Username/Password?
Go to registration at:
http://mevjournal.com/index.php/mev/user/register

Registration and login are required to submit items online and to check the status of current submissions.

Copy Editing and Proofreading

Every article accepted by MEV Journal shall be an object to **Grammarly**® writing-enhancement program conducted by MEV Journal Editorial Board.

Reference Management

Every article submitted to MEV Journal shall use reference management software e.g. **Endnote**® or **Mendeley**.

Open Access Policy

MEV Journal provides immediate open access to its content on the principle that making research freely available to the public to supports a greater global exchange of knowledge.

Processing Charges

Every article submitted to MEV Journal **will not have** any Article Processing Charges. This includes submission, peer-reviewing, editing, publishing, maintaining and archiving, and allows immediate access to the full text versions of the articles.

Plagiarism Check

iThenticate®

Plagiarism screening will be conducted by MEV Editorial Board using **Crossref Similarity Check™** powered by iThenticate® and also using **Grammarly**® Plagiarism Checker.

Crossmark

Check for updates

Every article will be published along with **Crossmark** button in the PDF and in the online abstract page. Crossmark gives readers quick and easy access to the current status of a piece of content.

Cited-by

Crossref Cited-by

Published article will be equipped with Crossref **Cited-by** service. Cited-by lets publishers show authors and readers what other Crossref content is citing their content.

Indexing & Abstracting

MEV has been covered by these following indexing services:

EBSCOhost, Google Scholar, Directory of Open Access Journal (DOAJ), Microsoft Academic Search, Science and Technology Index (SINTA), Crossref, Indonesian Scientific Journal Database (ISJD), Indonesian Publication Index (IPI), CiteULike, Cite Factor, Academic Journal Database, ResearchBib, Bielefeld Academic Search Engine (BASE), WorldCat, Sherpa Romeo, Index Copernicus, Open Academic Journal Index (OAJI), Open Access Articles, ROAD: the Directory of Open Access Scholarly Resources, Toronto Public Library, Western Theological Seminary, Ghent University Library, and Electronic Journals Library.

CC License

e-ISSN 2088-6985
p-ISSN 2087-3379

Journal of
Mechatronics, Electrical Power, and Vehicular Technology

Volume 10, Issue 2, 2019

Journal of

Mechatronics, Electrical Power, and Vehicular Technology

Volume 10, Issue 2, 2019

Journal of

Mechatronics, Electrical Power, and Vehicular Technology

Volume 10, Issue 2, 2019

FOREWORD FROM EDITOR-IN-CHIEF

Journal of Mechatronics, Electrical Power, and Vehicular Technology (MEV) is an international journal indexed by many internationally recognized indexers. Its Digital Object Identifier (DOI) Prefix is 10.14203. In this issue, five papers are published with the authors diversity came from Indonesia, Australia, and United Kingdom.

The papers come from multidisciplinary topics including mechatronics, electrical power, and mechanics. They may be classified as follows. Three papers fall in electrical power topic. The first paper presents simulation study for the effect of lightning strikes on the performance of arresters at 150 kV overhead lines. The second paper proposes a comprehensive guide and comparison surrounding the technologies supporting Smart Grid implementation especially on communication application. The third paper has the aim to identify the impact of synthetic textiles on earthing system performance through numerical analysis with the state-of-the-art software package. One paper is related to mechatronics which address the different exoskeleton designs and presents a working prototype of a surface electromyography (EMG) controlled exoskeleton to enhance the strength of the lower leg.

One paper deals with mechanical topic i.e. Three axis deviation analysis of CNC milling machine. Since the first volume, our journal provides discretion in financial term by waiving the article processing charge. We would like to acknowledge our immense gratitude to our International Editorial Board members, reviewers and authors.

We hope this publication would contribute to the enhancement of science and technology.

Bandung, December 2019

Editor-in-Chief

e-ISSN 2088-6985
p-ISSN 2087-3379

Journal of

Mechatronics, Electrical Power, and Vehicular Technology

Volume 10, Issue 2, 2019

LIST OF CONTENTS

The effect of lightning impulse characteristics and line arrester to the lightning protection performance on 150 kV overhead lines: ATP-EMTP computational approach
Fri Murdiya, Febrizal, Cecilia Stevany, Havel Alindo Sano, Firdaus.....49-59

Design and development of the sEMG-based exoskeleton strength enhancer for the legs
Mikecon Cenit, Vaibhav Gandhi.....61-71

Smart Grid communication applications: measurement equipment and networks architecture for data and energy flow
Tinton Dwi Atmaja, Dian Andriani, Rudi Darussalam.....73-84

Safety assessment of high voltage substation earthing systems with synthetic geotextile membrane
Mostafa Nazih.....85-91

Three axis deviation analysis of CNC milling machine
Dalmasius Ganjar Subagio, Ridwan Arief Subekti, Hendri Maja Saputra, Ahmad Rajani, Kadek Heri Sanjaya.....93-101

Journal of

Mechatronics, Electrical Power, and Vehicular Technology

Volume 10, Issue 2, 2019

ABSTRACTS SHEET

e-ISSN: 2088-6985
p-ISSN: 2087-3379

Fri Murdiya, Febrizal, Cecilia Stevany, Havel Alindo Sano, Firdaus (Department of Electrical Engineering, Faculty of Engineering, Universitas Riau, Indonesia)

The effect of lightning impulse characteristics and line arrester to the lightning protection performance on 150 kV overhead lines: ATP-EMTP computational approach

Journal of Mechatronics, Electrical Power, and Vehicular Technology, 2019, vol. 10, no. 2, p. 49-59, 21 ill, 3 tab, 29 ref.

This simulation study presents the effect of lightning strikes on the performance of arresters at 150 kV overhead lines. Lightning strikes have several parameters that affect the performance of line arresters (LA), namely lightning charge, and impulse energy. The simulation was attempted by injection of a direct strike to the ground wire with the peak voltage of 10 MV. The peak voltage was varied in terms of wavefront time (Tf) and the duration of lightning impulses (tau). In order to calculate current, charge and impulse energy of LA from various variations of Tf and tau, the trapezoidal numerical integration method is used. The current and impulse energy arising due to direct strikes and various variations of Tf and tau will be compared for each phase so that the influence of Tf and tau can be obtained from the performance of the LA and the current charge and impulse energy values are still within the limits of the IEEE C62.11 standard. The installation of LA and the position of arresters affected the peak voltage of lightning on the phase line when lightning struck it. The line arresters provide a drop in the peak voltage of lightning in phase lines. By installing line arresters in each tower, it will reduce the peak voltage of lightning on the phase line more significantly than the standalone line arrester. It is shown that the line arresters have to install at least six towers to reduce the peak voltage in the phase lines.

(Author)

Keywords: lightning impulse; line arrester; peak voltage; impulse energy; placement of arrester.

Mikecon Cenit, Vaibhav Gandhi (Department of Design Engineering and Mathematics, Middlesex University London, United Kingdom)

Design and development of the sEMG-based exoskeleton strength enhancer for the legs

Journal of Mechatronics, Electrical Power, and Vehicular Technology, 2019, vol. 10, no. 2, p.61-71, 12 ill, 0 tab, 73 ref.

This paper reviews the different exoskeleton designs and presents a working prototype of a surface electromyography (EMG) controlled exoskeleton to enhance the strength of the lower leg. The Computer Aided Design (CAD) model of the exoskeleton is designed, 3D printed with respect to the golden ratio of human anthropometry, and tested structurally. The exoskeleton control system is designed on the LabVIEW National Instrument platform and embedded in myRIO. Surface EMG sensors (sEMG) and flex sensors are used coherently to create different state filters for the EMG, human body posture and control for the mechanical exoskeleton actuation. The myRIO is used to process sEMG signals and send control signals to the exoskeleton. Thus, the complete exoskeleton system consists of sEMG as primary sensor and flex sensor as secondary sensor while the whole control system is designed in LabVIEW. FEA simulation and tests show that the exoskeleton is suitable for an average human weight of 62 kg plus excess force with different reactive spring forces. However, due to the mechanical properties of the exoskeleton actuator, it will require additional lift to provide the rapid reactive impulse force needed to increase biomechanical movement such as squatting up. Finally, with the increasing availability of such assistive devices on the market, the important aspect of ethical, social and legal issues have also emerged and discussed in this paper.

(Author)

Keywords: leg-exoskeleton; electromyography based exoskeleton; LabVIEW myRIO; ethical, societal, and legal concerns.

Tinton Dwi Atmaja [a], Dian Andriani [b], Rudi Darussalam [a] ([a] Research Centre for Electrical Power and Mechatronics, Indonesian Institute of Sciences, Indonesia; [b] Research Unit for Clean Technology, Indonesian Institute of Science, Indonesia)

Smart Grid communication applications: measurement equipment and networks architecture for data and energy flow

Journal of Mechatronics, Electrical Power, and Vehicular Technology, 2019, vol. 10, no. 2, p. 73-84, 10 ill, 5 tab, 63 ref.

Smart Grid is an advanced two way data and energy flow capable of self-healing, adaptive, resilient, and sustainable

with prediction capability of possible fault. This article aimed to disclose Smart Grid communication in a logical way to facilitate the understanding of each component function. The study was focused on the improvement, advantages, common used design, and possible feature of Smart Grid communication components. The results of the study divide the Smart Grid communication application into two main category i.e. measurement equipment and network architecture. Measurement equipment consists of Advance Metering Infrastructure, Phasor Measurement Unit, Intelligent Electronic Devices, and Wide Area Measurement System. The network architecture is divided based on three hierarchies; local area network for 1 to 100 m with 100 kbps data rate, neighbour area network for 100 m to 10 km with 100 Mbps data rate, and wide area network for up to 100 km with 1 Gbps data rate. More information is provided regarding the routing protocol for each network from various available protocols. The final section presents the energy and data flow architecture for Smart Grid implementation based on the measurement equipment and the network suitability. This article is expected to provide a comprehensive guide and comparison surrounding the technologies supporting Smart Grid implementation especially on communication applications.

(Author)

Keywords: Smart Grid application; phasor measurement unit; communication network; communication protocol; energy and data flow.

Mostafa Nazih (Building, Infrastructure and Advanced Facilities, Jacobs, Australia)

Safety assessment of high voltage substation earthing systems with synthetic geotextile membrane

Journal of Mechatronics, Electrical Power, and Vehicular Technology, 2019, vol. 10, no. 2, p. 85-91, 7 ill, 4 tab, 17 ref.

High voltage substations built within areas prone to vegetation or with unfavourable subgrade conditions are paved with the addition of punched geotextiles and non-conductive synthetic fabrics underneath switchyard surfacing. The aim of this research is to identify the impact of synthetic textiles on earthing system performance through numerical analysis with the state-of-the-art software package. The new layer interferes with the earthing grids performance with a different behaviour depending on the installation above or underneath the layer with considerable impact taking place when the earthing grid is installed above the geotextile layer. Rods penetrating the geotextile can alleviate the potential voltage distribution issues and improve the earthing system performance regardless of the native soil stratification.

(Author)

Keywords: substation earthing; synthetic geotextile; tolerable voltages; high voltage.

Dalmasius Ganjar Subagio, Ridwan Arief Subekti, Hendri Maja Saputra, Ahmad Rajani, Kadek Heri Sanjaya (Research Centre for Electrical Power and Mechatronics, Indonesian Institute of Sciences, Indonesia)

Three axis deviation analysis of CNC milling machine

Journal of Mechatronics, Electrical Power, and Vehicular Technology, 2019, vol. 10, no. 2, p. 93-101, 12 ill, 4 tab, 31 ref.

The manufacturing technology has developed rapidly, especially those intended to improve the precision. Consequently, increasing precision requires greater technical capabilities in the field of measurement. A prototype of a 3-axis CNC milling machine has been designed and developed in the Research Centre for Electrical Power and Mechatronics, Indonesian Institute of Sciences (RCEPM-LIPI). The CNC milling machine is driven by a 0.4 kW servo motor with a spindle rotation of 12,000 rpm. This study aims to measure the precision of the CNC milling machine by carrying out the measurement process. It is expected that the CNC milling machine will be able toperform in an optimum precision during the manufacturing process. Accuracy level testing is done by measuring the deviations on the three axes namely X-axis, Y-axis, and Z-axis, as well as the flatness using a dial indicator and parallel plates. The measurement results show the deviation on the X-axis by 0.033 mm, the Y-axis by 0.102 mm, the Z-axis by 0.063 mm, and the flatness of the table by 0.096 mm, respectively. It is confirmed that the deviation value is within the tolerance standard limits set by ISO 2768 standard. However, the calibration is required for this CNC milling machine to achieve more accurate precision. Furthermore, the design improvement of CNC milling machine and the application of information technology in accordance with Industry 4.0 concept will enhance the precision and realibility.

(Author)

Keywords: precision measurement; orthogonal axes; manufacturing machine; automation industry.

Journal of Mechatronics, Electrical Power, and Vehicular Technology 10 (2019) 49-59

Journal of Mechatronics, Electrical Power, and Vehicular Technology

e-ISSN: 2088-6985
p-ISSN: 2087-3379

www.mevjournal.com

The effect of lightning impulse characteristics and line arrester to the lightning protection performance on 150 kV overhead lines: ATP-EMTP computational approach

Fri Murdiya *, Febrizal, Cecilia Stevany, Havel Alindo Sano, Firdaus

Department of Electrical Engineering, Faculty of Engineering, Universitas Riau
Jl. H.R Subrantas km 12,5 Kampus Binawidya Panam, Pekanbaru, 28293, Indonesia

Received 14 January 2019; accepted 15 November 2019

Abstract

This simulation study presents the effect of lightning strikes on the performance of arresters at 150 kV overhead lines. Lightning strikes have several parameters that affect the performance of line arresters (LA), namely lightning charge, and impulse energy. The simulation was attempted by the injection of a direct strike to the ground wire with the peak voltage of 10 MV. The peak voltage was varied in terms of wavefront time (Tf) and the duration of lightning impulses (tau). In order to calculate current, charge and impulse energy of LA from various variations of Tf and tau, the trapezoidal numerical integration method is used. The current and impulse energy arising due to direct strikes and various variations of Tf and tau will be compared for each phase so that the influence of Tf and tau can be obtained from the performance of the LA and the current charge and impulse energy values are still within the limits of the IEEE C62.11 standard. The installation of LA and the position of arresters affected the peak voltage of lightning on the phase line when lightning struck it. The line arresters provide a drop in the peak voltage of lightning in phase lines. By installing line arresters in each tower, it will reduce the peak voltage of lightning on the phase line more significantly than the standalone line arrester. It is shown that the line arresters have to install at least six towers to reduce the peak voltage in the phase lines.

Keywords: lightning impulse; line arrester; peak voltage; impulse energy; placement of arrester.

I. Introduction

Overhead lines for 70 kV, 150 kV and 275 kV, which stretch along the island of Sumatra, are very susceptible to the disruption caused by lightning strike. This is proven by the lightning activity in Sumatra Island, which includes the high category. This happens because Indonesia is located in the humid tropics which results in very high thunderstorm days compared to other regions (100-200 days of thunder per year). Based on the calculation using IEEE flash software as shown in Figure 1, the back flashover rate (BFOR) and shielding failure flashover rate (SFFOR) are directly proportional to the ground flash density (GFD) for the 150 kV overhead lines in Sumatra. With GFD of 9-13 flash/km^2/year, the 150 kV overhead lines in Sumatra are often hit by the lightning strikes. The data show that from 2011 to 2014, the phase lines were struck by lightning as many as 305 times as shown in Figure 2.

The recorded failures of the 150 kV overhead lines in central Sumatra from 2011 to 2014 occurred throughout the year. This failure was recorded as a failure due to lightning. These data also show that the central Sumatra has a high lightning density which is a threat and disruption to the distribution of electricity. The data in Figure 1 and Figure 2 indicates that the 150 kV overhead lines in central Sumatra need to be protected according to the safety standard.

High-voltage transmission poles are tall objects and are subject to lightning strikes. It is not only the shielding failure caused by lightning struck that should be calculated, but the back flashover needs to also be estimated. The efforts that have been attempted by the Electric Company in Sumatra to reduce the outages caused by lightning strikes include checking and resetting the grounding rod at

* Corresponding Author. Hp: +62 812 8881 6276
E-mail address: frimurdiya@eng.unri.ac.id

doi: https://dx.doi.org/10.14203/j.mev.2019.v10.49-59

Accreditation Number: (RISTEKDIKTI) 1/E/KPT/2015 (Sinta 2).

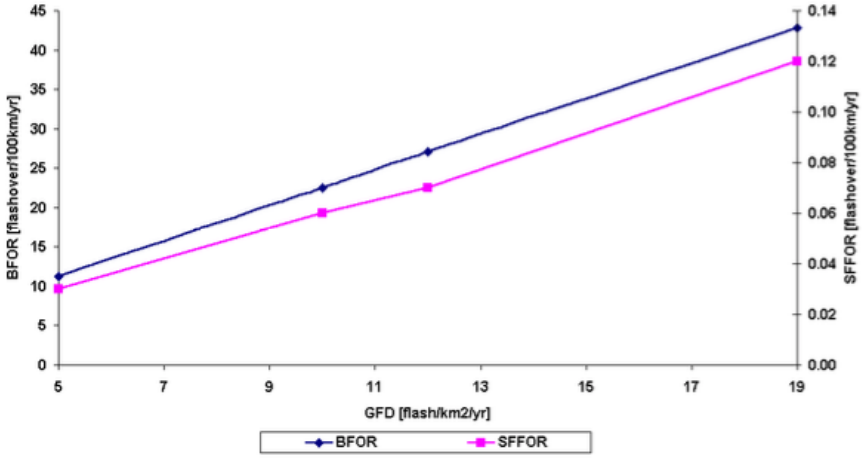

Figure 1. BFOR and SFFOR for 150 kV in Sumatra

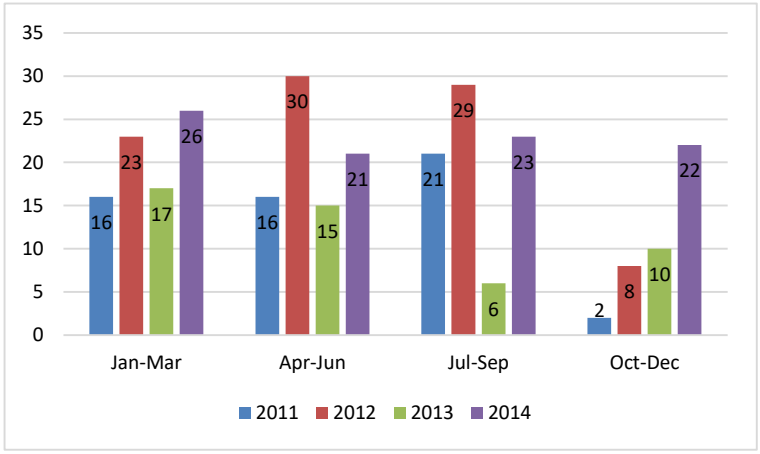

Source: Electric Company in Sumatra

Figure 2. The number of the outage of the 150 kV overhead lines caused by lightning struck

least under 5 Ohms, checking and repairing the ground static wire clamps, as well as the installations of transmission lightning arrester (TLA), lightning protection termination early streamer emission (ESE), and static wire insulated ground (i-GSW) for areas that are often struck by lightning. Another effort was also carried out by installing jet stream arc-quenching lightning protection gap. External ground wires contribute to reduce flashover rate. Those efforts are done by [1][2][3][4][5][6][7][8]. The recommendation for back flashover rate improvement has been proposed by [9] using multi chamber insulator arresters (MCIA) to substitute the string insulators. From the improvement efforts carried out by the electric company in Sumatra, there are some interesting things to be evaluated further, such as whether, the installed TLA is related to the characteristics of the lightning impulses and their effects to decrease the lightning peak voltage hence improving the 150 kV lines performances. In this manuscript, the simulations were carried out by means of ATP-EMTP software. The impulse generator model uses the Heidler model which is an impulse current function model and is widely used as a model of lightning. Equation (1) and Equation (2) are momentary current equations that calculate lightning currents in this model [10][11][12][13]. This Heidler model is given in Figure 3.

$$i(t) = \frac{I_0}{\eta} \cdot \frac{\left[\frac{t}{\tau_1}\right]}{\left[\frac{t}{\tau_1}\right]^n + 1} \cdot e^{\left[\frac{-t}{\tau_2}\right]} \quad (1)$$

$$\eta = e^{\left[-\left[\frac{\tau_1}{\tau_2}\right]\left[\frac{\eta\tau_2}{\tau_1}\right]^{\frac{1}{n}}\right]} \quad (2)$$

where I_0 is lightning peak current (kA), τ_1 is current rising time constant, τ_2 is current dropping time constant, and η is current crest factor.

The TLA model of 150 kV overhead lines is shown in Figure 4. This model has also been derived from IEEE standards [14][15][16]. This model will be used in the simulation with the ATP-EMTP software. The

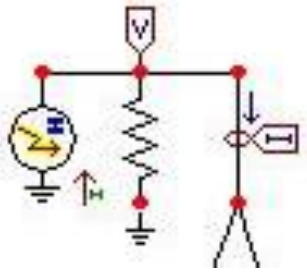

Figure 3. Lightning current model

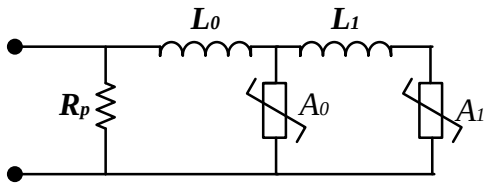

Figure 4. Pinceti and Giannettoni model

Table 1.
Data of arrester MOV

I (A)	U (V)	
	A_0	A_1
10	271,250	0
100	298,530	238,390
1,000	325,500	263,500
2,000	337,280	277,140
4,000	348,750	286,750
6,000	352,780	290,780
8,000	362,390	296,360
10,000	368,280	300,390
12,000	373,860	302,250
14,000	381,610	306,280
16,000	387,500	308,140
18,000	397,110	310,000
20,000	407,030	311,860

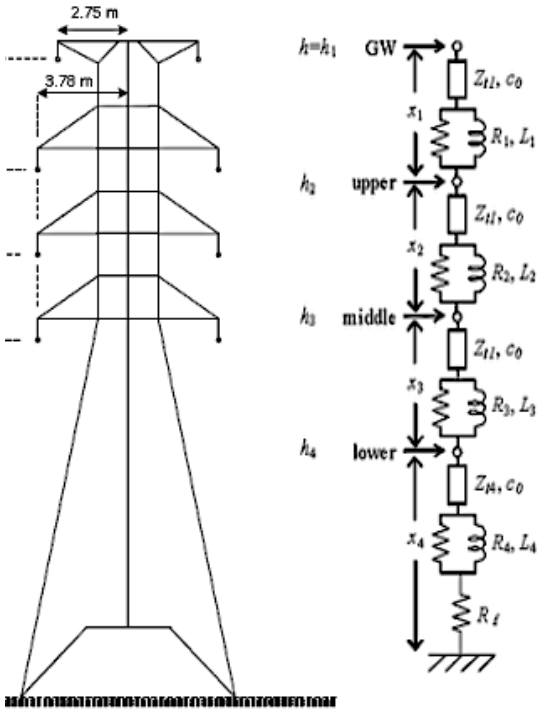

(a) (b)

Figure 5. The well-known models: (a) 150 kV tower and (b) Multi-storey tower for ATP-EMTP model

Pinceti and Giannettoni model is a simplified model of the IEEE W.G 3.4.11 standard. This model eliminates the capacitance C because of its negligible effect. The two parallel resistances with inductance are replaced by one R resistance (about 1 MΩ) between the input terminals. The non-linear resistor characteristics A_o and A_1 are identical to the IEEE W. G 3.4.11 model. The L_o and L_1 parameters of this simplified surge arrester model are calculated from the following Equation (3) and Equation (4) [17][18].

$$L_1 = \frac{1}{4} \cdot \frac{V_{r1/T_2} - V_{r8/20}}{V_{r8/20}} \cdot V_n \quad (3)$$

$$L_0 = \frac{1}{12} \cdot \frac{V_{r1/T_2} - V_{r8/20}}{V_{r8/20}} \cdot V_n \quad (4)$$

where V_n is arrester rated voltage, V_{r1/T_2} is impulse voltage with a waveform of 1,2/5 μs, $V_{r8/20}$ is impulse voltage with waveform 8/20 μs. The values of non-linear resistance A_0 and A_1 are taken from the data of ZnO arrester presented in Table 1. By using Equation (3) and Equation (4), the values of L_1 is 0.002448 mH and L_0 is 0.000816 mH. The values of A_0 and A_1, V_{ref} is twice of residual voltage for the current of 10 kA and waveform of 8/20 μs. The transmission tower is modelled for 150 kV with four parameters illustrated in Figure 5. One of the well-known models is the multistory model designed by Masaru Ishii. The multistory tower model consists of a line of parameters distributed with parallel RL circuits and has been recommended by Japanese standards for designing/coordinating insulation against lightning. This model is widely used for lightning wave analysis in Japan [13][19][20]. The velocity of propagation is 300 m/s. The recommended surge impedance value from the tower model above can be seen in Table 2. The values of R and L every section on the tower are defined as in Equation (5) and Equation (6) as follows:

$$R_i = \Delta R_i x_i \quad (5)$$

$$L_i = 2\tau R_i \quad (6)$$

where *i = 1,2,3,* and *4* for every section of the tower, tower height *h*, x_1 is the distance of ground wire (GW) to phase line 1, x_2 is the distance of phase line 2 to phase line 1, x_3 is the distance of phase line 3 to phase line 2, and x_4 is the distance of phase line 3 to ground. The formula of ΔR_i is determined by Equation (4) and

Table 2.
Recommended value of lightning parameters

System voltage	Lighting current	Tower height/ geometry (m)				Surge imp. (Ω)		Footing res. (Ω)
(kV)	(kA)	*H*	x_1	x_2	x_3	Z_{t1}	Z_{t4}	R_f
1100	200	107	12.5	18.5	18.5	130	90	10
500	150	79.5	7.5	14.5	14.5	220	150	10
275	100	52.0	9.0	7.6	7.6	220	150	10
154 (110)	60	45.8	6.2	4.3	4.3	220	150	10
77 (66)	30, 40	28.0	3.5	4.0	3.5	220	150	10-20

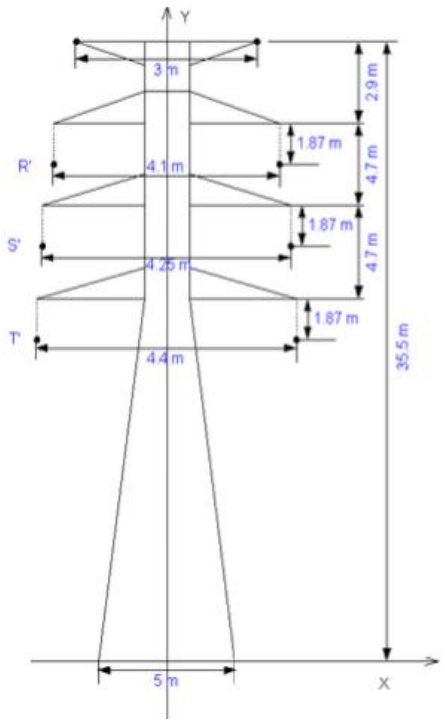

Figure 6. Tower configurations

Equation (5) where Z_{t1} and Z_{t4} are data from Table 1 for system voltage of 154 kV/110 kV and time of traveling wave on the tower: $\tau = {}^{h}/_{c_0}$, the attenuation constant: and propagation velocity: $c_0 = 300\,{}^{m}/_{\mu s}$.

$$\Delta R_1 = \Delta R_2 = \Delta R_3 = \frac{2Z_{tl}}{h-x_4} ln\left(\frac{1}{\alpha_1}\right) \quad (7)$$

$$\Delta R_4 = \frac{2Z_{tl}}{h-x_4} ln\left(\frac{1}{\alpha_1}\right) \quad (8)$$

Transmission lines in Japan use a vertical twincircuit configuration with two ground wires and 6 phase wires. This configuration model is used for the transmission line model on EMTP called the frequency-dependent line model of the EMTP. However, the influence of distributed-line models with a fixed propagation velocity, more attenuation, and surge impedance is explained in EMTP which is often used for transient overvoltage simulations [21]. The frequency-dependent effect of a tower used in the simulation is a combination of the frequency-dependent tower impedance with the Semlyen or Marti line model in EMTP [22][23][24][25][26]. The current charge is the area of lightning or integral current with time. This current charge (Q) is formulated in Equation (9), where *i* is the lightning current strength in kA and t is a time in seconds.

$$Q = \int i\,dt \text{ (C)} \quad (9)$$

Integral Quadratic Current (E) is impulse energy which is a mechanical effect, and lightning heat can be formulated in Equation (10),

$$E = \int i^2 t\,dt \text{ (J)} \quad (10)$$

By following the simulation rules above, the effects of lightning impulse characteristics and transmission lines arrester (TLA) on the design of TLA laying in 150 kV overhead lines in Sumatra were carried out. The number of TLA used needs to be proven by simulations to determine the effectiveness of TLA installation on 150 kV overhead lines in Sumatra.

II. Research Methodology

Analysis of lightning strikes on arrester work at 150 kV overhead lines in this study was carried out using the ATP (Alternative Transient Program). The simulation process was carried out in several stages, namely: field data collection, transmission line parameter calculation, modelling all channel parameters into ATP-EMTP, analyzing current charge and impulse energy in arresters in each phase and analyzing the installation of arresters in each transmission tower.

The data retrieval was carried out by collecting equipment data, tower data, power transformer data, arrester data used at the substation and lines, and the components needed for the modelling process. The conductor data used in this study are divided into two: shield wires and phase wires. Shield wires are made of the galvanized steel wire with a cross-sectional area of 55 mm^2, and the sag length is 4,576 m. Phase conductor is made of Zebra ACSR with a cross-sectional area of 428 mm^2, R_{max} resistance is 0.0397 Ohm/km, X_{max} reactance is 0.272 Ohm/km, L_{max} inductance is 0.433 mH/km and C_{max} capacitance is 6.645 nF/km. Sag length is 5.4 m. The tower configuration is shown in Figure 6. Shield wires and phase wires are tabulated in Table 3.

Table 3.
The positions of shield wires and phase wires

Conductor No.	Operating Phase-Phase [kV]	Phase Angle [^{0}]	Function	Phase Coordinates	
				X [m]	Y [m]
1	-	-	Shield	-1.5	35.5
2	-	-	Shield	1.5	35.5
3	150	0	R	-2.05	30.73
4	150	240	S	-2.125	26.03
5	150	120	T	-2.2	21.33
6	150	0	R'	2.05	30.73
7	150	240	S'	2.125	26.03
8	150	120	T'	2.2	21.33

Span (Average) = 300 m
Surge Impedance = 139 ohm

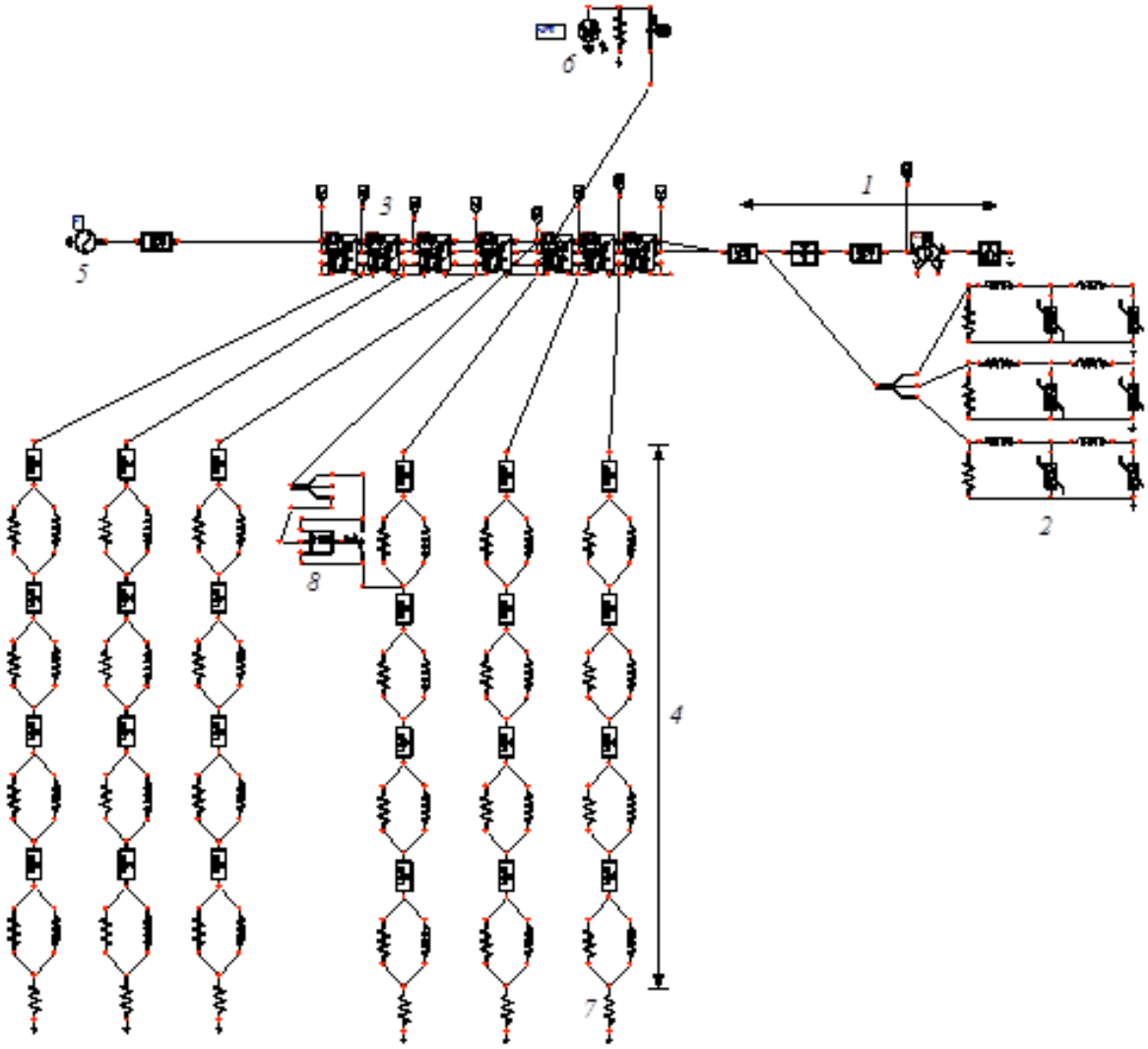

Figure 7. 150 kV overhead lines model: (1) Substation; (2) Lightning arrester; (3) LCC/Lines; (4) Multistory tower; (5) Power generator; 6. Impulse generator; (7) Footing resistance (R_f); (8) Switch for back flashover

By entering tower configuration data into Equations (5-8), the parameters for the tower replacement circuit were obtained in the ATP-EMTP software. Lines phases were modelled with LCC and the configuration of the circuit of sixline phases and two ground wires. The power transformer used was 150 kV rms with a frequency of 50 Hz. Arrester was used by the model in Figure 4.

The simulation method looked at the effect of lightning wave front (Tf) and lightning wave duration (tau) on lightning charge and lightning energy compared to the IEEE C62.11 standard. The peak voltage of the impulse generator (Heidler model) was 10 MV. After overvoltage on the tower, a simulation was carried out to see the effect of TLA installation on the 150 kV transmission line. The back flash over model was also created with an automatical switch in microsecond order, for example, number 6 in Figure 7. According to Table 2, the tower ground resistance is 10 Ohm. The number of TLA and TLA positions is the objective of this research. The model used in the simulation is given in Figure 7.

III. Results and Discussions

The variation of Tf of the lightning impulse modelled at ATM-EMTP is shown in Figure 8. The Tf value imputed on the Hiedler impulse generator model is 1.2, 2.4, 3.6, 4.8 µs. Next, the wavefront start value and tau value are set at 0.1 and 50 µs. After the Tf and data parameters are set, the impulse current flows through arresters in phase A because the isolator flashover process occurs in phase A. The characteristics of lightning impulse currents through arresters in phase A for variations of Tf are given in Figure 9. By using the trapezoidal numerical method, the current charge and impulse energy values can be solved by using current impulse data flowing in arrester A with a variation of Tf. For the comparison of the current charge, the change in Tf is still within the arrester resistance limit, which is in the range of 3.5 C. However, the impulse energy values that occur in arresters on phase A have exceeded the energy resistance limit of the arrester, which is 11 kJ. The value of the current charge and impulse energy with variations of Tf is given in Figure 10 and Figure 11. It

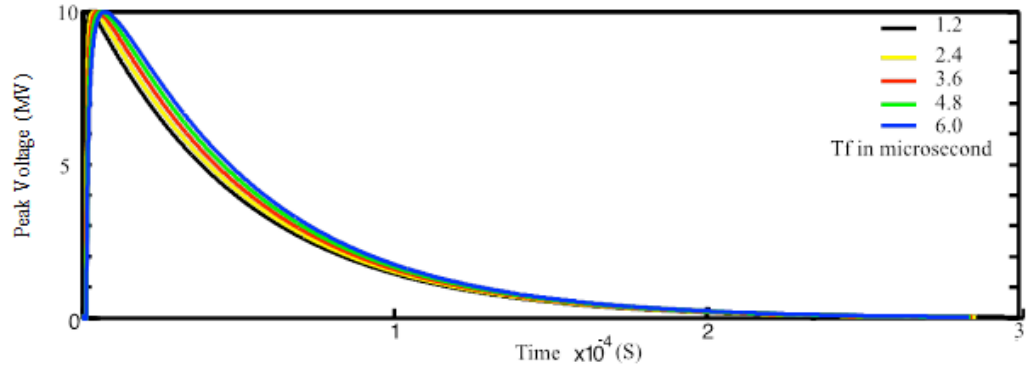

Figure 8. Lightning impulse with Tf variations

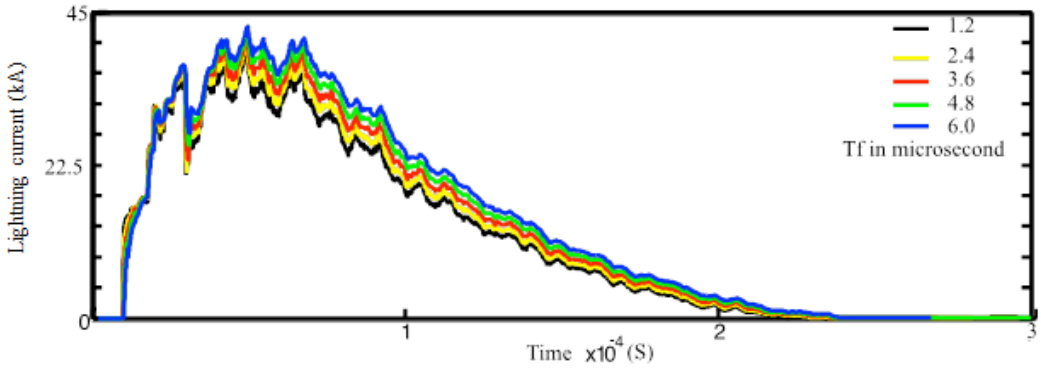

Figure 9. Current waves passing through arresters in phase A to variations of Tf

shows that the variation Tf of the lightning impulse influences the current charge and impulse energy values. Current and impulse energy values are proportional to Tf. By keeping the peak voltage of the impulse 10 MV and varying the Tf values, the impulse energy received by the arrester is greater than the standard value while the charge values are still below the standard. Impulse energy that exceeds this standard could result in a shorter lifetime of the arrester.

In order to find out the effect of changes in tau value, this simulation was carried out by varying the tau values of 50, 70, 90, 110 and 130 µs. As for the values of Tsta and Tf are fixed, which is 0.1 and 1.2 µs. The value of the variation of the lightning impulse is shown in Figure 12 and Figure 13. By injecting lightning impulses into a 150 kV overhead lines model, this will cause arresters in phase A to work because the arresters are passed by the current after a flashover event of the insulator in phase A. The current charge and impulse energy can be solved using current data flowing in the arrester in phase A. These values are given in Figure 14 and Figure 15. It is shown that the tau value is proportional to the current charge. If the tau values exceed the 70 µs, the arrester will exceed the limit value (shown in yellow line). However, the value also affects the impulse energy value, which exceeds the standard value of arresters according to IEEE C62.11. The values of tau could affect the values of the charge and impulse energy that exceeds the standard. It is shown that tau can influence the arrester performance where the lifetime of arrester will be shorter than the variation of Tf.

In order to figure out the effect of arrester performance, the installation locations of arresters are varied in this study. Figure 16 shows a simulation of a series of a lightning strike that grabs the ground

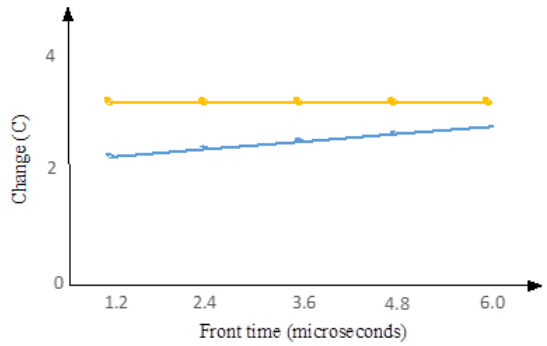

Figure 10. Comparison of current charge values to variations of Tf

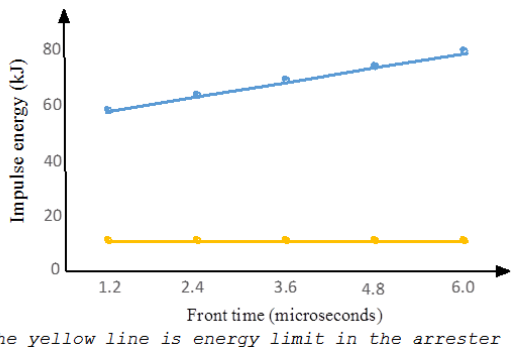

The yellow line is energy limit in the arrester

Figure 11. Comparison of impulse energy values with Tf variations

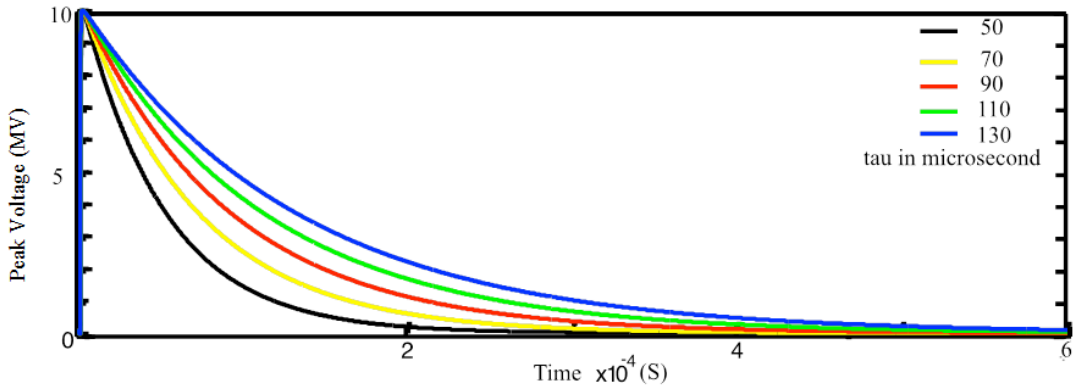

Figure 12. Lightning impulse with tau variations

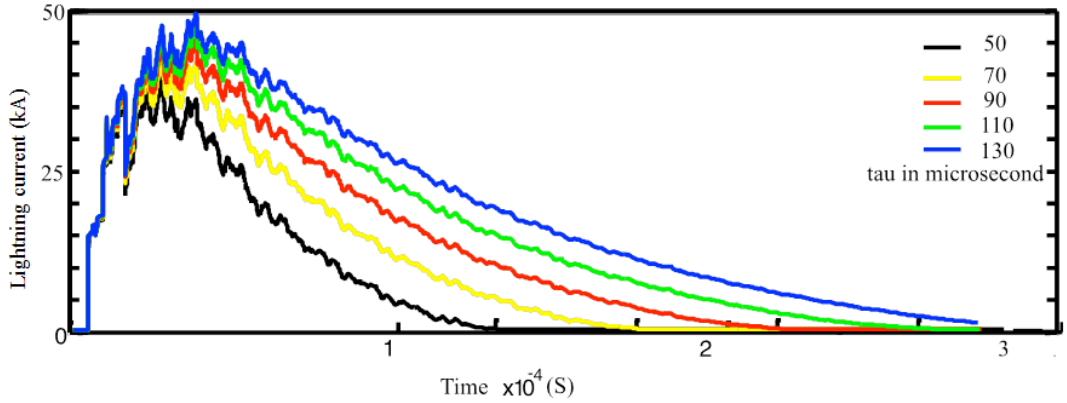

Figure 13. Current waves through arrester in phase A after lightning currents are injected with variations of tau

wire and propagates throughout the transmission lines. The carry out model is the insulator on tower number 4 during the flashover event and it causes an increase of voltage on the phase wire. The Tf, Tsta and tau values in this simulation are 1.2, 3, and 90 ms, respectively. The simulation results that were run on a series of a lightning strike on ground wires without mounting arresters can be seen in Figure 16. The values of the peak voltage of phase wire are 6.5078 MV, 7.7113 MV, 8.6198 MV, 10 MV, 8.8588 MV, and 8.3243 MV for tower numbers 1 to 6, respectively. This simulation also examines the effect of arrester performance in various arrester installation locations. Figure 17 shows a simulation of a series of the lightning strike with arresters placed on tower 1. The arrester on tower 1 has a voltage drop of 89.05 % with a voltage level of 0.7124 MV. Meanwhile, towers 2 to 6 did not experience significant decreases of peak voltage, with the values of 10.99 %, 0.54 %, 0 %, 0.81 %, and 0.8 %, respectively.

The peak voltage of phase wires for towers 2 to 6 are 6.9173 MV, 8.5731 MV, 10 MV, 8.7873 MV, and 8.2579 MV, respectively. Figure 18 shows the simulation result with the placement of TLA on towers 1 and 5. The peak lightning voltage on the phase wires in each tower is different. The highest to

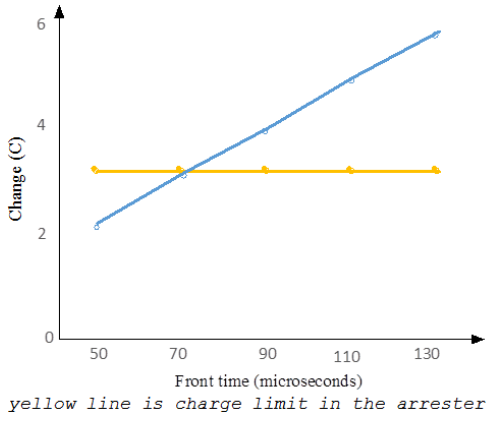

Figure 14. Comparison of current charge values to tau variations

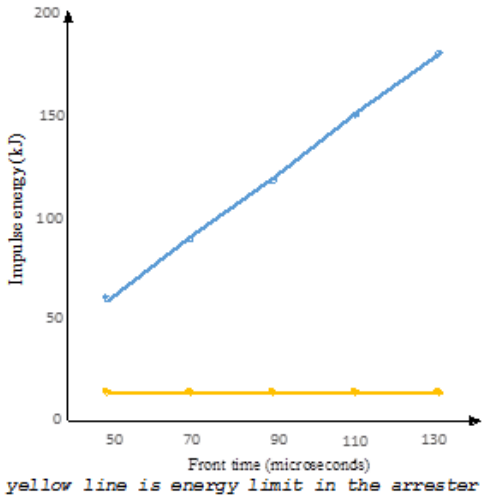

Figure 15. Comparison of impulse energy values to tau variations

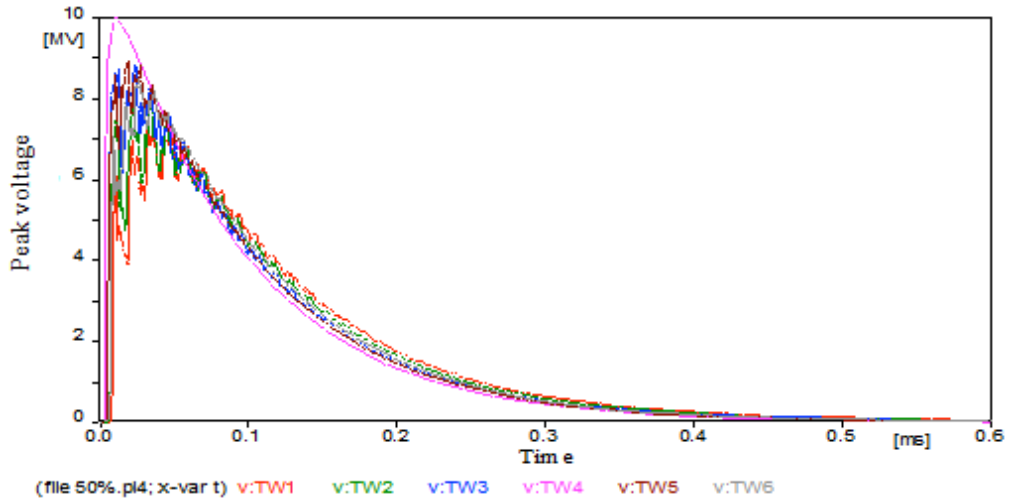

Figure 16. Simulation result of the output of the lightning strike circuit without arrester

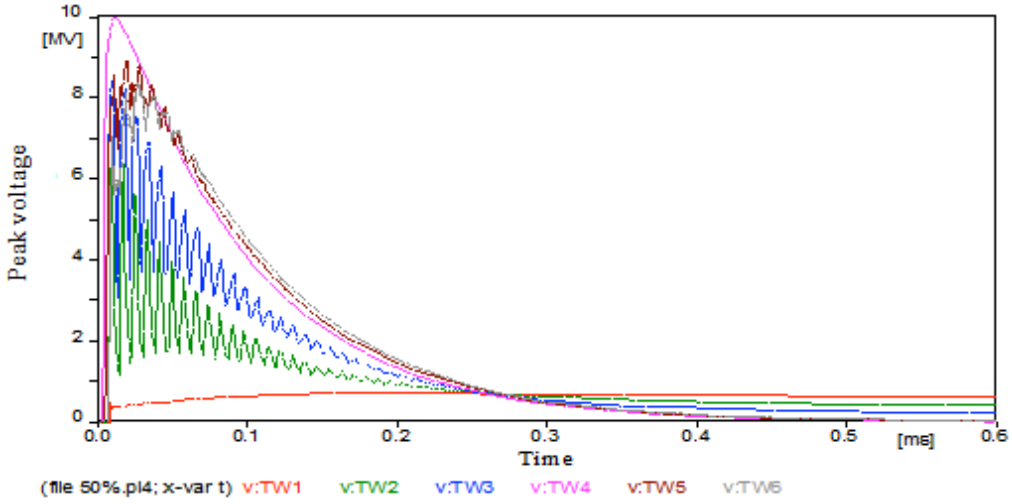

Figure 17. Simulation results show a series of lightning strikes on transmission lines with arresters placed on tower 1

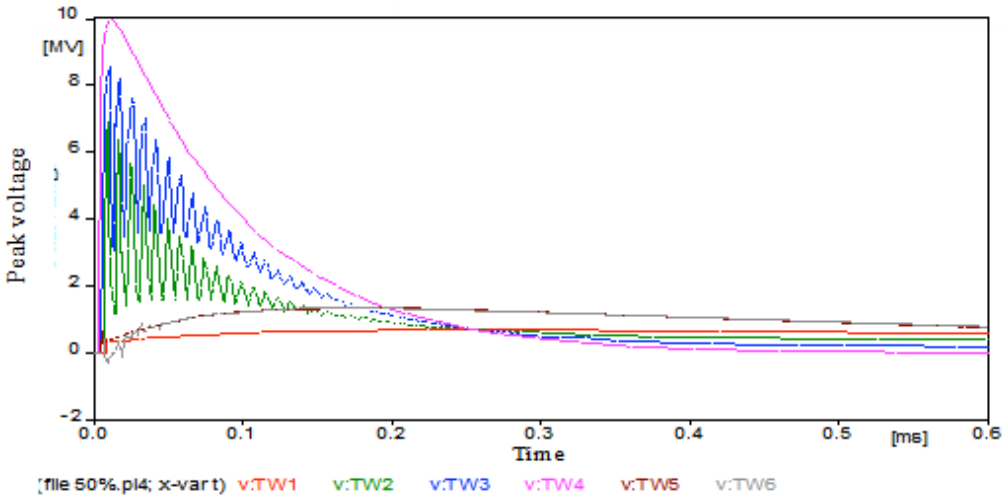

Figure 18. Simulation result of a lightning strike on transmission lines with arresters placed on towers 1 and 5

the lowest peak voltage is found in towers 4, 3, 2, 6, 5, and 1. The most significant decrease in peak voltage on phase wires is found between towers 1 and 5. The peak voltage drop on phase wires from towers 1 to 6 are 89.67 %, 11 %, 0.52 %, 0 %, 84.61 %, 83.49 %, respectively, while the recorded peak voltage was 0.7113 MV, 6.9167 MV, 8.5746 MV, 10 MV, 1.3636 MV, 1.3746 MV, respectively. Moreover, the simulation results for the installation of arresters in towers 1, 2 and 6 can be seen in Figure 19. From the graph above,

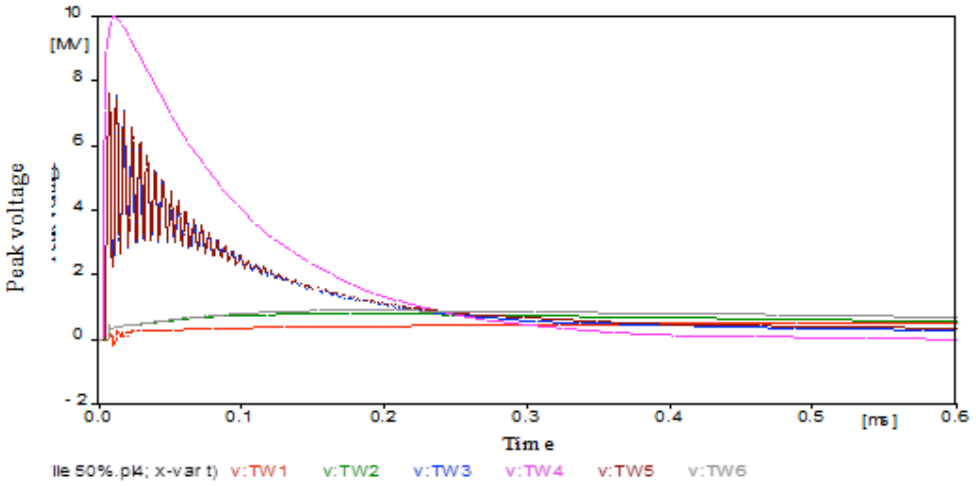

Figure 19. Simulation result of a lightning strike on transmission lines with arresters placed on towers 1, 2 and 6

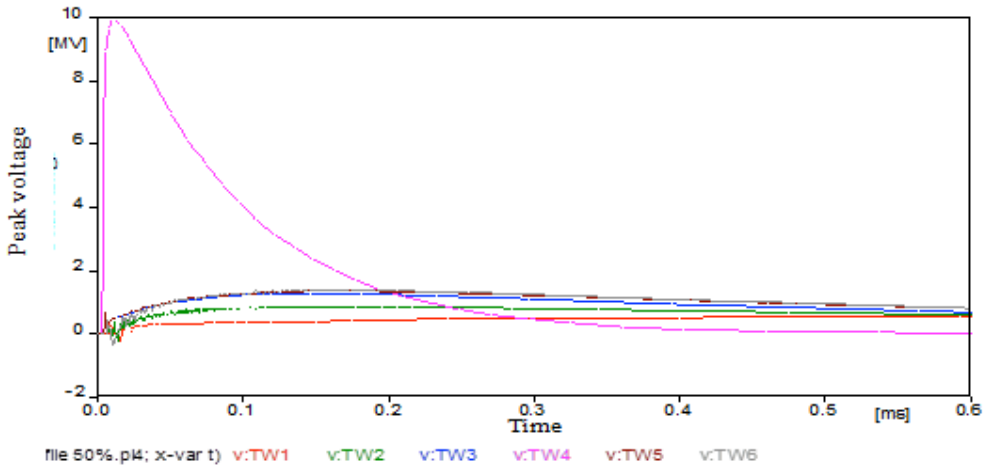

Figure 20. Simulation result of a lightning strike on transmission lines with arresters placed on towers 1, 3, 4 and 5

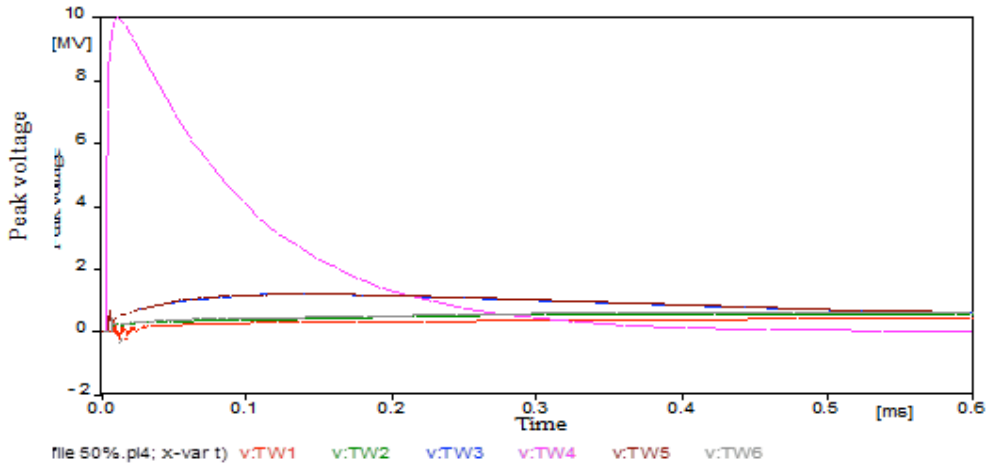

Figure 21. Simulation result of a lightning strike on transmission lines with arresters placed on towers 1, 2, 3, 4, 5 and 6

the data obtained for peak voltage on phase wires in towers 1 to 6 include 0.5153 MV, 0.8021 MV, 7.6114 MV, 10 MV, 7.613 MV, 0.8971 MV, respectively and the percentages of reduction of peak voltage are 92.08 %, 89.68 %, 11.69 %, 0 %, 14.04 %, 89.22 % for towers 1 to 6, respectively.

The simulation results for the installation of arresters in towers 1, 3, 4 and 5 can be seen in Figure 20. From the graph above, the data are as follows: the peak voltages of lightning on phase wire are 0.5471 MV (decreased 91.59 %), 0.8519 MV (decreased 89.04 %), 1.284 MV (decreased 85.1 %), 10 MV (decreased 0 %), 1.3615 MV (decreased 84.63 %), and 1.3811 MV (decreased 83.41 %) for towers 1 to 6, respectively. Figure 21 is a simulation result with the placement of arresters in towers 1, 2, 3, 4, 5, and 6.

The lightning peak voltages on phase wire are 0.4679 MV, 0.5674 MV, 1.2248 MV, 10 MV, 1,2322 MV, and 0.6219 MV for towers 1 to 6, respectively. The voltage drop values are as follows: 92.81 %, 92.64 %, 85.79 %, 0 %, 86.09 %, and 92.53 % for towers 1 to 6, respectively.

In addition, the location of lightning strikes on overhead lines does not have a significant effect on travelling waves with the theory of wave reflection and waves transmitted on the system. However, the location of the lightning strike still influences the overvoltage in the substation by changing the distance of the travelling wave towards the substation [27]. Then, the simulation results also show that the installation of arresters for all phases in several towers can reduce the overvoltage in the tower. This is in a good agreement with [28][29]. However, for economic and maintenance reasons, the installation of arresters should be on a tower that often gets lightning strikes.

IV. Conclusion

Based on the simulation and data analysis that has been done, some conclusions can be drawn: the variations of the wave front time duration (Tf) and strike duration (tau) on lightning impulses affect the current and integral currents that occur in arresters. Tsta variations in lightning impulses do not affect the current charge and impulse energy. Tf is proportional to current charge and impulse energy. The small tau leads to the current toward zero faster. Lightning strikes of 10 MV on the ground wire without mounting arresters resulted in the increases of voltage on the phase wires on tower 1 until 6 were 6.5078 MV, 7.7113 MV, 8.6198 MV, 10 MV (tower had flashover event), 8.8588 MV and 8.3243 MV, respectively. After the installation of arresters in each tower for phase wires, the subsequent decrease of peak voltage on tower 1 until 6 were 0.4679 MV (92.81 %), 0.5674 MV (92.64 %), 1.2248 MV (85.79 %), 10 MV (0 %), 1.2322 MV (86.09 %) and 0.6219 MV (92.53 %), respectively. Protection of the transmission line to reduce overvoltage in phase wires by installing arresters in each tower is better than installing the standing alone arrester or without installing any arresters.

Acknowledgement

We thank all those who have supported this research.

Declarations

Author contribution

F. Murdiya contributed as the main contributor of this paper. All authors read and approved the final paper.

Funding statement

This research did not receive any specific grant from funding agencies in the public, commercial, or not-for-profit sectors.

Conflict of interest

The authors declare no conflict of interest.

Additional information

No additional information is available for this paper.

References

[1] A. Borghetti *et al.*, " Lightning protection of a multi-circuit HV-MV overhead line," *Electric Power Systems Research*, Vol. 180, pages 106-119, available online 3 December 2019.

[2] A. Rahiminejad and B. Vahidi, "LPM-Based Shielding Performance Analysis of High-Voltage Substations Against Direct Lightning Strokes," *IEEE Trans. Power Deliv.*, 32, 2218–2227, 2017.

[3] R. Zoro, G. K. Atmajaya and B. Denov, "Lightning protection system for high voltage transmission line in Indonesia," 2nd International Conference on High Voltage Engineering and Power Systems (ICHVEPS), Denpasar, Bali, Indonesia, pp. 1-5, 2019.

[4] J. Wang *et al.*, "Research and application of jet stream arc-quenching lightning protection gap (JSALPG) for transmission lines," *IEEE Trans. Dielectr. Electr. Insul.*, 22, 782–788, 2015.

[5] F. M. Gatta *et al.*, "Tower Grounding Improvement Versus Line Surge Arresters: Comparison of Remedial Measures for High-BFOR Subtransmission Lines," *IEEE Trans. Ind. Appl.*, 51, 4952–4960, 2015.

[6] S. Mladen and Banjanin,"Line Arresters Application in Lightning Protection of High Voltage Substations with Non-standard Configuration," *Electric Power Components and Systems*, 45:11, 1173-1181, 2017.

[7] Mladen S *et al.*, "Lightning protection of overhead transmission lines using external ground wires," *Electric Power Systems Research*, Volume 127, Pages 206-212, 2015.

[8] M. S. Savic and A. M. Savic, "Substation Lightning Performance Estimation Due to Strikes Into Connected Overhead Lines," *IEEE Trans. Power Deliv.*, 30, 1752–1760, 2015.

[9] K. T. M. U. Hemapala, O. V. G. Swathika, and K. P. R. D. S. K. Dharmadasa, "Techno-economic feasibility of lighting protection of overhead transmission line with multi-chamber insulator arrestors", *Development Engineering*, Volume 3, Pages 100-116, 2018.

[10] A. S. Ghoniem, "Effective elimination factors to the generated lightning flashover in high voltage transmission network," *International Journal on Electrical Engineering and Informatics,* Volume 9, Number 3, September 2017.

[11] O. E. Gouda, A. Z. El Dein, and G. M. Amer, "Parameters Affecting the Back Flashover across the Overhead Transmission Line Insulator Caused by Lightning." *Proceedings of the 14th International Middle East Power Systems Conference (MEPCON' 10)*, Cairo University, Vol. 111, 2010.

[12] S. H. Taheri, A. Gholami, and M. Mirzaei, "Study on the behavior of polluted insulators under lightning impulse stress." *Electric Power Components and Systems,* 37.12, 1321-1333, 2009.

[13] N. Zawani *et al.*, "Modelling of 132 kV overhead transmission lines by using ATP/ EMTP for shielding failure pattern recognition," *Procedia Engineering*, vol. 53, 278–287, 2013.

[14] M. A. Abd-Allah, M. N. Ali, and A. Said, "Towards an accurate modeling of frequency-dependent wind farm components under transient conditions," *WSEAS Transactions on Power Systems*, Volume 9, Art. #40, pp. 395-407, 2014.

[15] P. Pinceti and M. Giannettoni, "A simplified model for zinc oxide surge arresters," in *IEEE Transactions on Power Delivery*, vol. 14, no. 2, pp. 393-398, April 1999.

[16] F. Fernandes, R. Diaz, "Metal-oxide surge arrester model for fast transient simulations," *IPST Conference,* 2001.

[17] D. Lovrić, S. Vujević, and T. Modrić, 'Comparison of Different Metal Oxide Surge Arrester Models', *Int. J. Emerg. Sci*, 4 December, pp. 545–554, 2011.

[18] L. Shoubin *et al*., "Applicability Analysis of Simulation Model of Metal Oxide Arrester and Experimental Study," *Advances in Intelligent Systems Research (AISR)*, volume 151, 2018.

[19] M. Ishii *et al*., "Multistory transmission tower model for lightning surge analysis," in *IEEE Transactions on Power Delivery*, vol. 6, no. 3, pp. 1327-1335, July, 1991.

[20] H. W. Dommel, *EMTP Theory Book*: B.P.A., Aug. 1986.

[21] A. Semlyen and A. Dabuleanu, "Fast and accurate switching transient calculations on transmission lines with ground return using recursive convolutions," in *IEEE Transactions on Power Apparatus and Systems*, vol. 94, no. 2, pp. 561-571, March 1975.

[22] J. R. Marti, "Accurate modeling of frequency-dependent transmission lines in electromagnetic transient simulations," *IEEE Trans. Power App. Syst*., vol. PAS-101, no. 1, p. 147, 1982.

[23] N. Nagaoka, "Development of frequency-dependent tower model," *Trans. IEE Japan*, vol. 111-B, p. 51, 1991.

[24] J. V. G. R. Rao, K. S.Kalyani, and K. R. Charan, "Optimal Surge Arrester Placement for Extra High Voltage Substation", *International Journal of Engineering and Advanced Technology (IJEAT)*, Volume-8 Issue-6, August 2019.

[25] N. H. N Hassan *et al*., "Analysis of discharge energy on surge arrester configurations in 132 kV double circuit transmission lines," *Measurement*, Volume 139, Pages 103-111, 2019.

[26] J. R. Martí and A. Tavighi, "Frequency-Dependent Multiconductor Transmission Line Model With Collocated Voltage and Current Propagation," in IEEE Transactions on Power Delivery, vol. 33, no. 1, pp. 71-81, Feb., 2018.

[27] M. I. Jambak *et al*., "Analysis of Transmission Lightning Arrester Locations Using Tflash," *Telkomika*, volume 14, number 4, 2016.

[28] Q. Xia, "Surge Arrester Placement for Long Transmission Line and Substation," Master Theses, Arizona State University, May 2018.

[29] J. He *et al*., "Statistical Analysis on Lightning Performance of Transmission Lines in Several Regions of China," *IEEE Trans. Power Deliv*., 30, 1543–1551, 2015.

This page intentionally left blank

Journal of Mechatronics, Electrical Power, and Vehicular Technology 10 (2019) 61-71

Journal of Mechatronics, Electrical Power, and Vehicular Technology

e-ISSN: 2088-6985
p-ISSN: 2087-3379

www.mevjournal.com

Design and development of the sEMG-based exoskeleton strength enhancer for the legs

Mikecon Cenit, Vaibhav Gandhi *

Department of Design Engineering and Mathematics, Middlesex University London
The Burroughs, Hendon, London, NW4 4BT, United Kingdom

Received 30 July 2019; accepted 28 November 2019

Abstract

This paper reviews the different exoskeleton designs and presents a working prototype of a surface electromyography (EMG) controlled exoskeleton to enhance the strength of the lower leg. The Computer Aided Design (CAD) model of the exoskeleton is designed, 3D printed with respect to the golden ratio of human anthropometry, and tested structurally. The exoskeleton control system is designed on the LabVIEW National Instrument platform and embedded in myRIO. Surface EMG sensors (sEMG) and flex sensors are used coherently to create different state filters for the EMG, human body posture and control for the mechanical exoskeleton actuation. The myRIO is used to process sEMG signals and send control signals to the exoskeleton. Thus, the complete exoskeleton system consists of sEMG as primary sensor and flex sensor as a secondary sensor while the whole control system is designed in LabVIEW. FEA simulation and tests show that the exoskeleton is suitable for an average human weight of 62 kg plus excess force with different reactive spring forces. However, due to the mechanical properties of the exoskeleton actuator, it will require an additional lift to provide the rapid reactive impulse force needed to increase biomechanical movement such as squatting up. Finally, with the increasing availability of such assistive devices on the market, the important aspect of ethical, social and legal issues have also emerged and discussed in this paper.

Keywords: leg-exoskeleton; electromyography based exoskeleton; LabVIEW myRIO; ethical, societal, and legal concerns.

I. Introduction

Assisted exoskeleton technology seems to be still in the development stage, and needs to be improved to meet the individual needs [1]. Some examples of this exoskeleton are Berkeley Lower Extremity Exoskeleton [2], Raytheon XOS2 [3], Exosuit [4][5], DARPA Soft Exosuit [6], Ekso Bionics [7] and many more [8]. These full body exoskeletons all have some limitation with their design, such as the lack of appropriate power supply suitable to their target specifications. Specialised exoskeleton suits come in many varieties which are used as an aid for medical rehabilitation [9][10], industrial [11], military [12] and commercial [13]. These specialised exoskeletons allow individuals with any lower limb weakness including those who are paralyzed below to move and mimic the biomechanical movement of walking. Any technology that can reduce casualties or enhance one's survival in a harsh environment and open new strategical advantages will always find itself in military use. The concept of specialised exoskeletons is specific to one job but limits the energy consumption to a great extent. On the other hand, the whole body's exoskeletons require a far greater power supply as the exoskeleton is needed to carry the weight of other parts of the suit that might not be used [14]. Such technology may not be popular compared to a humanoid robot in the future, as it is specifically designed for medical and military use and is also expensive and far from generalizing for the general public. It is also impractical for daily life use as it is designed for a harsher environment than the civilian population or is made to help and strengthen one's need for biomechanical movement. Military concept exoskeleton is generally more developed according to the harsher environments [15]. Potential commercial uses are also considered in this review for completeness [16].

A good example of exoskeleton suit that is used medically is the Lifesuit prototype. A man called Monty K. Reed, broke his back due to a parachute

* Corresponding Author. Tel: +44 208 411 5511
E-mail address: V.Gandhi@mdx.ac.uk

doi: https://dx.doi.org/10.14203/j.mev.2019.v10.61-71

Accreditation Number: (RISTEKDIKTI) 1/E/KPT/2015 (Sinta 2).

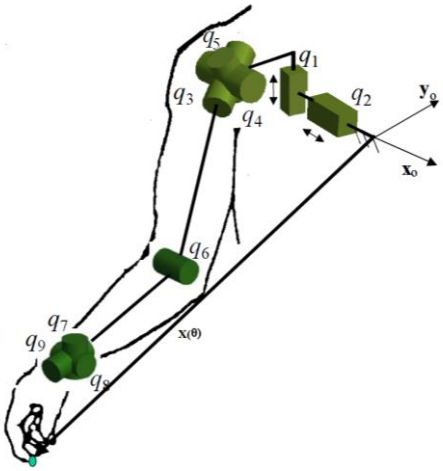

Figure 1. 9-DOF of the human upper limb [72]

accident, created a Lifesuit I prototype in 1986 [17]. His idea of a powered exoskeleton emerged when he was reading Robert Heinlein's spaceship during his time in the hospital while recovering from his injuries. Reed then demonstrated his findings at the university of Washington Engineering Day event and had set a world record for the 8-inches high jump and a land-speed distance record for walking 5 km in powered exoskeletons in 90 minutes at Saint Patrick's Day Dash 2005 [17]. The LS12 Lifesuit prototype used to manage the record also caused some disadvatages to the pilot user. Over time the material used to make the Lifesuit had worn out and became loose, causing minor injuries to the pilot's left outer thigh. The previous prototype also caused some minor injuries when the pilot conducted the experiments. However, the potential risk had been removed and improved with successors [18]. Finding initial risks early within the project can be beneficial as the design can be improved. The lifesuit prototype exoskeleton framework became more ergonomic and more user-friendly as sophisticated systems are improved and added, for example, using the pneumatic power supply, pneumatic actuator and handheld controllers [18]. The handheld controller concept has pro and cons as the user's hand is being mastered but this gives the pilot some manual control over the pneumatic actuators.

Mechanical robotic rehabilitation suits can be divided into the upper limb and lower limb usage [19]. Exoskeletons for upper limb have a shared structure that mimics the human upper limb (Figure 1 and Figure 3). Since the exoskeleton is attached to several upper limb locations difference in a human size, it makes it difficult for the robot to adapt [20]. The upper limb exoskeleton can also be arranged to help certain muscles during rehabilitation by regulating and algorithmic combination that adapts to the forces applied by the exoskeleton to the end user's arm. Most of the exoskeletons work around the biomechanical mechanism of the human flexion elbow movement and shoulder spherical movement [21]. On the other hand, some research on exoskeletons has also included the wrist movement and hand grasping movement [22][23]. Some examples of the upper exoskeletons are Armin 3 and IntelliArm [24]. These exoskeletons have an integrated design 3-DOF to help shoulder depression and elevation movements. The Medarm's exoskeleton has included depression, elevation, retraction and protraction actuator system, while other designs have utilized passive DOF to support the ankle. Passive DOF helps the ankle to move and allows greater freedom of movement, and this minimizes the generated actuation force that is given at the joint [25][26][27]. Lower limb exoskeletons (Figure 2 and Figure 4) focuses more on the ankle rehabilitation. The most common problems addressed in ankle rehabilitation studies is the gait pattern of the patient as the

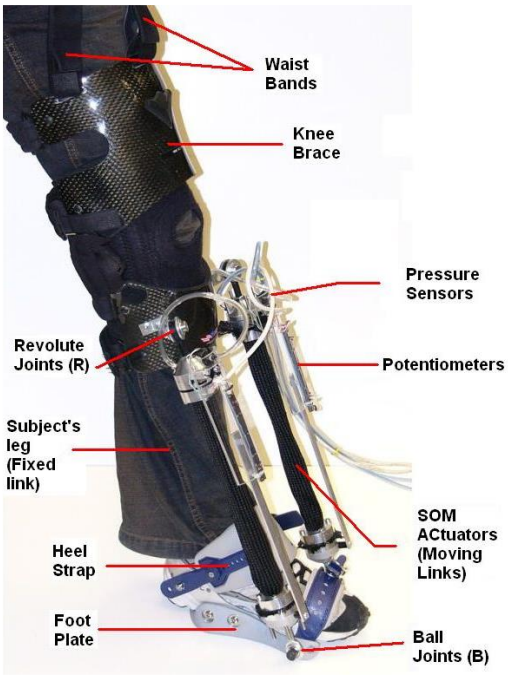

Figure 2. Robotic gait trainer [73]

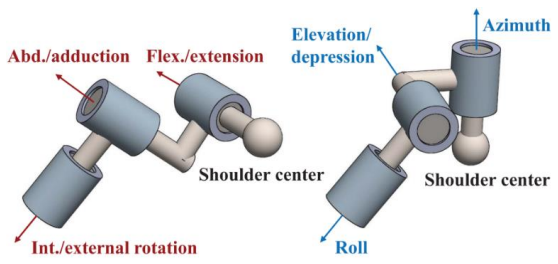

Figure 3. Two rotation conventions for the glenohumeral joint model: (a) flexion–abduction–rotation and (b) azimuth–elevation–roll [29]

exoskeleton systems manipulate the applied force to improve the gait pattern of the end user [28]. The generalised design of robotic devices provides the actuated motion that affects the foot plantar flexion and dorsiflexion. On the other hand, some devices include passive and/or controlled inversion and eversion movements. Stiffness control of an actuator is commonly used rather than actuators that provide a massive amount of assistive force, but this is mainly due to the biomechanical movement of the ankle joint [29].

Military categorised exoskeletons are more generalised to the entire human body (for example, Raytheon XOS clothing), unlike the medically categorised exoskeletons that are specific to certain key elements of the human body that focuses on say for example only the ankle and not the whole of the human body [30]. The Raytheon Sarcos's XOS2 robotic suit is roughly 50 % more energy efficient than the XOS1 and weighs around 95 kg. The structure is built with high strength aluminium and steel alloy and utilizes actuators, controllers and sensors to perform the required task [31]. The exoskeleton can take a heavy object with a ratio of 17:1, and this is due to the high-pressure hydraulics used, but this again increases the overall weight of the exoskeleton itself. The system analyses the user's limb movements and range awareness so it does not cause damage to itself. This prevents damage from unwanted movements such as sneezing and coughing. The motors have multiple speeds to overcome and produce the appropriate speed and power. Although, XOS2 is more energy efficient than its predecessor but it still has the limitation of the power source. The only power source provided to the system is through a wire tether that connect to the outside power supply. Supplying it with an expensive on-board battery can be violated on the battlefield and can cause friendly casualty [32].

Figure 4. Anklebot [28]

This paper proposes a low-cost and reasonably simple exoskeleton design with a focus on only assisting the user's lower body. The paper is organized into six sections. Section I introduces the exoskeleton designs in general. Section II provides a brief description of exoskeleton aspects, and especially surface EMG (sEMG) control, which is used as a primary sensor in the proposed design. Section III details the proposed lower body one leg sEMG-controlled exoskeleton. Section IV discusses the evaluation/testing of the proposed system. Section V discusses the significant aspects of ethical, social and legal facets in new robotic technologies. Section VI concludes the paper with a brief summary.

II. EMG based Exoskeleton Control

There are several methods for moving and exoskeletons manoeuvring, however, the most sought-after concept is the use of electromyography (EMG) [33][34][35]. EMG signals can be classified into two types: intramuscular EMG signals, detected from inside of the muscles; and surface EMG signals (sEMGs), detected from the skin surface [36]. EMG-based exoskeletons are usually designed with muscles that are easily accessible from the skin surface. For this reason, sEMG electrode circuit is used in this work. The sEMG-based system works by recording and processing the myoelectric signals from the user so that they can communicate and control the actuators. sEMG signals of flexor Digitorum Superficialis from the finger flexure and Pollicis Longus from the tumb flexure are commonly used as control (actuation) signals. Among the muscles that are part of the upper/lower body limb exoskeleton [37][38], the muscle signals mentioned above are commonly used to create and control an exoskeleton or assistance robotic device that involves hand movements. This is due to the grasping movement, lower noise and the potential ergonomic value, as electrodes can be mounted on the forearm [39]. A better understanding of human anatomy, electrode placements, and the basic principles of muscle contraction can be found in Peter Konrad *et al.* research [40]. Placement of the electrodes from the main voluntary muscles enables control to the specialized exoskeleton. Usually using voluntary EMG muscle signals that are partners with the right part of an exoskeleton creates far more natural movement with respect to the biomechanical movement of the human body. exoskeleton or auxiliary robots can also work without the correct paired muscle such as the case with amputated personnel [35]. Different muscle types can be trained and used to mimic the EMG signal required for natural movements. For example, a person without fingers can make a robot to capture an object by using the EMG from different muscle group that does not interfere with other signals [39][41][42].

Zaheer *et al.* [43] discuss the sensor site for ideal electrodes placement based on the results of the

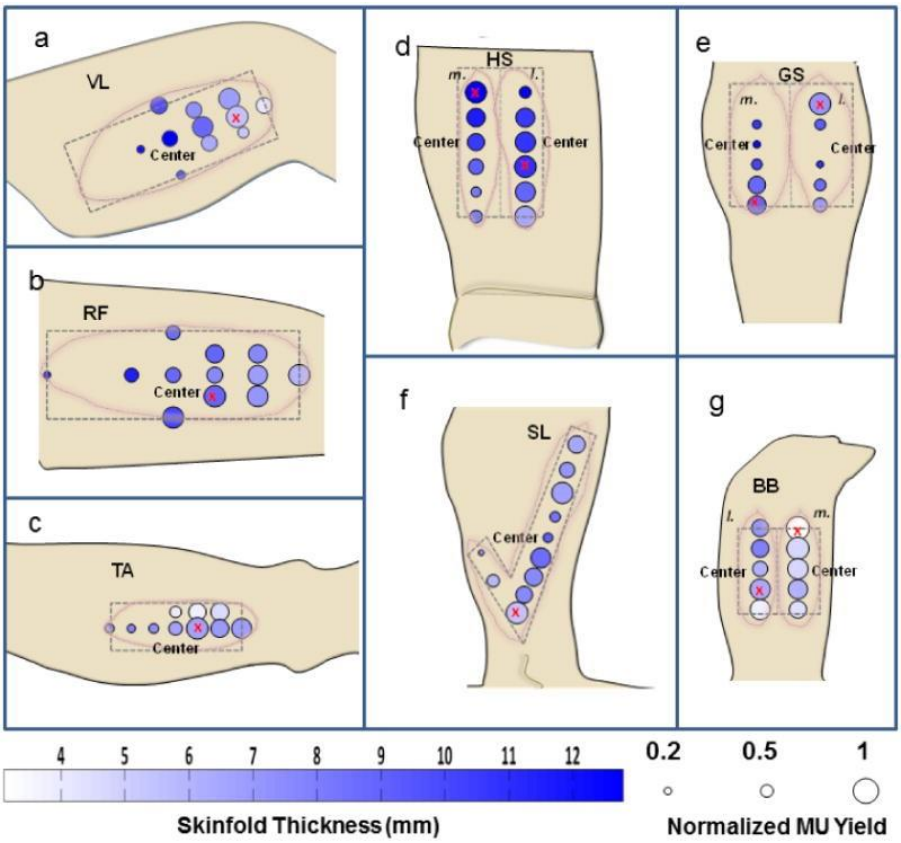

Figure 5. Electrode placement locations from the seven tested muscles topographically mapped by the normalized MU yield per sensor site with increasing circle sizes reflecting greater yields. Average skinfold thickness is indicated by the hue of the color. The values for each muscle are as follows: (a) Vastus Lateralis: the normalized MU yield ranges from 0.3 - 0.9 and the skinfold ranges from 4 to 12.6 mm; (b) Rectus Femoris: the normalized MU yield ranges from 0.3 - 0.8 and the skinfold ranges from 5.9 to 12.4 mm; (c) Tibialis Anterior: the normalized MU yield ranges from 0.4 - 1 and the skinfold ranges from 3.3 to 6.7 mm; (d) Hamstrings Medial: the normalized MU yield ranges from 0.4 - 0.9 and the skinfold ranges from 7.8 - 11.5 mm; Hamstrings Lateral: the normalized MU yield ranges from 0.5 - 0.9 and the skinfold ranges from 6.4 to 12.5 mm; (e) Gastrocnemius Medial: the normalized MU yield ranges from 0.3 - 0.9 and the skinfold ranges from 6 to 12.6 mm, Gastrocnemius Lateral: the normalized MU yield ranges from 0.3 - 1 and the skinfold ranges from 6 to 12 mm; (f) Soleus: the normalized MU yield ranges from 0.2 - 0.9 and the skinfold ranges from 5.4 – 9 mm; (g) Biceps Brachii Medial: the normalized MU yield ranges from 0.7 - 1 and the skinfold ranges from 3.1 to 6.7 mm, Biceps Brachii Lateral: the normalized MU yield ranges [43]

normalised motor unit and skin thickness. These concepts of the ideal electrode placement sites are located between the centre mass and the muscle tendency area (Figure 5 for a mapped area). The signal to noise ratio of the detected sEMG signal correlates with the motor unit yield. The signal to noise ratio is inversely related to the muscle fibres and thickness of the subdermal cell tissue between the sensor and muscles [43]. However, the concept of ideal electrode placement varies in different muscle groups [44] as well as from one subject to the other. Inter-subject and intra-session variation is common knowledge in EMG study [36][45]. Subcutaneous fat has also been understood to inhibit sEMG signals [46][47], resulting in a lack of sEMG compared to the invasive EMG needle method [48]. However, the location of this ideal sensor sites by F. Zaheer *et al.* [43] is slightly different from the preferred sensor site of the kinesiology EMG studies [49][50]. The general kinesiology EMG studies are performed using stem electrodes with the intention of acquiring global muscle activities [50].

This study also confirms that reasonable motor unit results can be obtained from almost anywhere in the central mass of the selected muscle group. On the other hand, the results that muscles have localised regions that provide greater motor unit yields are likely related to variations in the EMG signal resulting from the subdermal tissue throughout the muscle surface, and the quality of electrode contact of the sensor and the skin. This also shows evidence that correlates the direct relationship between the motor unit results and the signal to noise ratio of the EMG signal. The poor sources of the sEMG signal are likely due to increasing distance between the electrode sensors and the muscle due to the subdermal tissue, which reduces the sEMG signal amplitude. However, based on some of the ideal electrode placement site results, the relationships of decreasing signal to noise ratio and increasing subdermal network seems inconsistent. Therefore, some other factors may influence the motor unit results such as the muscle innervation zone.

Studies also show that the sEMG signal read in the skin area near the innervation zones produces signals with lower amplitude, resulting in a lower signal to noise ratio due to the cancellation of the action potentials moving in the opposite directions [42]. In summary, the sEMG signal near the muscle innervation seems to have higher frequencies and lower amplitudes. Every area of the human body provides either adequate or poor EMG signals that can vary from person to person. However, certain biomechanical movements of the muscles have

preferred sites that provide richer motor unit results. They are generally located between the centre of the muscle mass when contracted and the tendinous area. Another ideal electrode placement is in the area of the skin with the thinnest subdermal tissues. Therefore, the electrodes placement will be located in the area as shown in Figure 5 of vastus lateralis and rectus femoris.

III. Proposed sEMG based Exoskeleton

A. Overall design and software

The development of exoskeleton size depends on anthropometry [51] i.e., the physical measure of human size. For the proposed design, the leg to body height ratio of 49 % with respect to the average male size of 175 cm is considered. The research also includes ±1, 2 or 3 mean value bases of the 49 % comparison to different racial origins. Thus, the most appropriate exoskeleton size is based on the average human height. Smaller exoskeletons can be made to adapt to the average size of the female. Therefore, the size of the exoskeleton is made on the basis of 85.75 cm due to the 49 % of the male average of 175 cm.

The proposed exoskeleton (Figure 6 to Figure 9) consists of flex sensors and actuators that are controlled by using the NI myRIO (LabVIEW) [52] based control system (Figure 10). The start-up sensors used is from the BITalino hardware and software tools kit [53]. BITalino hardware and software are specifically designed to read body signals such as electrocardiography (ECG), sEMG and many more; and has a configurable sampling rate of 1, 10, 100, and 1000 Hz [54]. Flex sensors are used in the development of the exoskeleton as a secondary controller while maintaining the BITalino sEMG sensor [55] as the primary sensor. The sEMG sensor cannot be removed and provides bipolar differential measurement. The raw sEMG signals should be filtered using appropriate techniques such as Savitzsky-Golay (SG) [56], or advanced techniques as Recurrent Quantum Neural Network [57][58] and many others [59][60][61]. In the current work, raw

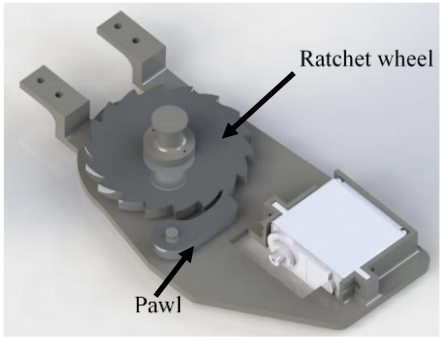

Figure 6. Ratchet and Pawl

sEMG signals from the BITalino are sampled at 100 Hz, filtered and refined using the SG convolution filter concept. Flex sensors are installed at the top of the knee joint to read the user's posture, create a condition for the control system software, and appear to provide information with a good level of precision, reliability and repeatability [62]. The default analogue value that is read then sent to a state condition that provides Boolean control for the system. The state condition is calibrated to fit the user's sensitivity preference over the exoskeleton, and provides the user's posture state. Depending on the posture, different numeric polynomial sequences and side points are provided for the SG filter LabVIEW program. Memory shape materials can be used as actuators for exoskeleton systems because it does not require external or onboard functioning energy, thereby increasing energy efficiency [63][64]. There are numerous forms of memory materials that can be used, but for the proposed exoskeleton, a tension spring is used as it mimics kinetic movement properties of the pneumatic air muscle when contracting to support the user when squatting and storing the energy. The stored energy is subsequently used to support the user to squat up. A mechanical ratchet and pawl (designed in-house) (Figure 6, Figure 7) is used to hold down the extension of the tension spring from releasing the stored potential energy.

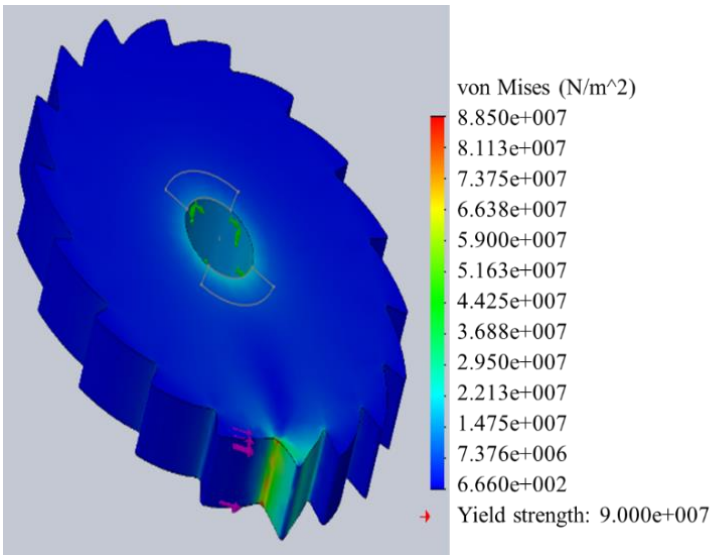

Figure 7. FEA simulation of ratchet gear

Figure 8. CAD prototype of the exoskeleton

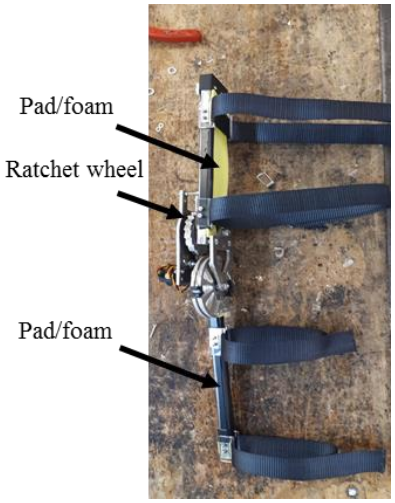

Figure 9. Physical prototype of the exoskeleton

The CAD design (Figure 8) incorporates the rapid prototyping of a grey 3D printer. The ratchet turns as the user squats down and is held by the mechanical pawl. The design concept is to control the reactive force of a spring. The pawl is controlled using a servo motor. The position of the servo motor changes according to the user proclaimed by the system after user calibration. The exoskeleton structural framework is made using aluminium metal to stop potential electrical problems. The good advantage of using aluminium for developing the exoskeleton is due to the machinery available to be used and also the anti-rusting nature. The metals is cut using a water jet cutter that immerses the material in an aqueous environment.

Carbon fibre is planned as the final material to be used for commercial development of the exoskeleton. The red spring is installed in-between the aluminium frames to concentrate the spring strength and share the load between the frames (Figure 8). The complex 3D parts that are manufactured using the 3D printer had weak tensile strength, therefore a material change is needed. Improving the previous prototype design, the revised design incorporates layered sheet build due to the water jet cutting machine is only able to cut flat aluminium material. The 1060-H14 grade aluminium alloy is used as the main body material in the production of the exoskeleton as it is widely recognized for its excellent corrosion resistance, high durability and highly reflective blue/silver appearance (Figure 9). The strap has been added to attach to the exoskeleton, and is locked and joined using Velcro to allow different leg sizes. The yellow soft foam padding is added in a place where the exoskeleton will make surface contact with the user. This creates a soft feeling for the user instead of cold metal and also improve the ergonomic design.

When the parameters set for the sEMG signal are triggered, a Boolean output is given. The condition parameters are set to check the value provided by the flex sensor. The result is two Boolean outputs telling the control system that the user's posture must stand

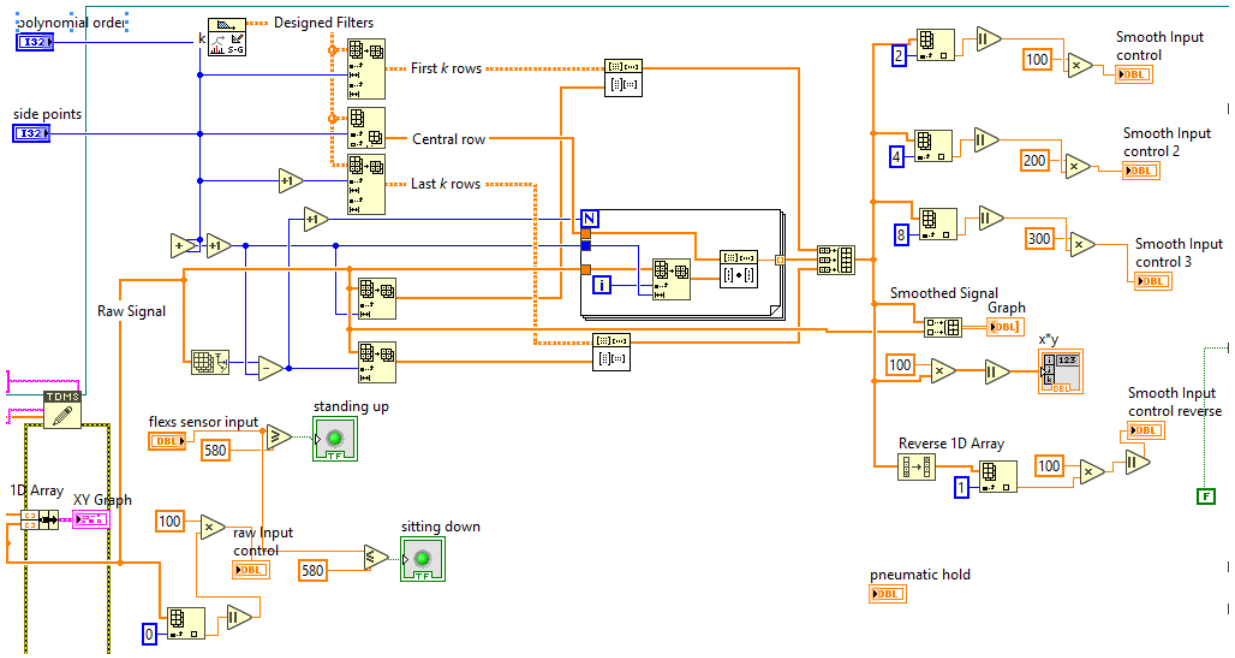

Figure 10. NI LabVIEW control system model

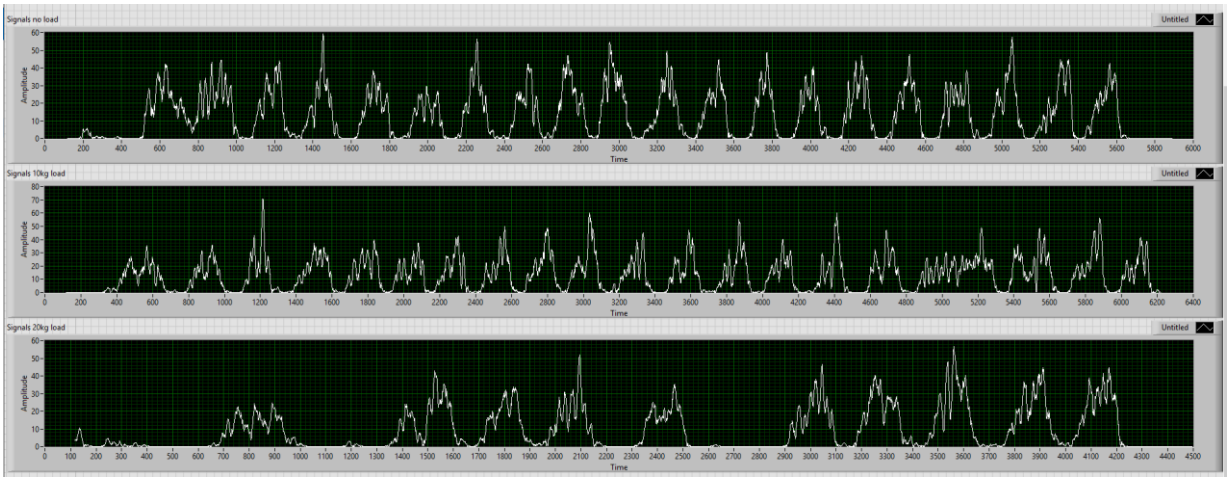

Figure 11. Squat sEMG signal of the quadricep with different spring load *x*-axis [100 = 1 second] *y*-axis [100mV]

or sit on the base of the angle range of the knee. The Boolean output results are sent to the state condition to control the servo position (Figure 10).

IV. Testing and Evaluation

A. Structural test

Ratchet is the only mechanical part that holds the reactive force of the spring potential energy. The 1060-H14 aluminium alloy has a shear modulus of 2.63+010 N/m^2. The force applied on Finite Element Analysis (FEA) simulation of the ratchet gear is set on 607.6 N. The average human weight is 62 kg = 607.6 N. To ensure the system can handle enough spring force to carry the weight of the average human body plus the excess force of overweight users. The FEA simulation shows the highest 8.850e+007 von Mises of the ratchet gear is way below the shear modulus of the 1060-H14 aluminium alloy (Figure 7).

B. sEMG signal based on different spring reactive force

'No-load signal' is the exoskeleton fitted on the user while adjusting the reaction force of the spring to eliminate the weight of the exoskeleton. This establishes the initial basis to show that the exoskeleton can compensate for its own weight without providing support value. Both '10 kg signal load' and '20 kg signal load' are defined as additional reactive force with the additional negative reactive force required to nullify the weight of the exoskeleton (Figure 11). To create a simple average of quadricep sEMG activity while squatting requires some categorization. 10 samples close to the specification and classification are used to create this average value of the sEMG signal shown in Figure 12. The classification of data works by collecting the array of amplitude values from the start of the squat to the end of the squat in a certain amount of time and between breaks. The rest time between each repetition of squat is 4 seconds which is double the time of the 2 second full squat. Once the classification of the data is done, each data set is layered on top of one another to find the most suitable one.

Based on the sEMG signal graph of 'no-load signal' shown on Figure 12(a), it shows; four amplitude spikes: the first and second amplitude spike is located at 0 to 90 *y*-axes when the user is squatting down, as expected due to the quadriceps and hamstring muscle support the body to descend. Once the user reached the target, squat down the legs muscle pass most of the load to the gluteus maximus as shown on the sEMG amplitude which drops at 90 to 105 *y*-axes. On the other hand, the third sEMG amplitude spike up is located at 105 to 132 *y*-axes, this is due to the user squatting up. The body requires a massive workload impact force to move the body weight against gravity. The muscle relaxes as it reaches its baseline point/standing, as shown at 140 to 200 *y*-axes. Once the user stands up, the weight load is transferred parallel from the leg muscle on the bones to the foot.

The comparison of the average sEMG signal with different reactive spring force shown in Figure 12 shows; exoskeleton supports the user well as the strength of body weight pushes the legs down due to squatting. There is an overall lower average sEMG amplitude as the reactive force provided by the spring actuator increases. As the reactive force of the spring increases, the time needed for the user to squat down also increase as the downward force is damped by the spring. On the other hand, the squat up process time is reduced as the stored potential energy inside the spring helps the user to stand up. Therefore, as the spring reactive force increases, the working time of a full squat increase in the process. The actuator memory form material has a good property of absorbing the body weight strength. In the first half of the sEMG signal, where the user squats down, the sEMG signal indicates a lower sEMG amplitude value as the spring reactive force increases.

Due to its mechanical properties, the memory shape actuator fails to provide a quick impulse reactive force required to increase the squatting biomechanical movement. An additional actuator is required to compensate for the additional reactive force to increase the squatting biomechanical movement. Adding more shape memory foam to the system can provide a bigger reactive force impulse. However, the process flow chart would change to accommodate the biomechanical time and movement that needed to convert more kinetic force from squatting down to potential energy stored in the spring shape of the memory.

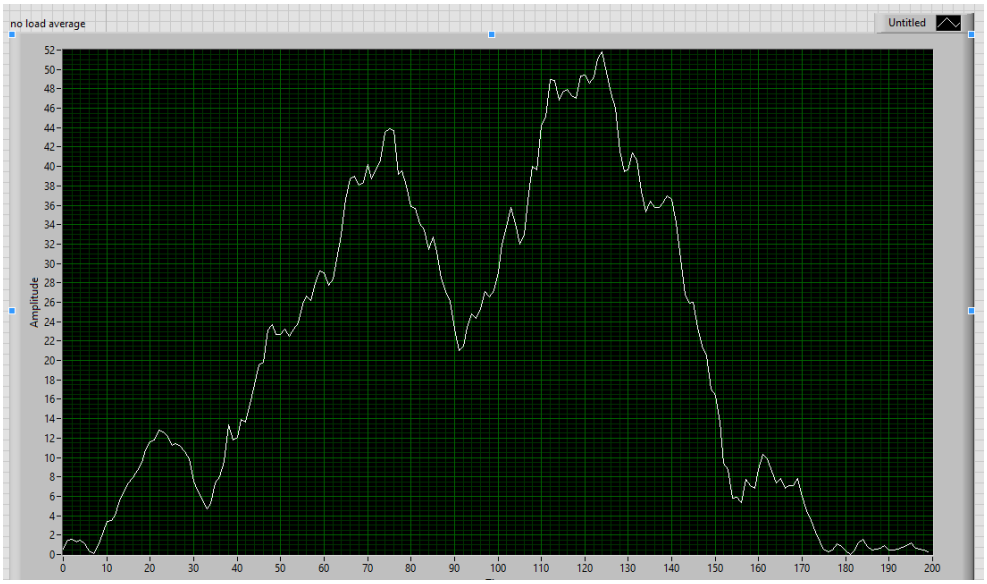

(a)

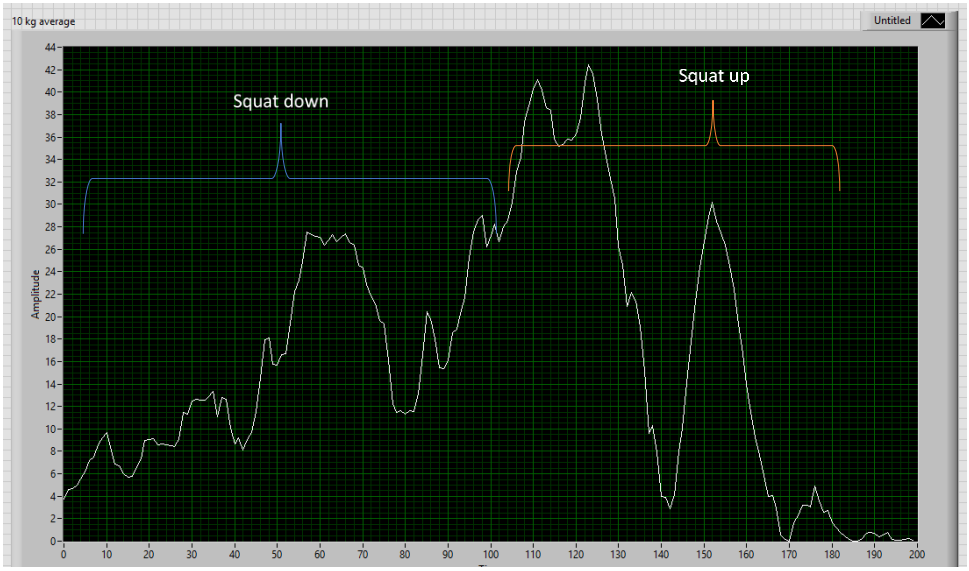

(b)

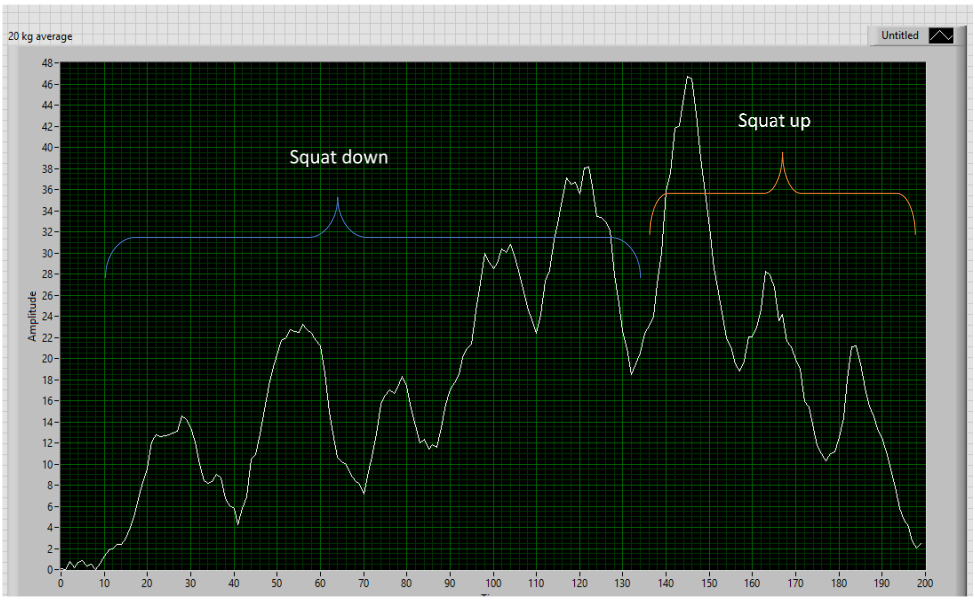

(c)

Figure 12. sEMG signal with varying load reactive forces (a) No load reactive force; (b) 10 kg reactive force; (c) 20 kg reactive force. x-axis [100 = 1 second], y-axis [100mV]

V. Ethical, Societal, and Legal (ELS) Aspects in Wearable Robotics

According to Salvini [65], in the coming years, the western societies will have population aged of 60 more than younger people and, to make things even worse, the family caregivers are no longer willing to look after their older relatives, thus obliging them to use wearable robots. This is where assistive devices such as the one discussed here can play an important role. However, with the increasing availability of such assistive devices, an important aspect of ethical, social, legal and standardization aspects have emerged [66][67][68][69]. A comprehensive and a very recent work on ELS issues in Wearable Robotics, identifying relevant values and ethical, philosophical, legal and social concerns related to the design, dissemination and practical use of wearable robots can be found in Felzmann *et al.* work [69]. There are several other works in this field such as that by Greenbaum *et al.* [70], which talks about the specifics related mainly to exoskeleton designs. Greenbaum *et al.* also raises an important open question as a way of dealing with the high costs of exoskeletons in relation to social justice of access/affordability for all who need it (especially with the increasing ageing population), as well as the dependence on expensive technologies that eventually occurs. It seems that for the wider society, exoskeletons and other technological enhancement raise much longer and complex questions that will force human to redefine how human themselves are being perceived [70]. Calo in [71] examines very well and probably for the first time what is the meaning of the introduction of equally transformative new technologies for cyberlaw and policies regarding integrating robotics and such new technologies.

VI. Conclusion

The sEMG-based exoskeleton concept of using a spring as a mechanical actuator works well but it is limited to the energy a spring can store. The memory shape material actuator has a good property of absorbing the body weight force while supporting the user to squat down. On the other hand, the time a person takes to squat down increases as the downwards force is dampened by the spring, slowing down the full squatting action. The amplitude value of sEMG control signal does not have a repetitive arrangement value over time as the muscle contraction varies with minute changes across the environment and the user. In addition, the sEMG electrode placement varies from subject to subject. The entire area of the leg muscle provides sEMG signals that can be decomposed to produce the firing instances and shapes of several motor unit. However, muscles have preferred a place that provides richer motor unit yields. They are generally located between the centre of the abdominal muscle and the muscle tendon area. These sites are associated with regions where the easily measured skinfolds have the least thickness. Therefore, the required amplitude control is set to a lower range to trigger the system to change the servo position. The squat down process shows the greatest change with the different sEMG signal and increased spring reactive force. However, minute changes occur with sEMG signal of squat up. On the other hand, the implantable surgical subdermal electrode implant may provide reliable data as it will no longer be interfered by the skin and the outer layer fat. There is room for further improvement in using the tension spring as a mechanical actuator such as, optimizing the ideal reactive force of the spring and increase the amount of either the tension spring or longer extension range of a spiral spring. The spring(s) can be charged up to the maximum after two or more squat down then releases the stored potential energy in one squat up. Another improvement is to use various types of advanced actuators to create hybrid exoskeleton consisting of mechanical and pneumatic components. Nevertheless, the proposed sEMG driven mechanical exoskeleton is proven to help users with squatting biomechanical movement, however, it will require further improvement.

Declarations

Author contribution

M. Cenit conceived the original idea. V. Gandhi supervised and revised the work critically. Both authors read and approved the final paper.

Funding statement

This research was internally funded by the Faculty of Science and Technology, Middlesex University London, UK.

Conflict of interest

The authors declare no conflict of interest.

Additional information

No additional information is available for this paper.

References

[1] H. S. Lo and S. Q. Xie, "Exoskeleton robots for upper-limb rehabilitation: State of the art and future prospects," *Med. Eng. Phys.*, vol. 34, (3), pp. 261-268, 2012.

[2] A. B. Zoss, H. Kazerooni and A. Chu, "Biomechanical design of the Berkeley lower extremity exoskeleton (BLEEX)," *IEEE/ASME Transactions on Mechatronics*, vol. 11, (2), pp. 128-138, 2006.

[3] M. Hanlon, "Raytheon XOS 2: Second-Generation Exoskeleton. Robotics Suit, United States of America," Gizmag: Website: *www.Gizmag.Com/Raytheon-significantly-Progresses-Exoskeletondesign/1647*9, 2015

[4] K. Tsuneyasu, A. Ohno, Y. Fukuda, K. Ogawa, T. Tsuji and Y. Kurita, "A soft exoskeleton suit to reduce muscle fatigue with pneumatic artificial muscles," in *Proceedings of the 9th Augmented Human International Conference*, 2018.

[5] A. T. Asbeck, R. J. Dyer, A. F. Larusson and C. J. Walsh, "Biologically-inspired soft exosuit," in *2013 IEEE 13th International Conference on Rehabilitation Robotics (ICORR)*, 2013.

[6] C. Walsh, A. T. Asbeck, I. G. Bujanda, Y. Ding, R. J. Dyer, A. F. Larusson, B. T. Quinlivan, K. Schmidt, D. Wagner and M. Wehner, "Soft Exosuit for Assistance with Human Motion," 2016.

[7] L. Brenner, "Exploring the psychosocial impact of Ekso Bionics Technology," *Arch. Phys. Med. Rehabil.*, vol. 97, (10), pp. e113, 2016.

[8] C. M. Wilkins, "An Experimental Study of the Human Interface with One Atmosphere Diving Suit by Appendages," 2016.

[9] A. S. Gorgey, "Robotic exoskeletons: The current pros and cons," *World Journal of Orthopedics*, vol. 9, (9), pp. 112, 2018.

[10] M. Mekki, A. D. Delgado, A. Fry, D. Putrino and V. Huang, "Robotic rehabilitation and spinal cord injury: a narrative review," *Neurotherapeutics*, vol. 15, (3), pp. 604-617, 2018.

[11] M. Fontana, R. Vertechy, S. Marcheschi, F. Salsedo and M. Bergamasco, "The body extender: A full-body exoskeleton for the transport and handling of heavy loads," *IEEE Robotics & Automation Magazine*, vol. 21, (4), pp. 34-44, 2014.
[12] W. Van Diik, T. Van de Wijdeven, M. M. Holscher, R. Barents, R. Könemann, F. Krause and C. L. Koerhuis, "Exobuddy-A non-anthropomorphic quasi-passive exoskeleton for load carrying assistance," in *2018 7th IEEE International Conference on Biomedical Robotics and Biomechatronics (Biorob)*, 2018.
[13] F. Lunardini, C. Casellato, A. d'Avella, T. D. Sanger and A. Pedrocchi, "Robustness and reliability of synergy-based myocontrol of a multiple degree of freedom robotic arm," *IEEE Transactions on Neural Systems and Rehabilitation Engineering*, vol. 24, (9), pp. 940-950, 2015.
[14] R. Bogue, "Exoskeletons and robotic prosthetics: a review of recent developments," *Industrial Robot: An International Journal*, 2009.
[15] N. Fotion and G. Elfstrom, "Military ethics: guidelines for peace and war," 1986.
[16] M. Vukobratovic *et al*, *Biped Locomotion: Dynamics, Stability, Control and Application*. Springer Science & Business Media, vol. 7, 2012.
[17] M. K. Reed, "LIFESUIT exoskeleton gives the gift of walking so they shall walk," in *IEEE Global Humanitarian Technology Conference (GHTC 2014)*, 2014.
[18] C. Kopp, "Exoskeletons for warriors of the future," *Defence Today*, vol. 9, (2), pp. 38-40, 2011.
[19] S. Hesse, H. Schmidt, C. Werner and A. Bardeleben, "Upper and lower extremity robotic devices for rehabilitation and for studying motor control," *Curr. Opin. Neurol.*, vol. 16, (6), pp. 705-710, 2003.
[20] K. Bharadwaj, T. G. Sugar, J. B. Koeneman and E. J. Koeneman, "Design of a robotic gait trainer using spring over muscle actuators for ankle stroke rehabilitation," 2005.
[21] C. T. Freeman, E. Rogers, A. Hughes, J. H. Burridge and K. L. Meadmore, "Iterative learning control in health care: Electrical stimulation and robotic-assisted upper-limb stroke rehabilitation," *IEEE Control Syst. Mag.*, vol. 32, (1), pp. 18-43, 2012.
[22] L. Lucas, M. DiCicco and Y. Matsuoka, "An EMG-controlled hand exoskeleton for natural pinching," *Journal of Robotics and Mechatronics*, vol. 16, pp. 482-488, 2004.
[23] M. Krawczyk, Z. Yang, V. Gandhi, M. Karamanoglu, F. M. Franca, L. Priscila, W. Xiaochen and T. Geng, "Wrist movement detector for ROS based control of the robotic hand," *Advances in Robotics and Automation*, vol. 7, (1), 2018.
[24] T. Nef, M. Guidali and R. Riener, "ARMin III–arm therapy exoskeleton with an ergonomic shoulder actuation," *Applied Bionics and Biomechanics*, vol. 6, (2), pp. 127-142, 2009.
[25] A. H. Stienen, E. E. Hekman, Van Der Helm, Frans CT and H. Van Der Kooij, "Self-aligning exoskeleton axes through decoupling of joint rotations and translations," *IEEE Transactions on Robotics*, vol. 25, (3), pp. 628-633, 2009.
[26] Y. Ren, H. Park and L. Zhang, "Developing a whole-arm exoskeleton robot with hand opening and closing mechanism for upper limb stroke rehabilitation," in *2009 IEEE International Conference on Rehabilitation Robotics*, 2009.
[27] C. Carignan, J. Tang and S. Roderick, "Development of an exoskeleton haptic interface for virtual task training," in *2009 IEEE/RSJ International Conference on Intelligent Robots and Systems*, 2009.
[28] A. Roy, H. I. Krebs, S. L. Patterson, T. N. Judkins, I. Khanna, L. W. Forrester, R. M. Macko and N. Hogan, "Measurement of human ankle stiffness using the anklebot," in *2007 IEEE 10th International Conference on Rehabilitation Robotics*, 2007.
[29] J. Lu, K. Haninger, W. Chen, S. Gowda, M. Tomizuka and J. M. Carmena, "Design of a passive upper limb exoskeleton for macaque monkeys," *Journal of Dynamic Systems, Measurement, and Control*, vol. 138, (11), 2016.
[30] S. Oh, E. Baek, S. Song, S. Mohammed, D. Jeon and K. Kong, "A generalized control framework of assistive controllers and its application to lower limb exoskeletons," *Robotics and Autonomous Systems*, vol. 73, pp. 68-77, 2015.
[31] J. Zhu and H. Zhou, "Realization of key technology for intelligent exoskeleton load system," in *Advances in Information Technology and Industry Applications*, 2012.
[32] D. M. Dao, P. D. Pham, T. X. Tran and T. T. T. Le, "Study on the transient response of lower limb rehabilitation actuator using the pneumatic cylinder," *Journal of Mechatronics, Electrical Power, and Vehicular Technology*, vol. 9, (2), pp. 65-72, 2018.
[33] V. Krasin, V. Gandhi and Z. Yang, "EMG based elbow joint powered exoskeleton for biceps brachii strength augmentation," in July 12-17, 2015.
[34] R. M. Singh, S. Chatterji and A. Kumar, "Trends and challenges in EMG based control scheme of exoskeleton robots-a review," *Int J Sci Eng Res*, vol. 3, (9), pp. 933-940, 2012.
[35] L. J. Myers, M. Lowery, M. O'malley, C. L. Vaughan, C. Heneghan, A. S. C. Gibson, Y. Harley and R. Sreenivasan, "Rectification and non-linear pre-processing of EMG signals for cortico-muscular analysis," *J. Neurosci. Methods*, vol. 124, (2), pp. 157-165, 2003.
[36] D. Copaci, D. Serrano, L. Moreno and D. Blanco, "A High-Level Control Algorithm Based on sEMG Signalling for an Elbow Joint SMA Exoskeleton," *Sensors*, vol. 18, (8), pp. 2522, 2018.
[37] G. Weddell, B. Feinstein and R. E. Pattle, "The electrical activity of voluntary muscle in man under normal and pathological conditions." *Brain: A Journal of Neurology*, 1944.
[38] D. Denny-Brown and J. B. Pennybacker, "Fibrillation and fasciculation in voluntary muscle," *Brain*, vol. 61, (3), pp. 311-312, 1938.
[39] O. Fukuda, T. Tsuji, M. Kaneko and A. Otsuka, "A human-assisting manipulator teleoperated by EMG signals and arm motions," *IEEE Trans. Rob. Autom.*, vol. 19, (2), pp. 210-222, 2003.
[40] P. Konrad, "A Practical Introduction to Kinesiological Electromyography," *The ABC of EMG*, vol. 1, 2005.
[41] C. J. De Luca, A. Adam, R. Wotiz, L. D. Gilmore and S. H. Nawab, "Decomposition of surface EMG signals," *J. Neurophysiol.*, vol. 96, (3), pp. 1646-1657, 2006.
[42] C. J. De Luca, S. Chang, S. H. Roy, J. C. Kline and S. H. Nawab, "Decomposition of surface EMG signals from cyclic dynamic contractions," *J. Neurophysiol.*, vol. 113, (6), pp. 1941-1951, 2015.
[43] F. Zaheer, S. H. Roy and C. J. De Luca, "Preferred sensor sites for surface EMG signal decomposition," *Physiol. Meas.*, vol. 33, (2), pp. 195, 2012.
[44] N. U. Ahamed, K. Sundaraj, R. B. Ahmad, M. Rahman and M. A. Islam, "Analysis of right arm biceps brachii muscle activity with varying the electrode placement on three male age groups during isometric contractions using a wireless EMG sensor," *Procedia Engineering*, vol. 41, pp. 61-67, 2012.
[45] C. Amma, T. Krings, J. Böer and T. Schultz, "Advancing muscle-computer interfaces with high-density electromyography," in *Proceedings of the 33rd Annual ACM Conference on Human Factors in Computing Systems*, 2015.
[46] R. H. Chowdhury, M. B. Reaz, Ali, Mohd Alauddin Bin Mohd, A. A. Bakar, K. Chellappan and T. G. Chang, "Surface electromyography signal processing and classification techniques," *Sensors*, vol. 13, (9), pp. 12431-12466, 2013.
[47] M. A. Hemingway, H. Biedermann and J. Inglis, "Electromyographic recordings of paraspinal muscles: variations related to subcutaneous tissue thickness," *Biofeedback Self.*, vol. 20, (1), pp. 39-49, 1995.
[48] M. R. Al-Mulla, F. Sepulveda and M. Colley, "A review of non-invasive techniques to detect and predict localised muscle fatigue," *Sensors*, vol. 11, (4), pp. 3545-3594, 2011.
[49] K. Woŷniak, D. Piątkowska, M. Lipski and K. Mehr, "Surface electromyography in orthodontics–a literature review," *Medical Science Monitor: International Medical Journal of Experimental and Clinical Research*, vol. 19, pp. 416, 2013.
[50] I. Campanini, A. Merlo, P. Degola, R. Merletti, G. Vezzosi and D. Farina, "Effect of electrode location on EMG signal envelope in leg muscles during gait," *Journal of Electromyography and Kinesiology*, vol. 17, (4), pp. 515-526, 2007.
[51] C. Hansen, F. Gosselin, K. B. Mansour, P. Devos and F. Marin, "Design-validation of a hand exoskeleton using musculoskeletal modeling," *Appl. Ergon.*, vol. 68, pp. 283-288, 2018.
[52] *Hardware Integration with NI LabVIEW*. Available online 5th March 2019.
[53] J. Guerreiro, R. Martins, H. Silva, A. Lourenço and A. L. Fred, "BITalino-A multimodal platform for physiological computing," in *Icinco (1)*, 2013.
[54] H. P. Da Silva, J. Guerreiro, A. Lourenço, A. L. Fred and R. Martins, "BITalino: A novel hardware framework for physiological computing." in *PhyCS*, 2014.
[55] *Electromyography (EMG) Sensor Data Sheet*. 2016.
[56] A. Savitzky and M. J. E. Golay, "Smoothing and differentiation of data by simplified least squares procedures," *Anal. Chem.*, vol. 36, (8), pp. 1627-1639, 1964.
[57] V. Gandhi and T. M. McGinnity, "Quantum neural network based surface EMG signal filtering for control of robotic hand," in *IEEE International Joint Conference on Neural Networks*, 2013.
[58] W. Lu, C. Huang, K. Hou, L. Shi, H. Zhao, Z. Li and J. Qiu, "Recurrent neural network approach to quantum signal: coherent state restoration for continuous-variable quantum key

distribution," *Quantum Information Processing*, vol. 17, (5), pp. 109, 2018.
[59] N. Miljković, N. Popović, O. Djordjević, L. Konstantinović and T. B. Šekara," ECG artifact cancellation in surface EMG signals by fractional order calculus application," *Comput. Methods Programs Biomed.*, vol. 140, pp. 259-264, 2017.
[60] A. Phinyomark, E. Campbell and E. Scheme, "Surface electromyography (EMG) signal processing, classification, and practical considerations," in *Biomedical Signal Processing,* available online 13 November 2019.
[61] C. Gilliam, A. Bingham, T. Blu and B. Jelfs, "Time-varying delay estimation using common local all-pass filters with application to surface electromyography," in *2018 IEEE International Conference on Acoustics, Speech and Signal Processing (ICASSP)*, 2018.
[62] A. Syed, Z. T. H. Agasbal, T. Melligeri and B. Gudur, "Flex sensor based robotic arm controller using micro controller," 2012.
[63] D. Copaci, E. Cano, L. Moreno and D. Blanco, "New design of a soft robotics wearable elbow exoskeleton based on shape memory alloy wire actuators," *Applied Bionics and Biomechanics*, vol. 2017, 2017.
[64] D. Copaci, D. Blanco, A. Martin-Clemente and L. Moreno, "Flexible shape memory alloy actuators for soft robotics: Modelling and control," International Journal of Advanced Robotic Systems, vol. 17, (1), pp. 1729881419886747, In Press: September 28, 2019.
[65] P. Salvini, "On ethical, legal and social issues of care robots," in *Intelligent Assistive Robots,* 2015.
[66] Z. Dolic, R. Castro and A. Moarcas, "Robots in Healthcare: A Solution or a Problem?," *Policy Department for Economic, Scientific and Quality of Life Policies*, Directorate General for Internal Policies, European Parliament, 2019.
[67] P. Maurice, L. Allienne, A. Malaisé and S. Ivaldi, "Ethical and social considerations for the introduction of human-centered technologies at work," in *2018 IEEE Workshop on Advanced Robotics and its Social Impacts (ARSO)*, 2018.
[68] E. Fosch-Villaronga, C. Lutz and A. Tamò-Larrieux, "Gathering expert opinions for social robots' ethical, legal, and societal concerns: Findings from four international workshops," *International Journal of Social Robotics*, pp. 1-18, 2019.
[69] H. Felzmann, A. Kapeller, A. Hughes and E. Fosch-Villaronga, "Ethical, legal and social issues in wearable robotics: Perspectives from the work of the COST action on wearable robots," in *International Conference on Inclusive Robotics for a Better Society*, 2018.
[70] D. Greenbaum, "Ethical, legal and social concerns relating to exoskeletons," *ACM SIGCAS Computers and Society*, vol. 45, (3), pp. 234-239, 2016.
[71] R. Calo, "Robotics and the Lessons of Cyberlaw," *Calif. Law Rev.*, pp. 513-563, 2015.
[72] J. Yang, K. Abdel-Malek and K. Nebel, "The Reach Envelope of a 9 Degree-of-Freedom Model of the Upper Extremity," *International Journal of Robotics and Automation*, vol. 20, pp. 240–259, 2005.
[73] K. Bharadwaj and T. G. Sugar, "Kinematics of a robotic gait trainer for stroke rehabilitation," in *Proceedings 2006 IEEE International Conference on Robotics and Automation (ICRA 2006),* 2006.

This page intentionally left blank

Journal of Mechatronics, Electrical Power, and Vehicular Technology 10 (2019) 73-84

Journal of Mechatronics, Electrical Power, and Vehicular Technology

e-ISSN: 2088-6985
p-ISSN: 2087-3379

www.mevjournal.com

Smart Grid communication applications: measurement equipment and networks architecture for data and energy flow

Tinton Dwi Atmaja [a, *], Dian Andriani [b], Rudi Darussalam [a]

[a] *Research Centre for Electrical Power and Mechatronics, Indonesian Institute of Sciences*
Komp LIPI Bandung, Gd 20, Lt 2, Bandung, West Java, 40135 Indonesia
[b] *Research Unit for Clean Technology, Indonesian Institute of Sciences*
Komp LIPI Bandung, Gd 50, Bandung, West Java, 40135 Indonesia

Received 13 September 2019; accepted 25 November 2019

Abstract

Smart Grid is an advanced two way data and energy flow capable of self-healing, adaptive, resilient, and sustainable with prediction capability of possible fault. This article aimed to disclose Smart Grid communication in a logical way to facilitate the understanding of each component function. The study was focused on the improvement, advantages, common used design, and possible feature of Smart Grid communication components. The results of the study divide the Smart Grid communication application into two main category i.e. measurement equipment and network architecture. Measurement equipment consists of Advance Metering Infrastructure, Phasor Measurement Unit, Intelligent Electronic Devices, and Wide Area Measurement System. The network architecture is divided based on three hierarchies; local area network for 1 to 100 m with 100 kbps data rate, neighbour area network for 100 m to 10 km with 100 Mbps data rate, and wide area network for up to 100 km with 1 Gbps data rate. More information is provided regarding the routing protocol for each network from various available protocols. The final section presents the energy and data flow architecture for Smart Grid implementation based on the measurement equipment and the network suitability. This article is expected to provide a comprehensive guide and comparison surrounding the technologies supporting Smart Grid implementation especially on communication applications.

Keywords: Smart Grid application; phasor measurement unit; communication network; communication protocol; energy and data flow.

I. Introduction

Recent researches on Smart Grid have been focused on addressing readability, adaptability, and fault prediction issues [1]. Further challenges on Smart Grid research should include demand handling, service quality, grid flexibility, power sustainability, end to end full control, market enabling, cost reduction, performance optimization, self-healing, and grid restoration [2].

The increase of distributed generation (DG) penetration brings an increased number of parameters including networks constrain, thermal overload, voltage limits, and hardwire connection complexities. Communication application is the key component to provide reliable Smart Grid operation by facilitating a real-time connection for measuring, monitoring, and controlling the grid assets [3][4][5]. Two way communications with high speed data rate in Smart Grid communication will give a dynamic infrastructure for power exchange [6][7][8].

Developing a smart communication system and subsystem requires monitoring and metering capability which covers the entire domain from the generation up to distribution [9]. Advanced metering infrastructure (AMI) can be assumed as the upgraded version of the conventional automated meter reading and automated meter management. AMI involves smart meter, communication network, and data management system [10].

Phasor measurement unit (PMU) can also be considered as the upgrade of the conventional system. Supervisory control and data acquisition (SCADA) played a significant role in the power system until the communication technology has evolved and the grid is demanding a fast unlimited data access at so many network node [11]. PMU deployment will lead to the

* Corresponding Author. Tel: +62-22-2503055
E-mail address: tinton_dwi@yahoo.com

doi: https://dx.doi.org/10.14203/j.mev.2019.v10.73-84

Accreditation Number: (RISTEKDIKTI) 1/E/KPT/2015 (Sinta 2).

implementation of some technologies which cannot be handled properly by the conventional power delivery system, such as high-voltage direct currents (HVDCs) and intelligent electronic devices (IEDs) [11]. PMU is also able to estimate the synchrophasor, frequency, and the rate of change of frequency (ROCOF or d f/dt) of the acquired voltage and/or current waveforms [12]. The common standards used by synchrophasor technology were IEEE 1344, IRIG-B, IEEE C37.118, and IEC61850 [13][14]. PMU has been dedicated as the most effective measurement device for monitoring, control, and protection of the evolved power system in correspondence to its capability on addressing technological update and covering the geographical extension of the modern power system [15].

Communication network should be the next focus after the measurement system. Smart Grid network should be classified in the typical payload, data sampling, latency, and reliability [16]. This study has divided the communication network basically by its data rate and coverage area [3][17]. Routing development of each network classification had been explained to describe the interaction of each component in a proper way with respect to the various Smart Grid applications. The connection protocols have been categorized on the existing approach for local area network, neighbor area network, and wide area network. Furthermore, open architecture with plug and play features should provide a better environment for smart sensor and control devices.

This article aimed to disclose Smart Grid communication components to facilitate the understanding of the further function of each component. The result of the study provides a detail explanation of the technologies' features, advantages, connectivity, and primary role in supporting Smart Grid implementation, especially on Smart Grid communication.

II. Materials and Methods

The article focused on the Smart Grid communication components by presenting their improvement, advantages, commonly used design, and possible feature. The Smart Grid communication application is divided into its measurement equipment and network architecture. The measurement equipment consists of Advance Metering Infrastructure, Phasor Measurement Unit, and Intelligent Electronic Devices. Meanwhile, the network architecture is divided based on their hierarchy; namely local area network, neighbor area network, and wide area network. Further information was provided regarding the routing protocol for each network. The final section was presenting the energy and data flow of Smart Grid implementation based on the communication application.

III. Smart Grid Communication Equipment

A. Advanced metering infrastructure

The advanced metering infrastructure consists of several components which provide two way intelligent links from the consumers to the system management [18][19][20]. The infrastructures commonly consist of three segments; namely the consumer data collection devices, the system management, and a communication network as the connector. Figure 1 shows the schematic representation of AMI [2][21]. The implementation of AMI is the first step to upgrade the conventional grid into the modern Smart Grid. It requires telecommunication system, wiring component, various standard, and numerous best practices. All the digitalized asset on the consumers will provide information for the system management to make an intelligent decision on the grid real-time condition. Digitalize asset all over the grid will enhance the service that lead to significant benefit for the customer and the management. Various supporting technology such as smart metering, HAN, utility application, etc. will enhance the two-way interactions among utilities, consumer, and the network.

Basically, AMI acts as the main backbone for the information flow between the consumer and the utility grid. The infrastructure will monitor and control the power generation system, the storage

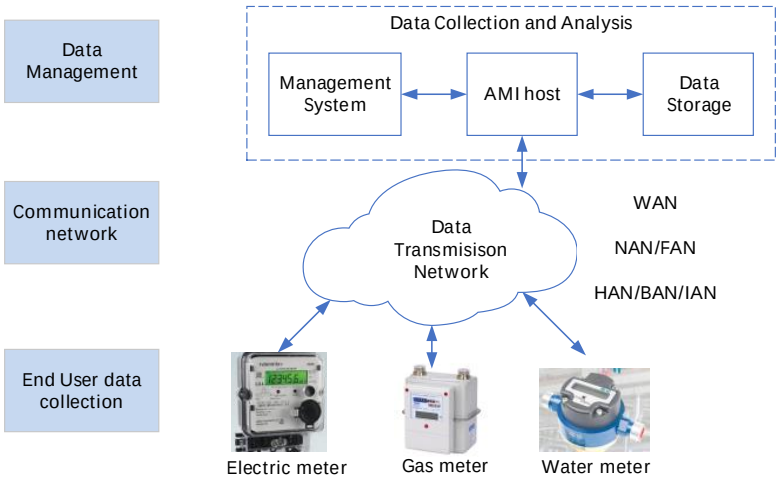

Figure 1. AMI implementation schematic

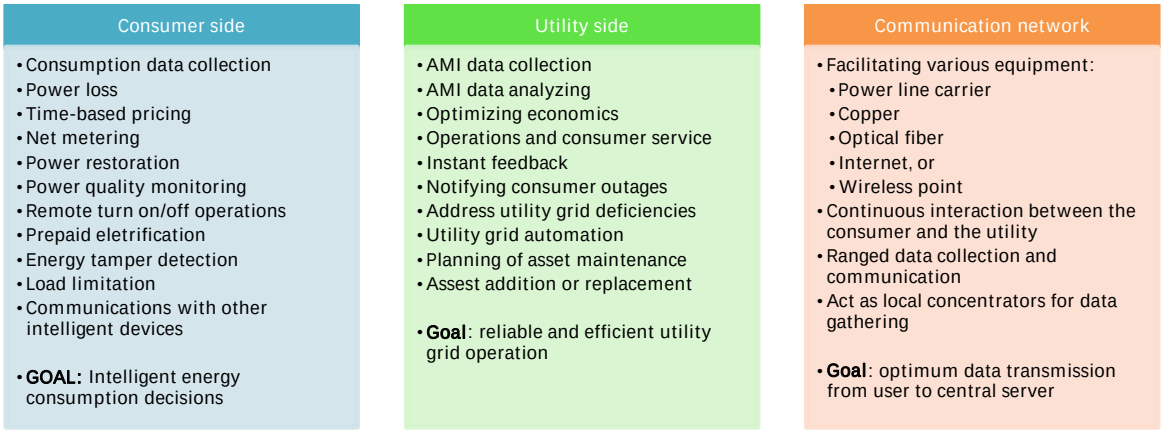

Figure 2. AMI features in each Smart Grid communication domain

units, data reception equipment, and perform a possible big data analysis. At the end user, smart metering devices can be combined with the power quality monitoring system to fasten the smart demand response for any power quality troubleshoots. Within the correct range, remote connection and disconnection is considered as a possible implementation to minimize on-field personnel and reduce the operational cost. This infrastructure was also implemented not only for data storage but also as a back up strategy for possible attack or anomaly. It can be equipped with forecasting neural network to detect possible failure followed with self-healing capability performed from data management center. AMI collected data provides granularity and timeliness information to improve asset management and operations. Figure 2 shows AMI feature presented on each side of the domain [21].

1) AMI subsystem

AMI assist the consumer portal layer to connect entirely with metering layer and also with the communication layer. All smart metering devices in the HAN and LAN will be connected and controlled in a very intelligent step toward modern power grid. AMI technology and interference is shown in Figure 3 [21]. The infrastructure covers the communication network, smart metering devices, HAN-LAN, gateways, local data concentrators, data center, and meter data management system. The final function of AMI is to add the collected data into big data platforms.

2) AMI communication technologies

Several communication technologies is available in the today's market such as long term evolution (LTE), LTE-Advanced, power line carrier (PLC), general packet radio service (GPRS), 802.22 wireless networking protocol, and Zigbee. Table 1 shows a comparison of some available communication technologies in correspondence with AMI requirement [2]. Although the comparison shows many advantages of LTE application, the utility companies still consider the cost and the spectrum as the main reason of not using the LTE. More modifications are encouraged to be implemented in the communication technology such as open standard on utility communication which can be lead to a better connection between communication systems.

B. Phasor measurement units

PMU is employing a general time source to measure the electrical wave on the utility grid [22][23][24]. PMU basic component consists of the

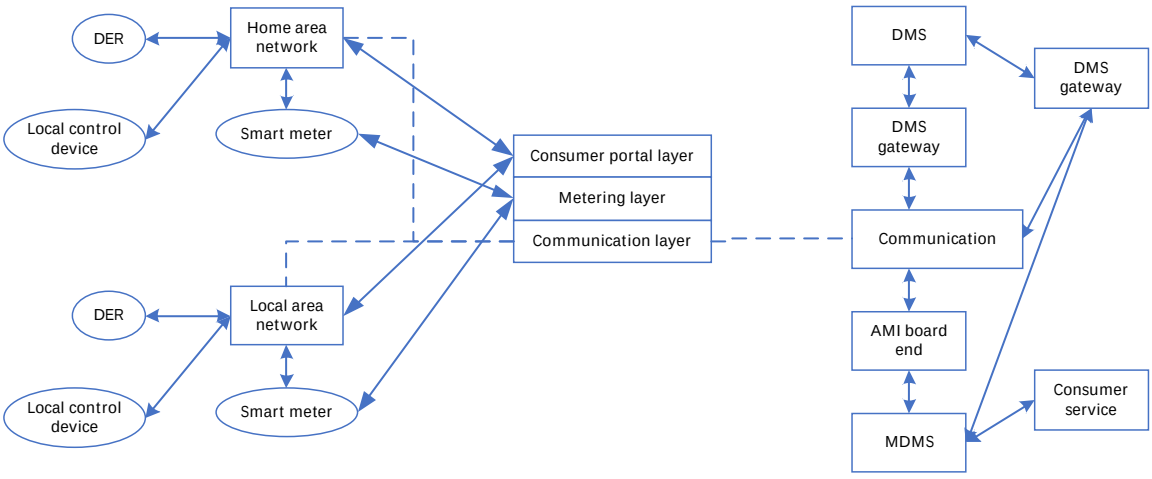

Figure 3. AMI subsystem technology and interferences

Table 1.
Comparison of the available communication technologies for AMI

Parameter	LTE-A	3G (HSPA+)	PLC	802.22
Latency (ms)	<5	<50	<10	<20
Date rate (Mbps) download/upload	1000/500	28/11	3/3	18/18
Range (km)	100	10	5	100
Main disadvantage	-	Limited number of supported connection	Alternate technology (bypass) needed at transformer	No QoS due to faulty spectrum sensing

current phasor, bus voltage phasor, location information, converter, and phasor microprocessor as shown in Figure 4 [11][21]. The current and the voltage signal are converted into digitalized AC waveforms. In the other segment, GPS receiver sends the coordinate to the phasor locked oscillator and create a high-speed synchronized sampling with 1 ms precision. The current-voltage and the phasor locked the oscillator output to combine with the 16-bits A/D converter. PMU is able to quantify 50 Hz AC waveforms (currents and voltages) at a common rate of 48 samples per cycle [25]. Time synchronization permits synchronized immediate measurements over many types of remote measurement points scattered within the grid. The result of the measurement is known as synchrophasor. With synchrophasor as the metered value, PMUs plays one of the most important role on measuring energy and data for the future power delivery systems.

The most advantageous aspect of the PMU is the GPS reference inclusion inside the unit. The time source is calibrated and synchronized into resultant time-stamped phasor that can be transmitted from various important cross points through the entire utility grid. With up to 120 samples per second, the user can visualize the whole grid in the precise angular among various locations. PMU mostly used to monitor and control the voltage around the wide area grid. PMU also prevent any possible blackout, mitigate potential congestion problem, and provide dynamic visibility into the source-consumer power system. With the increase of DG integration, PMU installation provides a real-time measurement system that covers the whole delivery system including generation, transmission, and distribution. Additional utility monitoring systems consist of dynamic line rating technology, electronic instrument transformers, batteries, temperature sensors, conductor sensors, insulation contamination leakage, backscatter radios technology, and monitoring system for CB and current frequency.

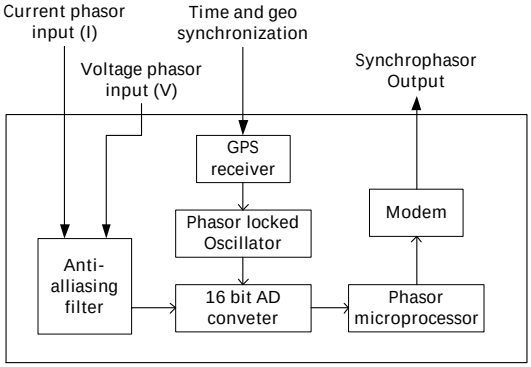

Figure 4. Basic components of a Phasor Measurement Unit

C. Intelligent electronic devices

Monitoring process on the power system line basically performed by SCADA system based on collected data from substations. As the grid evolved, the SCADA system limitation to support AMI and PMU has been covered by the inclusion of IED. IED is a microprocessor with the ability to exchange data and process a control signal between devices in the grid. It is considered as the prime supporter of any remote power management, including PMU unit, on how they provide continuous real time synchronization [26][27][28]. IED configuration shown in Figure 5 was aimed to improve monitoring, controlling, data acquisition, and data recording [21][29][30]. IED is mostly connected with Global Positioning System (GPS) as further support to the PMU.

IEDs measures control signal, phase current/voltage, internal relay, and oscilloscopic data with three common different types: circuit breaker monitor (CBM), digital fault recorder (DFR) and digital protective relay (DPR). CBM is responsible for the monitoring of the circuit condition and acts as a determinant for opening and closing process. DFR is the device to capture and store a short duration events such as power spike, harmonic disorder, frequency anomaly, RMS, and power factor disturbance. DPR was specifically designed for transmission line monitoring on possible fault or trip. DPR will respond to the surge on current, voltage, impedance, or frequency and inform it away to the substation. Table 2 shows the available synchrophasor IED to support PMU on Smart Grid communication system [11].

D. Wide area measurement systems

Wide Area Measurement Systems (WAMS) is the final component to integrate AMI and PMU [31][32][33]. Most likely in similar concept with the present SCADA system, measurements of the grid

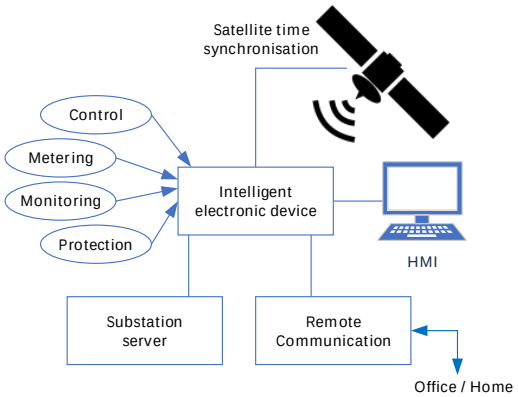

Figure 5. Functional architecture of IED

Table 2.
Commercial syncrophasor-based IEDs

Company	IED	Application
ABB	PVI-PMU (power management unit)	Photovoltaic system monitoring, active and reactive power control
	RES670 2.0 (relion 670 & 650 series)	Power system protection and control
	PSGuard	SCADA/EMS integration and communication, power system monitoring
General Electric, grid solutions	MiCOM P40 Agile	Feeder management
EATON	GearGard	Conditional remote monitoring and early failure warning solutions Real-time monitoring, statistical analysis, and condition-based maintenance decisions
Mehta Tec	Data fault recorder (DFR)/disturbance monitoring equipment (DME)/PMU	Online disturbance monitoring and data archiving
Macrodyne	1690	Phasor measurement systems for real-time data acquisition and control
	1692	Integrated recording units for transient fault and long-term disturbance events
	1698, 1698E	Satellite timing units for absolute time tagging and synchronous data sampling
Schweitzer Engineering Laboratories (SEL)	SEL-2411	Programmable automation controller
	SEL-T400L	Line protection with simple configuration, accurate fault locating, and high-resolution oscillography
	SEL-411L	Line current di erential, distance, and directional overcurrent protection, comprehensive monitoring, advanced automation and communication, high-accuracy fault locating
S&C electric company	6800 series	Control and manage distribution switches automatically
Power Standards Lab (PSL)	PQube (PMU)	Cyber-attacks detection, power consumption analysis, remotely understand commercial AC power grids, provide input for solar PV and storage control system development, simulation and data integration for solar planning tools, and short-term planning and operations
Siemens	SIGUARD PDP (phasor data processor)	Complete portfolio for network monitoring, power quality recording, fault recording, phasor measurement, and system software applications

system are conceded at a higher rate (up to 5-60 samples per second). Therefore, the system requires a wide area measurement which can perform continuous and simultaneous real-time information rendering [34][35]. More or less, WAMS was aiming to improve the grid performance by stability assessment, fault detection, remedial control actions and supporting more accurate state estimation [36][37].

Figure 6 shows the common WAMS architecture which deploys PMUs, PDCs, super PDCs (regional PDCs), and communication protocol [11]. PMU send

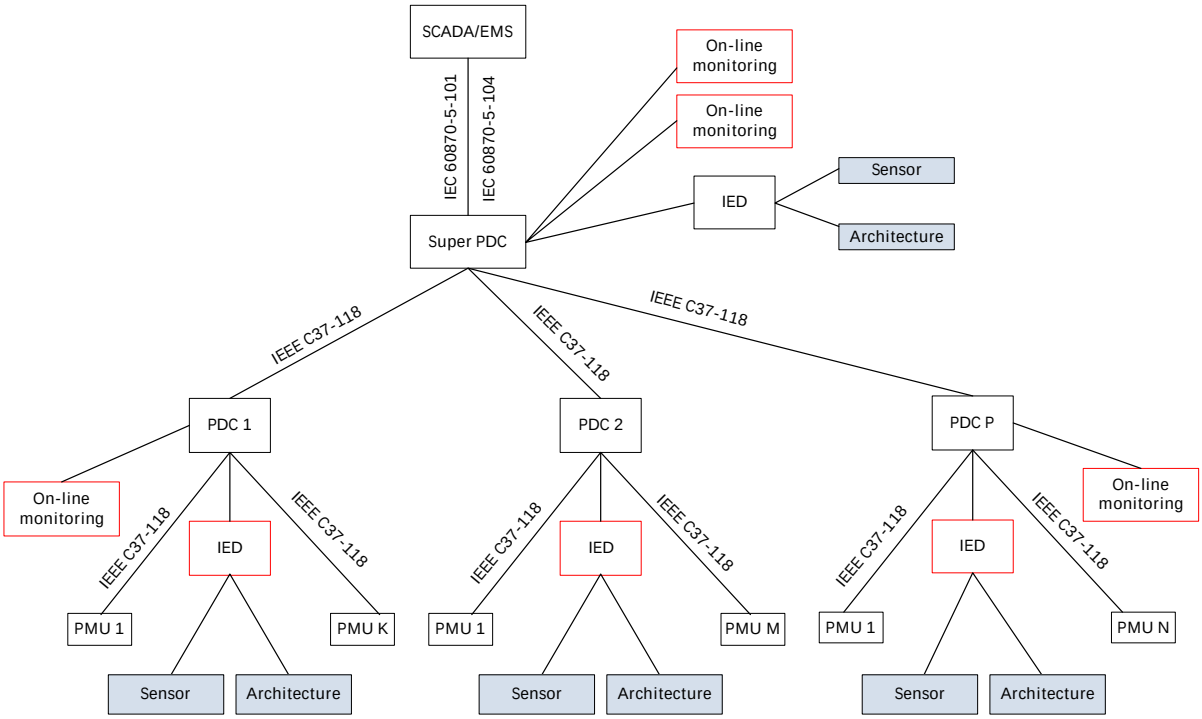

Figure 6. WAMS Architecture

voltage and current in phasor form to the local phase data concentrators (PDC) using IEEE C37.118.2 or IEC 61850-90-5 standards. PDC normally located in the primary substation where the collected data was analyzed [38]. PDCs are required to make a decision with a very low latency of 10– 100 ms. IED has shown to take an important part in this WAMS by integrating devices such as reclosers, switches, and capacitor banks so that PDCs or super PDCs will be able to protect and control the grid at the distribution or transmission level immediately [39]. Future concept can use IEC61850-90-5 to replace IEEE C37.118.2 protocol [40].

IV. Smart Grid Communication Networks

The designated communication network in Smart Grid concept is classified based on the coverage area and the rate speed (Figure 7) [17]. There are three common classes; namely local network, neighbour network, and wide network. The local network can be found in the form of home area network (HAN), building area network (BAN), or industrial area network (IAN). These networks usually cover single customer with several local applications, such as home automation and building automation, to perform electrical data collection and measurement within the small radius area between 1 to 100 m. This application can be implemented without high frequency transmission system, performed at low cost and low power consumption, and also can be used conveniently. Data rate requirement in this area was up to 100 kbps which sufficiently supported by Wifi, Zwave, ZigBee, PLC, Bluetooth, or Ethernet [41].

Neighbour network is usually called neighbour area network (NAN) or field area network (FAN). At this scale, the applications have a more complex requirement such as smart metering, demand response, and distribution automation. Data transmissions are required to cover a larger number of the customer which led to the deployment of data concentrator and small substation. The coverage of this network can be up to 10 km with a higher data rate between 100 kbps to 10 Mbps. NAN/FAN applications can be implemented over ZigBee mesh networks, WiFi mesh networks, PLC, as well as long distance wired and wireless technologies, such as WiMAX, Cellular, digital subscriber line (DSL) and Coaxial Cable [42].

Wide network commonly called wide area network (WAN) which apply the wide-area controlling, monitoring and protection. WAN requires a large number of higher frequency data points to allow stability control of a power system which can cover up to 100 km. Required data rate should be 10 Mbps to 1 Gbps which needs a utility control center due to its high capacity and low latency. Cellular, WiMAX, and satellite communication were highly recommended to provide redundant communications at critical transmission/distribution substation sites especially when the coverage of the network is a wide remote area. A comparison of various communication technologies that can support Smart Grid applications in terms of data rate and coverage distance is presented in Table 3 [17].

A. Local area network

Local area network usually limited to an individual or single user called home area network (HAN), building area network (BAN), or industrial area network (IAN) [43]. There always permission is given for the system to remotely control the digitalized appliance within the house or building. It also facilitates the communication between assets such as mobile phone, desktop computer, HVAC, electric vehicle, etc. via wireless or by wire connection [44]. HAN/BAN/IAN is the front line communication system that collects real-time data continuously and the primary media to facilitate the remote control provided by the data management system. It detects the peak time of the load demand, connect one smart appliance to another smart metering. This network also manages to conduct continuous monitoring system that enables to do early detection of possible failure or blackout. It also controls the automation of high consuming energy system so that the user could conduct self-energy usage optimization which leads to reduce electricity cost. This network also includes web-based monitoring system, AMI, and PMU.

B. Neighbour area network

Neighbour network commonly found in the form of Neighbour Area Network (NAN) or Field Area Network (FAN). NAN/FAN is a wireless or wired network consist of groups of individuals, system devices, buildings, or open area with digitalized assets; which cover a larger area than HAN/NAN/IAN [45]. Most of the architecture usually focused on optimization of interoperability and integration between different domains within the Smart Grid. NAN/FAN is able to find power generation domain within its coverage, it is commonly equipped with market service and plant control center with potential transmission-distribution line domain.

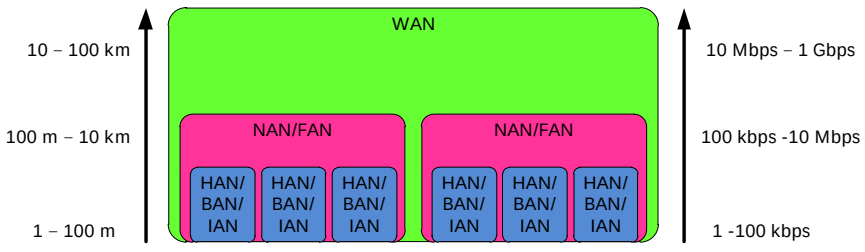

Figure 7. Smart Grid communication hierarchy with data rate and coverage range requirement

NAN/FAN is also considered as a substation connecting the local network with the wide network. It means that this network has quite large data storage to facilitate a large data collection system form the HAN/BAN/IAN. The neighbour network will connect many energy management systems, digitalized appliances, metering devices, more electric storages, and even consumer PHEVs. The connection to the consumer will primarily through the internet with the possible use of the large intranet. Depend on the area coverage, this network can be subdivided into transmission-distribution system using ISO/RTO technology. Therefore, this network is able to handle the utility of third party including billing system and larger early warning system.

C. Wide area networks (WAN)

WAN is the largest geographical coverage network compared to local or neighbour network, it usually interconnects multiple BAN/HAN/IAN or NAN/FAN [46]. WAN is commonly in the shape of point-to-point technology (PP), circuit-switched technology (CS), or packet-switched technology (PS). PP is a costly technology and usually in the form of the leased or dedicated line which is attached to the utility backbone and provided a secure line between the local domain. It usually on the state of normally-ON to ensure continuous line between network nodes on specified distance. CS technology needs a call-setup to make an action on the grid. Once the call has made, the data transfer will trigger the session and followed by engaging or disengaging a single or multiple domains. On-demand switched is usually a low speed response compared with the other technologies. The last technology is packet-switched which is the cheapest of all technologies due to it share a common infrastructure. Despite having the best performance in communication quality, however, it will cause inconsistent bandwidth.

V. Smart Grid Communication Routing Protocol

The goal of routing protocol is the reliability, security and QoS of the network performance [3][47][48]. The protocol has been classified into three classes i.e. routing for local network (HAN/BAN/IAN), routing for neighbour network (NAN/FAN), and routing for wide network (WAN). The breakdown of the routing protocol for each class can be found in Figure 8 [3].

A. Routing protocols for local network

Summary of routing protocols for the local network (HAN/BAN/IAN) can be found in Table 4 based on the adaptation layer and network layer [3]. The use of a specific protocol will affect the operational cost, performance of the network and the local network architecture.

B. Routing protocols for neighbour network

Smart Grid communications consist of several NAN/FAN with mostly hundreds of AMI. NAN routing protocol will ensure the collected data from the

Table 3.
Comparison of communication technologies for the Smart Grid

Technologies	Standard/ protocol	Theoretical data rate	Coverage range	Network		
				HAN/BAN/IAN	NAN/FAN	WAN
Wired communication technologies						
Coaxial Cable	DOCSIS	172 Mbps	Up to 28 km			
Ethernet	802.3x	10 Mbps - 10 Gbps	Up to 100 m	x	x	
PLC	Homeplug	14–200 Mbps	Up to 200 m	x		
	Narrowband	10–500 kbps	Up to 3 km		x	
DSL	ADSL	1–8 Mbps	Up to 5 km			
	HDSL	2 Mbps	Up to 3.6 km		x	
	VDSL	15–100 Mbps	Up to 1.5 km			
Fiber optic	PON	155 Mbps–2.5 Gbps	Up to 60 km			x
	WDM	40 Gbps	Up to 100 km			
	SONET/SDH	10 Gbps	Up to 100 km		x	
Wireless communication technologies						
Z-Wave	Z-Wave	40 kbps	Up to 30 m	x		
Bluetooth	802.15.1	721 kbps	Up to 100 m	x		
ZigBee	ZigBee	250 kbps	Up to 100 m	x	x	
	ZigBee Pro	250 kbps	Up to 1600 m			
WIFI	802.11x	2–600 Mbps	Up to 100 m			
WiMAX	802.16	75 Mbps	Up to 50 km			
Wireless Mesh	Various (e.g., RF mesh, 802.11, 802.15, 802.16)	Depending on selected protocols	Depending on deployment	x	x	
Cellular	2G	14.4 kbps	up to 50 Km		x	x
	2.5G	144 kbps				
	3G	2 Mbps				
	3.5G	14 Mbps				
	4G	100 Mbps				
Satellite	Satellite Internet	1 Mbps	100 - 6000 Km			x

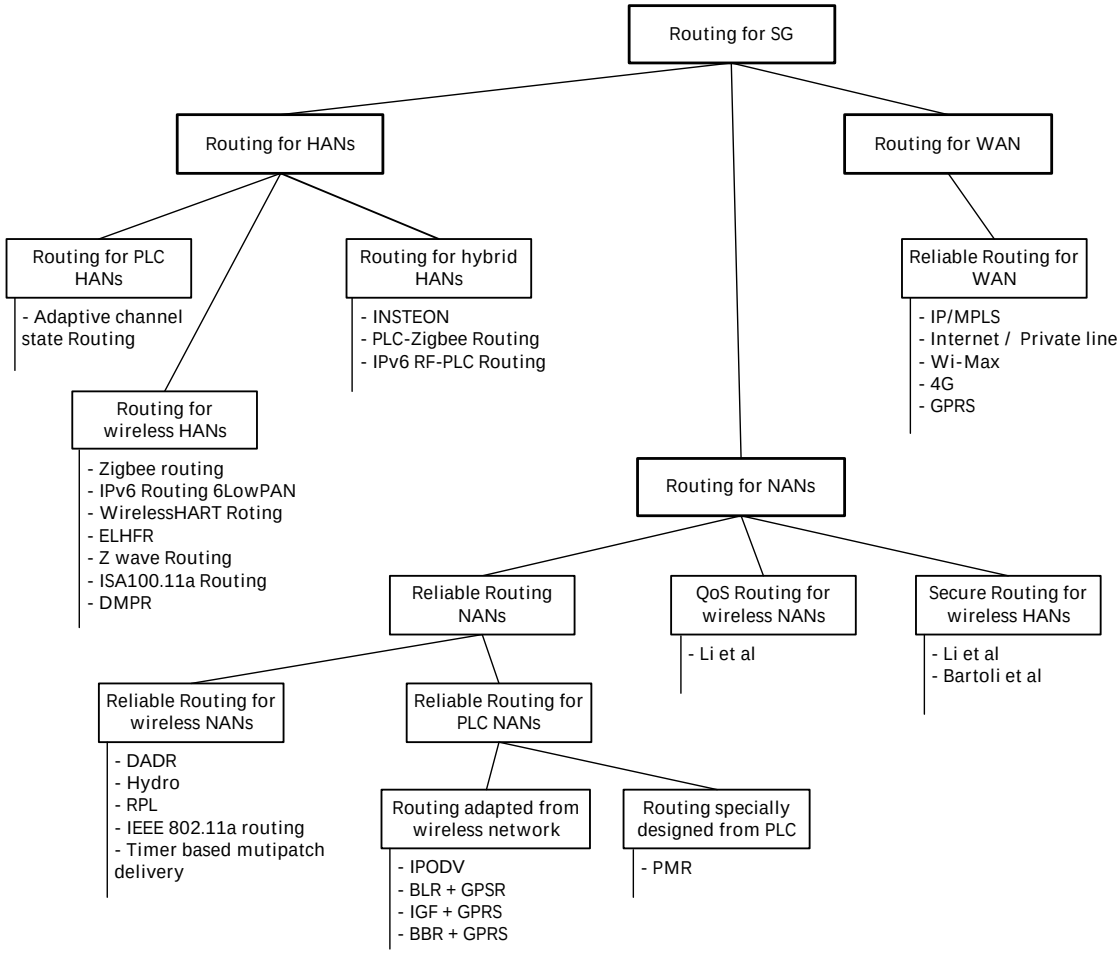

Figure 8. Routing protocol classification for Smart Grid communications

Table 4.
Summary of routing protocols for local network

Routing protocol	Adaptation layer	Data link	Network layer
ZigBee	n/a	CSMA/CA	Tree routing, on-demand mesh routing, source routing
Mesh under	Layer 2 mesh routing	CSMA/CA	n/a
Route over	n/a	CSMA/CA	RPL routing
Wireless-HART	n/a	TDMA	Graph and source routing
ISA100.11a	n/a	TDMA, CSMA/CA, graph routing and source routing	Backbone routing
Z-Wave	n/a	CSMA/CA	Source routing
INSTEON	n/a	TDMA	Simulcast

Table 5.
Routing protocol classification for NANs

Routing protocol	Point-to-point routing	One-to many routing	Many-to-one routing	Multipath	Scalable	Load balancing	Application
DADR		√	√	√	√	√	Wireless AMI
Hydro	√	√	√	√	√	√	Wireless AMI
Timer based multipath diversity routing		√	√	√			Wireless AMI, status management and monitoring
PMR		√		√			AMI-PLC

access point tier can report safely to the backhaul distribution tier. Routing challenge will vary based on the underlying communication. Therefore, there are three common protocols: Reliable Routing [49][50], Secure Routing [51][52][53], and QoS Routing protocols [54]. The comparison of each routing protocols can be seen in Table 5 [3].

C. Routing Protocols for Wide Network

Wide Network is different from local and neighbour network since it most likely consists of a core network or a backhaul network. Generally, WAN routing protocol is handled by the public network such as the internet and private lines. Fiber optic is the best offer to the required data rate and should be

followed by IP/multi-protocol label switching (MPLS) and Metro Ethernet. Another option is to apply Wi-MAC, 4G, or GPRS even though they depend on the quality of the physical layer, channels, radio, handoff, etc. The newest study showed that the deployment of multi-hop wireless WAN can be a proprietary network within a single instalment which have a complete substation, gateway, and data metering devices.

VI. Smart Grid Data and Energy Flow Architecture

The energy flow has been completely covered by the conventional utility grid. Nevertheless, the challenge on the Smart Grid implementation is covering the data flow within the entire grid. The first challenge is the digitalization of all the grid asset in order to be able to reach out the communication protocols. Combination of energy flow and data flow will then increase the controllability, flexibility, and more adaptive response. The data and energy flow should be covering all the domain including power generation, transmission-distribution, and customers' peripheral. Figure 9 shows the architecture of data and energy flow in Smart Grid with a wide multi-port system network node [21][55].

The architecture presented in Figure 9 covers the measurement equipment AMI and PMU, and consisting of three layers communication network. Local network mostly exists in the customer side which facilitates the control and monitoring of all digitalized appliances. Local network also connects the AMI to the energy management system (EMS), energy storage system (ESS), and possible use of plug-in hybrid electric vehicle (PHEV). The connection with PHEV would introduce the concept of vehicle to grid (V2G) where the charge and discharge action will depend completely on the time and location. Neighbour network would be consisting of at least two local networks, therefore, consisting of several AMI and possible local DG. AMIs in the customer side had connected to the substation's PMU in the distribution line, while each substation's PMU will connect each other in the transmission line. Moreover, the transmission line is the backbone network which unites the power generation side to the customer side. Power generation could be a large scale power plant in a remote location or could be small size DG within local neigbourhood. Each power plant would have its own substation, or multiple power plants covered by one substation. Substations' PMU at the power generation side will be connected to the backbone and coordinate with the PMUs at the consumer side.

These measurement devices and multi layers network contains different component with various characteristics and action. For example, DGs and load can connect or disconnect at any time without proper pattern. Therefore Smart Grid data management center must play the role of multi-agent to ensure that every node can be controlled in a specific manner. Every information provided by the AMIs and PMUs will be processed at the center and provide a control output to each of grid's digitalize asset. Farsighted the large number of AMIs and PMUs, it is

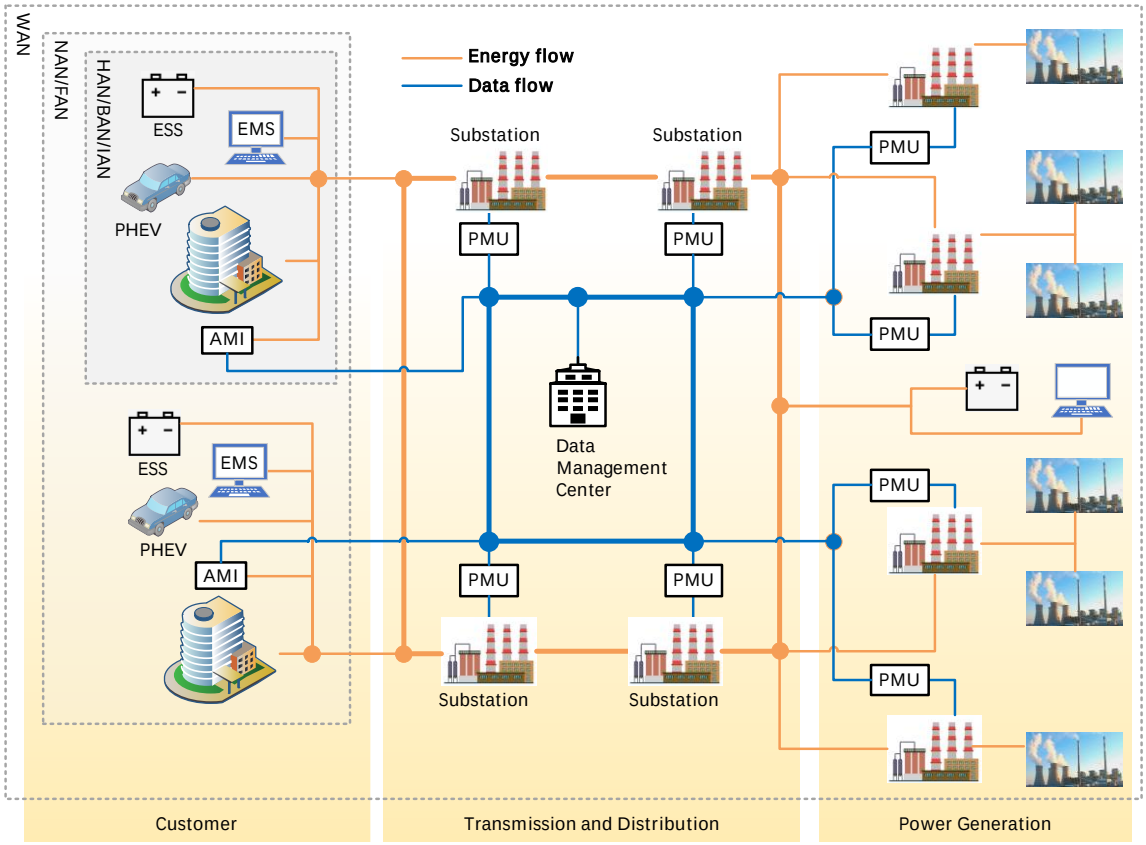

Figure 9. Data and energy flow architecture in Smart Grid

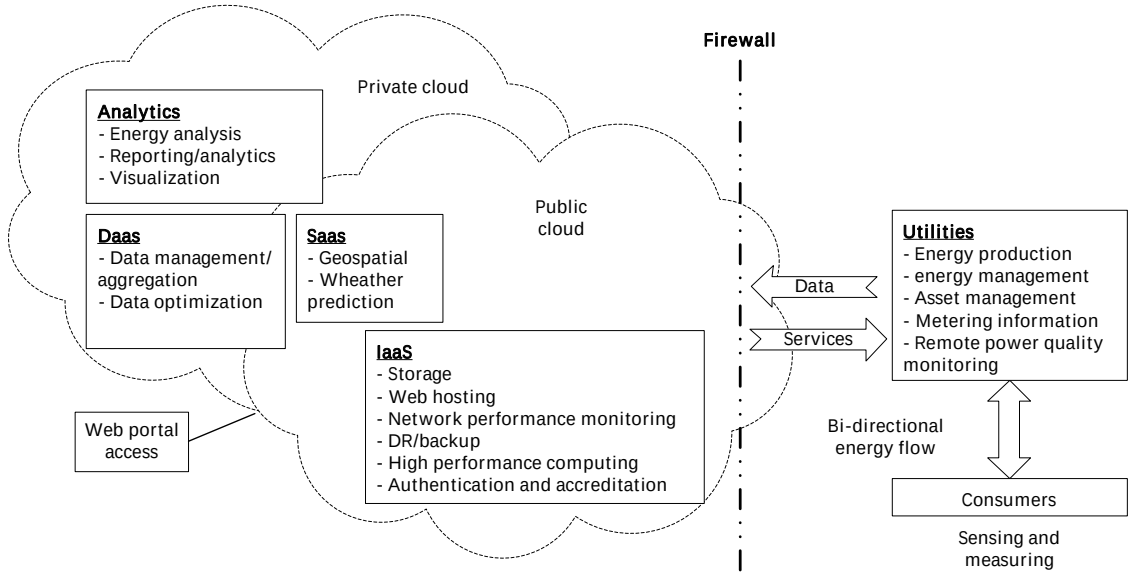

Figure 10. Smart Grid cloud architecture

recommended to adapt the cloud computing architecture to cover all the big data at the grid.

Cloud computing has served as an excellent method to handle a large volume of data in the coverage of all AMI and PMU [56][57]. Cloud computing can provide flexibility and scalable characteristic to cope with the data storage and vast transferable real-time data [58][59][60]. With the expanding area of the Smart Grid, cloud computing can easily adapt to present remote data storage, automatic updates, less utility cost, energy saving, and reduce human labor demand [61][62][63]. Cloud computing architecture for Smart Grid designed by Dileep G. [21] can be found in Figure 10.

This architecture can be adapted to create a cloud database which stores public and private information. Each information class can be managed as three basic cloud services i.e. Data as a service (DaaS), software as a service (SaaS), and infrastructure as a service (IaaS). The analytic can perform energy analysis within the grid, reporting and monitoring the grid's asset, and the most important is the visualization of the grid.

VII. Conclusion

This article presents an overview of the one key component of Smart Grid, the communication application including the related technologies. The study was done by conducting a review of its components, technologies, features, challenge, and advantages. It is known that efficiency, reliability, and security of interconnected devices are critical to enabling Smart Grid global implementation. The study explained various Smart Grid measurement technologies such as AMI, PMU, IED, and WAMS followed by the description of Smart Grid network classification divided in three classes i.e. HAN/BAN/IAN, NAN/FAN, and WAN. The AMI and PMU were covering the measurement system and data collection while the IED and WAMS was covering the secure and reliable data transfer from the consumer to the data management center. HAN/BAN/IAN is a local network which facilitates Smart Grid from the end user platform at low 100 kbps data rate for the least 1 to 100 m, while NAN/FAN is doing the similar task at the larger coverage area which is up to 10 km for 10 Mbps data rate. For the last, WAN is the one covering the whole local and neighbour network by approximately 100 km at 1 Gbps data rate. Related technologies are including routing protocol for each network that considers the underlying communications medium, reliability, security, and QoS. The primary function is to facilitate the measurement and monitoring process and then collect the data for the grid analysis at the data management center. This communication network will increase the flexibility to the attachment of DGs which will increase the usage of renewable energy. Smart Grid can be considered as a future technology to help environmental conservation and energy sustainability. It is expected that this article can offer a further understanding of communication network requirements for a complete Smart Grid implementation.

Acknowledgement

The author would like to thank all researchers at Research Centre for Electrical Power and Mechatronics and Research Unit for Clean Technology, Indonesian Institute of Science for the completion of this study.

Declarations

Author contribution

All authors contributed equally as the main contributor of this paper. All authors read and approved the final paper.

Funding statement

This research did not receive any specific grant from funding agencies in the public, commercial, or not-for-profit sectors.

Conflict of interest

The authors declare no conflict of interest.

Additional information

No additional information is available for this paper.

References

[1] J. A. Momoh, "Smart grid design for efficient and flexible power networks operation and control," in *2009 IEEE/PES Power Systems Conference and Exposition*, 2009, pp. 1–8.

[2] R. Rashed Mohassel, A. Fung, F. Mohammadi, and K. Raahemifar, "A survey on Advanced Metering Infrastructure," *Int. J. Electr. Power Energy Syst.*, vol. 63, pp. 473–484, Dec. 2014.

[3] N. Saputro, K. Akkaya, and S. Uludag, "A survey of routing protocols for smart grid communications," *Comput. Networks*, vol. 56, no. 11, pp. 2742–2771, Jul. 2012.

[4] M. Erol-Kantarci and H. T. Mouftah, "Energy-Efficient Information and Communication Infrastructures in the Smart Grid: A Survey on Interactions and Open Issues," *IEEE Commun. Surv. Tutorials*, vol. 17, no. 1, pp. 179–197, 2015.

[5] E. Ancillotti, R. Bruno, and M. Conti, "The role of communication systems in smart grids: Architectures, technical solutions and research challenges," *Comput. Commun.*, vol. 36, no. 17–18, pp. 1665–1697, Nov. 2013.

[6] J. Naus, G. Spaargaren, B. J. M. van Vliet, and H. M. van der Horst, "Smart grids, information flows and emerging domestic energy practices," *Energy Policy*, vol. 68, pp. 436–446, May 2014.

[7] J. Gao, Y. Xiao, J. Liu, W. Liang, and C. L. P. Chen, "A survey of communication/networking in Smart Grids," *Futur. Gener. Comput. Syst.*, vol. 28, no. 2, pp. 391–404, Feb. 2012.

[8] N. Kilic and V. C. Gungor, "Analysis of low power wireless links in smart grid environments," *Comput. Networks*, vol. 57, no. 5, pp. 1192–1203, Apr. 2013.

[9] S. Bruno, S. Lamonaca, M. La Scala, G. Rotondo, and U. Stecchi, "Improving Energy Efficiency in a Power Park by the Integration of a Hydrogen Steam Reformer," in *2009 Asia-Pacific Power and Energy Engineering Conference*, 2009, pp. 1–8.

[10] S. Paul, M. S. Rabbani, R. K. Kundu, and S. M. R. Zaman, "A review of smart technology (Smart Grid) and its features," in *2014 1st International Conference on Non Conventional Energy (ICONCE 2014)*, 2014, pp. 200–203.

[11] M. Hojabri, U. Dersch, A. Papaemmanouil, and P. Bosshart, "A Comprehensive Survey on Phasor Measurement Unit Applications in Distribution Systems," *Energies*, vol. 12, no. 23, p. 4552, Nov. 2019.

[12] I. Power and E. Society, *C37.118.1-2011 - IEEE Standard for Synchrophasor Measurements for Power Systems*, vol. 2011, no. December. 2011.

[13] K. E. Martin *et al.*, "Exploring the IEEE standard C37.118-2005 synchrophasors for power systems," *IEEE Trans. Power Deliv.*, 2008.

[14] V. Vyatkin, G. Zhabelova, N. Higgins, K. Schwarz, and N.-K. C. Nair, "Towards intelligent Smart Grid devices with IEC 61850 Interoperability and IEC 61499 open control architecture," in *IEEE PES T&D 2010*, 2010, pp. 1–8.

[15] D. K. Mohanta, C. Murthy, and D. Sinha Roy, "A Brief Review of Phasor Measurement Units as Sensors for Smart Grid," *Electr. Power Components Syst.*, vol. 44, no. 4, pp. 411–425, Feb. 2016.

[16] M. Jarrah, M. Jaradat, Y. Jararweh, M. Al-Ayyoub, and A. Bousselham, "A hierarchical optimization model for energy data flow in smart grid power systems," *Inf. Syst.*, vol. 53, pp. 190–200, Oct. 2015.

[17] M. Kuzlu, M. Pipattanasomporn, and S. Rahman, "Communication network requirements for major smart grid applications in HAN, NAN and WAN," *Comput. Networks*, vol. 67, pp. 74–88, Jul. 2014.

[18] I.-K. Yang, N.-J. Jung, and Y.-I. Kim, "Status of Advanced Metering Infrastructure development in Korea," in *2009 Transmission & Distribution Conference & Exposition: Asia and Pacific*, 2009, pp. 1–3.

[19] G. López, J. I. Moreno, H. Amarís, and F. Salazar, "Paving the road toward Smart Grids through large-scale advanced metering infrastructures," *Electr. Power Syst. Res.*, vol. 120, pp. 194–205, Mar. 2015.

[20] D. Wang, Z. Tao, J. Zhang, and A. A. Abouzeid, "RPL Based Routing for Advanced Metering Infrastructure in Smart Grid," in *2010 IEEE International Conference on Communications Workshops*, 2010, pp. 1–6.

[21] G. Dileep, "A survey on smart grid technologies and applications," *Renew. Energy*, vol. 146, pp. 2589–2625, available online 23 August 2010.

[22] A. Ahmadi, Y. Alinejad-Beromi, and M. Moradi, "Optimal PMU placement for power system observability using binary particle swarm optimization and considering measurement redundancy," *Expert Syst. Appl.*, vol. 38, no. 6, pp. 7263–7269, Jun. 2011.

[23] F. Aminifar, A. Khodaei, M. Fotuhi-Firuzabad, and M. Shahidehpour, "Contingency-Constrained PMU Placement in Power Networks," *IEEE Trans. Power Syst.*, vol. 25, no. 1, pp. 516–523, Feb. 2010.

[24] D. J. Brueni and L. S. Heath, "The PMU Placement Problem," *SIAM J. Discret. Math.*, vol. 19, no. 3, pp. 744–761, Jan. 2005.

[25] S. Das, D. Ghosh, T. Ghose, and D. K. Mohanta, "Simulation of wide area measurement system with optimal phasor measurement unit location," in *2014 International Conference on Signal Processing and Integrated Networks (SPIN)*, 2014, pp. 226–230.

[26] I.-H. Lim and T. S. Sidhu, "Design of a Backup IED for IEC 61850-Based Substation," *IEEE Trans. Power Deliv.*, vol. 28, no. 4, pp. 2048–2055, Oct. 2013.

[27] L. Zhu, D. Shi, and X. Duan, "Standard Function Blocks for Flexible IED in IEC 61850-Based Substation Automation," *IEEE Trans. Power Deliv.*, vol. 26, no. 2, pp. 1101–1110, Apr. 2011.

[28] U. C. Netto, D. de Castro Grillo, I. D. Lonel, E. L. Pellini, and D. V. Coury, "An ANN based forecast for IED network management using the IEC61850 standard," *Electr. Power Syst. Res.*, vol. 130, pp. 148–155, Jan. 2016.

[29] I.-H. Lim and T. S. Sidhu, "A new local backup scheme considering simultaneous faults of protection IEDs in an IEC 61850-based substation," *Int. J. Electr. Power Energy Syst.*, vol. 77, pp. 151–157, May 2016.

[30] T.-H. Yeh, S.-C. Hsu, C.-K. Chung, and M.-S. Lin, "Conformance Test for IEDs Based on IEC 61850 Communication Protocol," *J. Power Energy Eng.*, vol. 03, no. 04, pp. 289–296, 2015.

[31] D. Bhor, K. Angappan, and K. M. Sivalingam, "Network and power-grid co-simulation framework for Smart Grid wide-area monitoring networks," *J. Netw. Comput. Appl.*, vol. 59, pp. 274–284, Jan. 2016.

[32] T. Zseby and J. Fabini, "Security Challenges for Wide Area Monitoring in Smart Grids," *e i Elektrotechnik und Informationstechnik*, vol. 131, no. 3, pp. 105–111, May 2014.

[33] I. Albizu, E. Fernandez, P. Eguia, E. Torres, and A. J. Mazon, "Tension and Ampacity Monitoring System for Overhead Lines," *IEEE Trans. Power Deliv.*, vol. 28, no. 1, pp. 3–10, Jan. 2013.

[34] P. Hering, P. Janecek, and E. Janecek, "On-line Ampacity Monitoring from Phasor Measurements," *IFAC Proc. Vol.*, vol. 47, no. 3, pp. 3164–3169, 2014.

[35] R. G. Olsen and K. S. Edwards, "Closure on 'a new method for real-time monitoring of high voltage transmission line conductor sag,'" *IEEE Trans. Power Deliv.*, vol. 18, no. 4, pp. 1598–1599, Oct. 2003.

[36] A. Ashok, A. Hahn, and M. Govindarasu, "Cyber-physical security of Wide-Area Monitoring, Protection and Control in a smart grid environment," *J. Adv. Res.*, vol. 5, no. 4, pp. 481–489, Jul. 2014.

[37] Y. Mitani, T. Kudo, A. Satake, and K. H. Basri, "Monitoring the Wide Area Power System Dynamics by Phasor Measurement Units Based on Campus WAMS Strategy," *IFAC Proc. Vol.*, vol. 47, no. 3, pp. 2273–2278, 2014.

[38] C. Efthymiou and G. Kalogridis, "Smart Grid Privacy via Anonymization of Smart Metering Data," in *2010 First IEEE International Conference on Smart Grid Communications*, 2010, pp. 238–243.

[39] A. G. Phadke and B. Kasztenny, "Synchronized Phasor and Frequency Measurement Under Transient Conditions," *IEEE Trans. Power Deliv.*, vol. 24, no. 1, pp. 89–95, Jan. 2009.

[40] R. I. Müller and M. J. Booysen, "A Water Flow Meter for Smart Metering Applications," in *The 9th South African Conference on Computational and Applied Mechanics, SACAM2014*, 2014.

[41] W. Wang, Y. Xu, and M. Khanna, "A survey on the communication architectures in smart grid," *Comput. Networks*, vol. 55, no. 15, pp. 3604–3629, Oct. 2011.

[42] A. Aggarwal, S. Kunta, and P. K. Verma, "A proposed communications infrastructure for the smart grid," in *2010 Innovative Smart Grid Technologies (ISGT)*, 2010, pp. 1–5.

[43] V. C. Gungor *et al.*, "Smart Grid Technologies: Communication Technologies and Standards," *IEEE Trans. Ind. Informatics*, vol. 7, no. 4, pp. 529–539, Nov. 2011.

[44] Delphine, B. W. Jang, Y. S. Shin, S. T. Kang, and J. S. Choi, "Design

and implementation of building energy management system with quality of experience power scheduling model to prevent the blackout in smart grid network," in *16th International Conference on Advanced Communication Technology*, 2014, pp. 208–211.

[45] M. N. O. Sadiku and M. Ilyas, "Local Area Networks," in *Simulation of Local Area Networks*, CRC Press, 2018, pp. 1–16.

[46] S. Bera, S. Misra, and J. J. P. C. Rodrigues, "Cloud Computing Applications for Smart Grid: A Survey," *IEEE Trans. Parallel Distrib. Syst.*, vol. 26, no. 5, pp. 1477–1494, May 2015.

[47] T. Iwao *et al.*, "Dynamic Data Forwarding in Wireless Mesh Networks," in *2010 First IEEE International Conference on Smart Grid Communications*, 2010, pp. 385–390.

[48] J.-S. Jung, K.-W. Lim, J.-B. Kim, Y.-B. Ko, Y. Kim, and S.-Y. Lee, "Improving IEEE 802.11s Wireless Mesh Networks for Reliable Routing in the Smart Grid Infrastructure," in *2011 IEEE International Conference on Communications Workshops (ICC)*, 2011, pp. 1–5.

[49] S. Dawson-Haggerty, A. Tavakoli, and D. Culler, "Hydro: A Hybrid Routing Protocol for Low-Power and Lossy Networks," in *2010 First IEEE International Conference on Smart Grid Communications*, 2010, pp. 268–273.

[50] H. Gharavi and B. Hu, "Multigate Communication Network for Smart Grid," *Proc. IEEE*, vol. 99, no. 6, pp. 1028–1045, Jun. 2011.

[51] F. Li, B. Luo, and P. Liu, "Secure Information Aggregation for Smart Grids Using Homomorphic Encryption," in *2010 First IEEE International Conference on Smart Grid Communications*, 2010, pp. 327–332.

[52] A. Bartoli, J. Hernandez-Serrano, M. Soriano, M. Dohler, A. Kountouris, and D. Barthel, "Secure Lossless Aggregation for Smart Grid M2M Networks," in *2010 First IEEE International Conference on Smart Grid Communications*, 2010, pp. 333–338.

[53] T. Gamer, L. Völker, and M. Zitterbart, "Differentiated security in wireless mesh networks," *Secur. Commun. Networks*, vol. 4, no. 3, pp. 257–266, Mar. 2011.

[54] H. Li and W. Zhang, "QoS Routing in Smart Grid," in *2010 IEEE Global Telecommunications Conference GLOBECOM 2010*, 2010, pp. 1–6.

[55] Y. Kabalci, "A survey on smart metering and smart grid communication," *Renew. Sustain. Energy Rev.*, vol. 57, pp. 302–318, May 2016.

[56] S. Rusitschka, K. Eger, and C. Gerdes, "Smart Grid Data Cloud: A Model for Utilizing Cloud Computing in the Smart Grid Domain," in *2010 First IEEE International Conference on Smart Grid Communications*, 2010, pp. 483–488.

[57] M. Yigit, V. C. Gungor, and S. Baktir, "Cloud Computing for Smart Grid applications," *Comput. Networks*, vol. 70, pp. 312–329, Sep. 2014.

[58] I. Mezgár and U. Rauschecker, "The challenge of networked enterprises for cloud computing interoperability," *Comput. Ind.*, vol. 65, no. 4, pp. 657–674, May 2014.

[59] Q. Hu, F. Li, and C. Chen, "A Smart Home Test Bed for Undergraduate Education to Bridge the Curriculum Gap From Traditional Power Systems to Modernized Smart Grids," *IEEE Trans. Educ.*, vol. 58, no. 1, pp. 32–38, Feb. 2015.

[60] D. Li and S. K. Jayaweera, "Distributed Smart-Home Decision-Making in a Hierarchical Interactive Smart Grid Architecture," *IEEE Trans. Parallel Distrib. Syst.*, vol. 26, no. 1, pp. 75–84, Jan. 2015.

[61] M. Mital, A. K. Pani, S. Damodaran, and R. Ramesh, "Cloud based management and control system for smart communities: A practical case study," *Comput. Ind.*, vol. 74, pp. 162–172, Dec. 2015.

[62] A. Anwar and A. Mahmood, "Cyber Security of Smart Grid Infrastructure," in *The State of the Art in Intrusion Prevention and Detection*, Auerbach Publications, 2014, pp. 139–154.

[63] V. Ananda Kumar, K. K. Pandey, and D. K. Punia, "Cyber security threats in the power sector: Need for a domain specific regulatory framework in India," *Energy Policy*, vol. 65, pp. 126–133, Feb. 2014.

Journal of Mechatronics, Electrical Power, and Vehicular Technology 10 (2019) 85-91

Journal of Mechatronics, Electrical Power, and Vehicular Technology

e-ISSN: 2088-6985
p-ISSN: 2087-3379

www.mevjournal.com

Safety assessment of high voltage substation earthing systems with synthetic geotextile membrane

Mostafa Nazih *

Building, Infrastructure and Advanced Facilities, Jacobs
452 Flinders St., Melbourne, VIC 3000, Australia

Received 9 December 2019; accepted 21 December 2019

Abstract

High voltage substations built within areas prone to vegetation or with unfavourable subgrade conditions are paved with the addition of punched geotextiles and non-conductive synthetic fabrics underneath switchyard surfacing. The aim of this research is to identify the impact of synthetic textiles on earthing system performance through numerical analysis with the state-of-the-art software package. The new layer interferes with the earthing grid's performance with different behaviour depending on the installation above or underneath the layer with considerable impact taking place when the earthing grid is installed above the geotextile layer. Rods penetrating the geotextile can alleviate the potential voltage distribution issues and improve the earthing system performance regardless of the native soil stratification.

Keywords: substation earthing; synthetic geotextile; tolerable voltages; high voltage.

I. Introduction

Personal safety is paramount for HV substation earthing systems in addition to system requirements for neutral voltage reference, earth fault detection and electrostatic control [1]. Substation safety is assessed by comparing attained surface voltages, expressed as touch and step voltages as well as transferred voltages, to tolerable limits [2][3]. Surface voltages depend on soil stratification where fault currents prefer to go through layers of lower resistivities with less voltage gradients while high resistivity layers contribute to greater gradients and thus, touch and step voltages [4]. Polyester geotextiles with pores around 100 microns are laid underneath switchyard surface at an average depth of about 900 mm to control vegetation. Different types of geotextiles may be used to improve subgrade soil conditions during construction. The insulating nature of the geotextile interferes with the native soil stratification by introducing a very thin layer with very high resistivity. Example installation underneath a new switchyard is shown in Figure 1. The recent research review on native soil modifications indicates that the relations with high voltage substation earthing and synthetic geotextiles have not been studied [5][6][7][8][9][10][11][12][13]. This paper sheds some light on the subject since the trend to involve geotextiles is on the rise for substations within Australia and other parts of the world. The paper investigates the mechanism of action of the included layer as well as two case studies for green and brown field applications.

II. Materials and Methods

A. Fault current in soil

The introduction of geotextile underneath switchyard surface can be modelled as a thin layer with very high electrical resistivity. The level of earthing grids above or under the geotextile controls the surface voltage distribution and overall resistance to remote earth. For earthing grids above the geotextiles, fault current normally prefers to flow through the surface layer creating gradients proportional to the layer resistivity which can negatively impact the safety assessment. For earthing grids installed under the geotextiles, no significant changes are envisaged to grid resistance. Surface voltages will be very similar to the case with no geotextiles.

* Corresponding Author. Tel: +61-386683739
E-mail address: mostafa0020@yahoo.com

doi: https://dx.doi.org/10.14203/j.mev.2019.v10.85-91

Accreditation Number: (RISTEKDIKTI) 1/E/KPT/2015 (Sinta 2).

Figure 1. Installation of geotextile underneath new switchyard during construction

B. Geotextile modelling

Geotextiles are made of polyester, which is a dielectric material with a typical bulk resistivity of about 10^{11} to 10^{15} Ωm [14]. Although the commercially available geotextiles to control vegetation are permeable to water flow with surface flow rates vary between 100 to 200 litre/m^2/sec [14], it is considered to have a very high electrical resistivity since the pores are not sufficient to achieve reliable native soil contact through the geotextile in dry conditions.

The geotextiles are not normally tested for the electrical resistivity and an estimated value of 10,000 Ωm has been considered for the dry material based on corresponding values for a porous insulating material like wood [15]. Higher values reaching 50,000 Ωm are assumed for dry conditions. Various manufacturers have been approached for electrical testing of their material with negative feedback since the electrical testing of geotextile is a non-standard test.

Due its thin construction and insulating properties, it is not possible to measure or even detect the presence of a geotextile once installed using site based soil resistivity measurements (e.g. Schlumberger, Wenner methods) [16]. The geotextiles are envisaged to interference with the soil resistivity measurements by blocking the deeper soil layers interaction and a quick results saturation will be reached versus spacing.

The geotextiles are modelled in current distribution, electromagnetic interference, grounding and soil (CDEGS) structure analysis software embedded soil volume option. Since the soil model with geotextiles has a high degree of heterogeneity, memory allocation and processing time is considerably greater than cases with no geotextiles.

C. Safety criteria

Tolerable touch and step voltages are traditionally considered to compare versus attainable voltages within and around high voltage installations to assess the personal safety criteria parameters. With the use of high resistivity layer, the tolerable touch and step voltages, if the earthing grid is installed underneath the geotextile, will be impacted as the deeper native soil will be, theoretically, out of action and replaced by the high resistivity layer. Equation (1) from IEEE 80:2013 simplified formula for surface layer derating factor C_s [3]

$$C_s = 1 - \frac{0.09\left(1-\frac{\rho}{\rho_s}\right)}{2h_s+0.09} \quad (1)$$

where ρ represents the geotextile resistivity, ρ_s surface soil resistivity and h_s is the depth of the geotextile.

With estimated values ranging from 5,000 Ωm to 50,000 Ωm for geotextile resistivity depending on soil dryness and seasonal variations, the tolerable touch and step voltages will be higher than that with no geotextile, assuming a uniform soil model. The increase in a tolerable touch voltage is inversely proportional to the surface soil resistivity with behaviour shown in Figure 2 for 50 kg weight persons. The tolerable touch voltages ($V_{touch50kg}$) are calculated for fault duration t of 0.5 seconds based on IEEE 80:2013 Equation (2) [3]

$$V_{touch\ 50kg} = (1000 + 1.5 \times C_s \times \rho_s)\frac{0.116}{\sqrt{t}} \quad (2)$$

where native/surface soil resistivity is relatively low (less than 50 Ωm), an increase in the tolerable touch voltage of up to 350 % can be obtained in dry conditions where the geotextiles are assumed to have very high resistivity values in the range of 50,000 Ωm. in the other hand, where the soil is wet, as the water

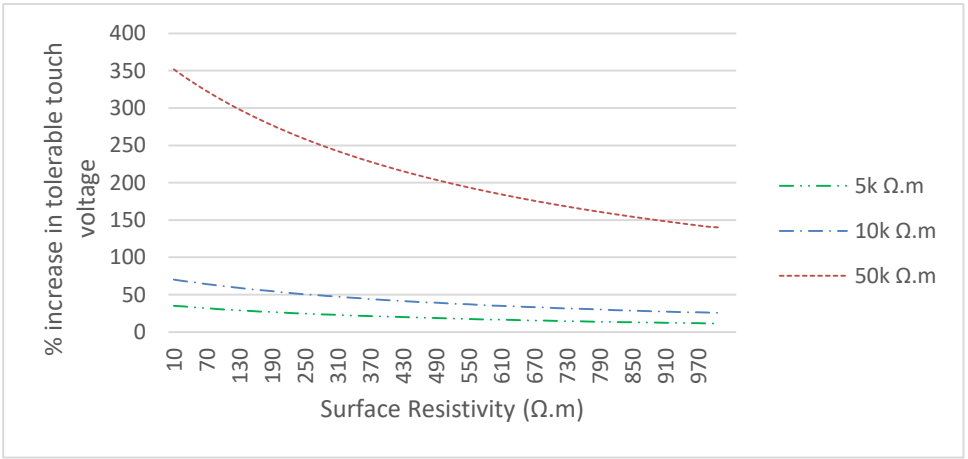

Figure 2. Touch voltage increase (%) versus surface soil resistivity (0.9 m deep geotextile)

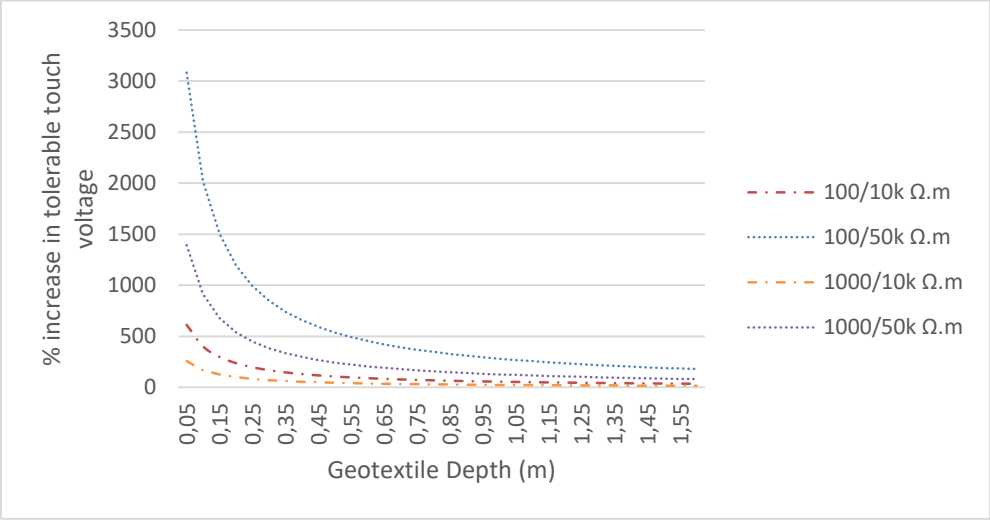

Figure 3. Touch voltage increase (%) versus surface textile depth

flows through the membrane, resistivity is assumed to decline sharply and less effect on tolerable touch voltage is envisaged.

The depth of the geotextile layer also affects the tolerable voltages as with shallow installations, the high resistivity layer will be near to the surface and hence, its effect will be greater. Variation of touch voltage with geotextile depth is typically depicted in Figure 3 with two different surfaces (native) soil resistivities 100 Ωm and 1000 Ωm. A sharp drop in the tolerable touch voltages is observed for geotextile installations deeper than 0.15 - 0.2 m from the finished surface. Typical geotextile installation depth is about 0.5 - 1 m.

III. Results and discussions

A. Case study I

The first case under study is for a new open terminal substation 500/220 kV with overall dimensions of 144 x 70 m. The native soil measurements at site modelled with CDEGS RESAP [17] with a 3-layer stratification as shown in Figure 4. High resistivity layers on a low one are considered in this case where deeper layers permit most of the current to propagate through away from the surface.

Earth fault current of 10 kA is used to represent the available 500 kV single phase to earth fault with a duration of 100 ms. Tolerable touch and step voltages

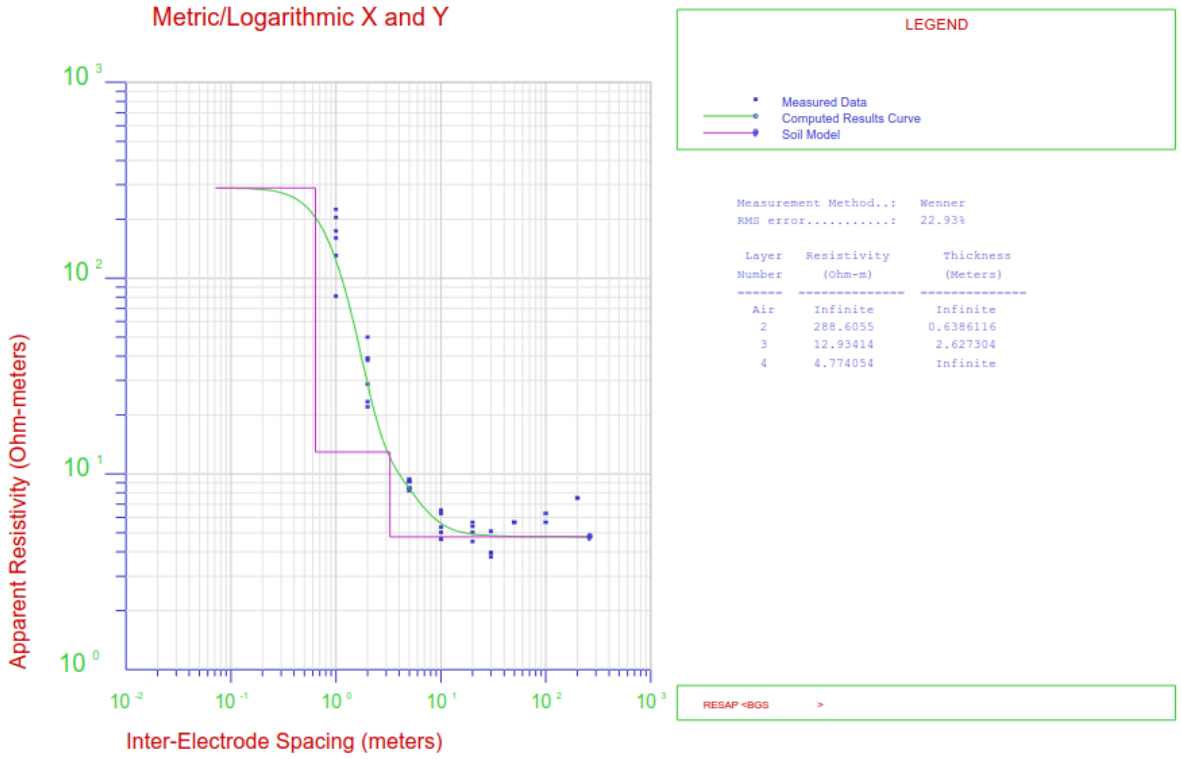

Figure 4. Native soil model showing 3-layer soil with high on low resistivity stratification

Table 1.
Modified soil model

Soil Layer	Soil Resistivity (Ω m)	Layer Thickness (m)
ρ 1	150.00	0.9
ρ 2	10000.00	0.05
ρ 3	288.61	0.63
ρ 4	12.93	2.63
ρ 5	4.77	Infinite

have been calculated using IEEE 80:2013 formulae [3]. Switchyard surfacing with an average resistivity of 150 Ωm is added as a top layer along with needle punched polyester geotextile with 100 micron pores to represent the final soil stratification as shown in Table 1. Tolerable touch and step voltages for the substation are tabulated in Table 2.

1) Initial grid design with no geotextile

Unsymmetrically spaced earthing grid with overall dimensions of 124 x 48 m and 10 x 1.5 m rods used for this substation initially without considering additional geotextile as shown in Figure 5. Substation Fence has a separate earthing ring not connected to the main grid. The initial grid design is meeting the tolerable touch and step criteria.

CDEGS results for the initial grid design with no textiles shows an earthing resistance of 0.122 Ω achieving the safety criteria within and around the site with tolerable touch voltages about 1100 V and 816 V, respectively (based on IEEE 80:2013 criteria for a 70 kg (inside) and 50 kg (outside) person including a footwear resistance of 2000 Ω per foot).

2) Modified grid design

Although the addition of geotextile raises tolerable touch voltage by about 25 %, the overall earthing resistance increases by about 61 % with unsafe touch voltages within the substation. Accordingly, the grid design is set for improvement by replacing 1.5 m rods with longer ones (3 m each) and an additional 13 x 3 m rods spread throughout the grid. The improvement is considered to utilize the deeper lower resistivity soil layers.

It is evident that the addition of geotextile completely covering the earthing grid increases the overall earthing system impedance to remote earth, which in turn may require additional remedial solutions in case that the associated touch and step voltages exceed the tolerable limits. Nevertheless, in this case, the increase in resistance and touch/step voltages with geotextiles is much more than the increase in tolerable voltages and hence, additional remedial solutions are required by installing additional rods.

B. Case study II

The second case under study is for an existing substation with overall dimensions of about 140 x 110 m and proposed extension of 90 x 70 m as shown in Figure 6 where geotextile is used under the earthing grid extension due to soil stability conditions. The existing earthing grid is adequately designed with tolerable touch and step voltages. The native soil measurements at site modelled with CDEGS RESAP [17] show a 2-layer stratification as shown in Figure 7 indicating a lower layer with high resistivity. This is a case of interest as the addition of rods is not supposed to significantly affect the earthing grid impedance. The extension does not include additional sources for fault current contributions and hence, the EPR is considered virtually constant (it will be practically lower than the existing situation since additional conductors within the extension area reduce the overall earthing system resistance and EPR accordingly).

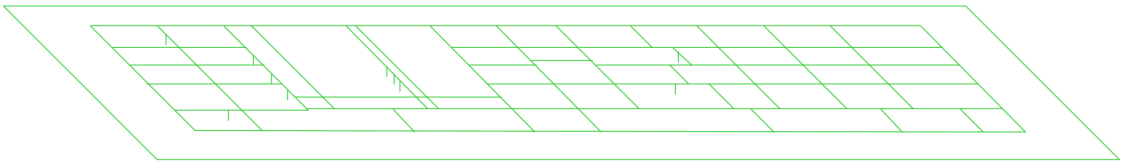

Figure 5. Earthing grid model in CDEGS with buried conductors and fenceline

Table 2.
Earthing grid performance parameters for case I

Parameter	No Fabric	Fabric	% Change	Modified design
Earthing system impedance (Ω)	0.122	0.197	61.5	0.133
Fault current (kA)	10	10	0.0	10
Earth potential rise (EPR) (V)	1225	1977	61.4	1335
Max. attainable touch voltage within substation (V)	958	1576	64.5	984
Tolerable touch voltage inside substation (V) – 70 kg	1105	1454	31.6	1454
Max. attainable touch voltage outside substation (V)	46	59	28.3	51
Tolerable touch voltage outside substation (V) – 50 kg	816	816	0.0	816
Max. attainable step voltage inside substation (V)	551	718	30.3	452
Tolerable step voltage inside substation (V) – 70 kg	2929	4326	47.7	4326
Max. attainable step voltage outside substation (V)	7	20	185.7	17
Tolerable step voltage outside substation (V) – 50 kg	2164	2164	0.0	2164

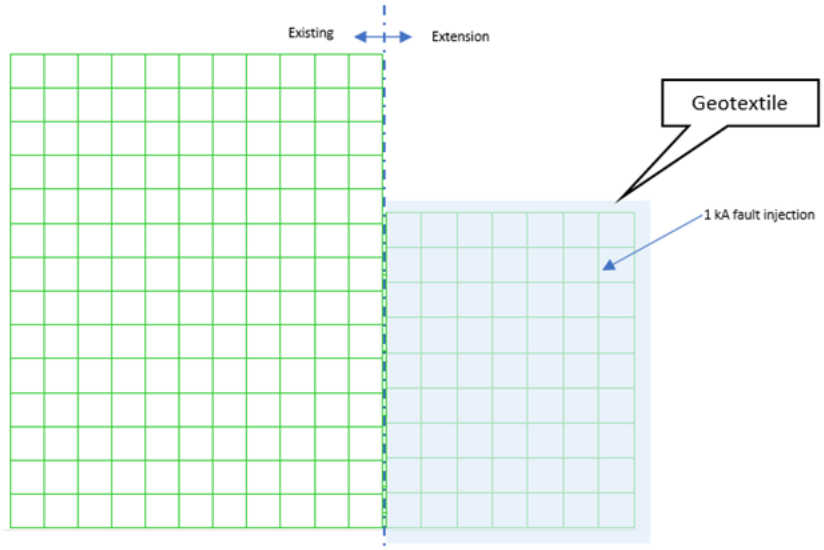

Figure 6. Earthing grid CDEGS model with existing and extension conductors

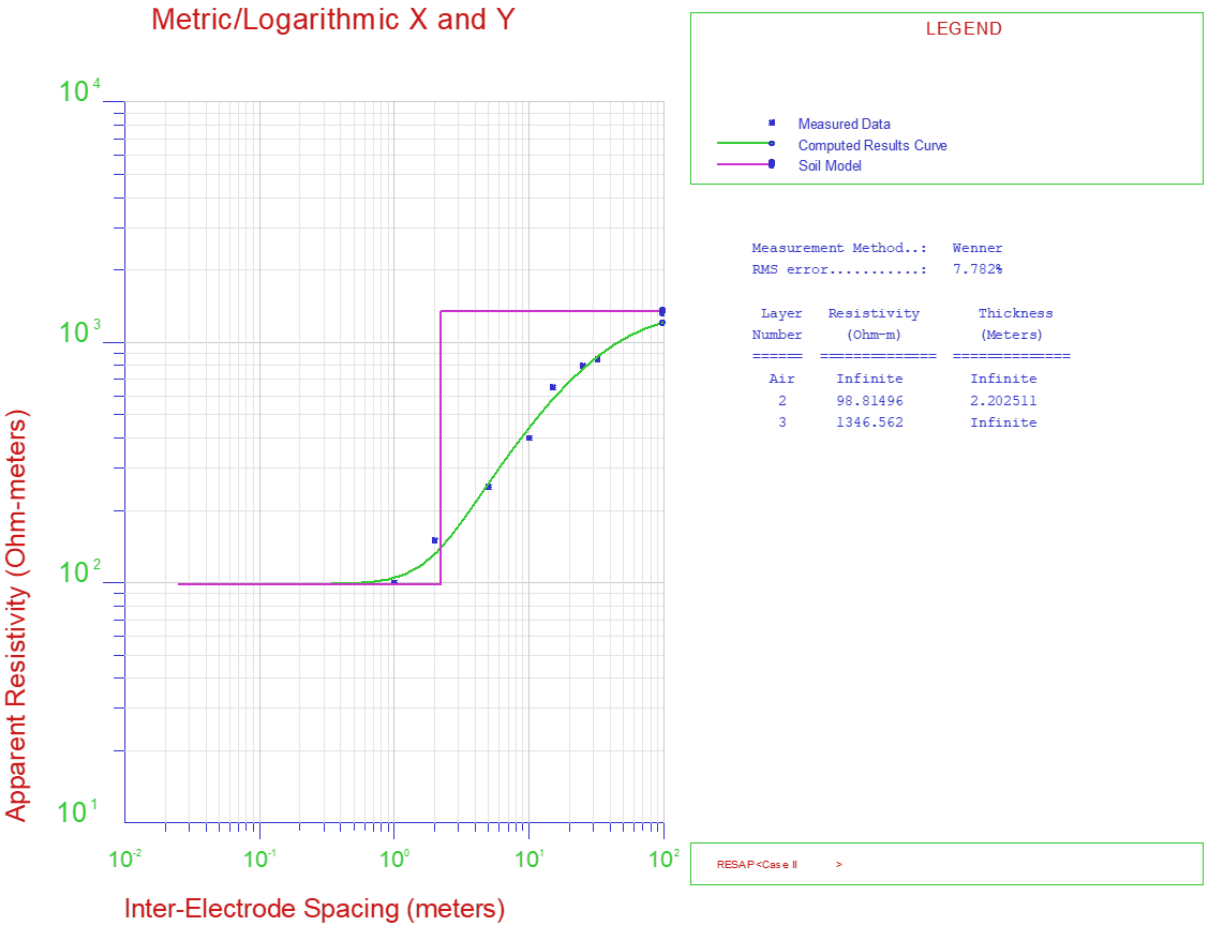

Figure 7. Native soil model showing 2-layer soil with low on high resistivity stratification

In the case of faulty equipment within the extension area, earth return fault current will leak from earthing conductors at the existing earthing grid rather than the new extension area as the immediate vicinity of the extension has a high resistivity layer underneath it. Nevertheless, a portion of the leakage current will flow upwards within the surface paving layer.

The leakage current density confirms the hypothesis due to the higher resistivity layer underneath the grid extension. The lower leakage current density results at higher surface voltages, touch, and step voltages accordingly since the voltage drop over top soil from the grid to surface is smaller with less current leaking into deeper soil. The increase in surface voltage and touch voltage is

Table 3.
Earthing grid performance parameters for case II

Parameter	Extended grid without fabric				Extended grid with fabric			
	Total	Existing	Extension	Ratio (%)	Total	Existing	Extension	Ratio (%)
Earthing system impedance (Ω)	2.76				2.77			
Fault current (kA)	1				1			
Earth potential rise (EPR) (V)	2760	2760	2760		2769	2769	2769	
Max. attainable touch voltage within substation (V)	117	117	112	-4.27	124	124	119	-4.03
Tolerable touch voltage inside substation (V)		675	675	0.00		675	897	32.89
Max. attainable touch voltage outside substation (V)	234	234	225	-3.85	247	247	239	-3.24
Tolerable touch voltage outside substation (V) - barefoot		267	267	0.00		267	267	0.00
Max. attainable step voltage inside substation (V)	66	52	66	26.92	77	51	77	50.98
Tolerable step voltage inside substation (V)		1758	1758	0.00		1758	2647	50.57
Max. attainable step voltage outside substation (V)	86	86	83	-3.49	96	85	96	12.94
Tolerable step voltage outside substation (V)		371	371	0.00		371	371	0.00

Table 4.
Earthing grid performance parameters for case II – with additional 3 x 3 m rods

Parameter	Extended grid without fabric				Extended grid with fabric			
	Total	Existing	Extension	Ratio (%)	Total	Existing	Extension	Ratio (%)
Earthing system impedance (Ω)	2.76				2.77			
Fault current (kA)	1				1			
Earth potential rise (EPR) (V)	2760	2760	2760		2769	2769	2769	
Max. attainable touch voltage within substation (V)	117	117	112	-4.27	124	124	119	-4.03
Tolerable touch voltage inside substation (V)		675	675	0.00		675	897	32.89
Max. attainable touch voltage outside substation (V)	234	234	225	-3.85	247	247	239	-3.24
Tolerable touch voltage outside substation (V) - barefoot		267	267	0.00		267	267	0.00
Max. attainable step voltage inside substation (V)	66	52	66	26.92	78	60	78	30.00
Tolerable step voltage inside substation (V)		1758	1758	0.00		1758	2647	50.57
Max. attainable step voltage outside substation (V)	86	86	83	-3.49	97	85	97	14.12
Tolerable step voltage outside substation (V)		371	371	0.00		371	371	0.00

accompanied by an increase in tolerable touch voltages as highlighted earlier. The increase in touch voltage is much less than the increase in tolerable limits. Comparative results are tabulated in Table 3.

The fabric has about 0.3 % effect on the overall resistance and EPR increase despite of the extension area representing about 29 % of total earthing system. Notwithstanding that, the surface voltage distribution and leakage current density are altered with the presence of geotextiles. Touch and step voltages appear to increase at both the geotextile covered and uncovered area. This behaviour is ascribed to higher surface voltages.

3 x 3 m rods are added to the corners of the extended grid to check the modified grid parameters. Additions of rods +2.2 m in length, although the deeper layer has a higher resistivity, stabilises the voltage and current distribution where provided, alleviating the effect of geotextile on step voltages increase. If the soil model has a lower deeper resistivity layer, rods will be more effective in diverting fault current into deeper layers and hence, less surface voltage gradients. Table 4 summarises the findings with additional rods. Due to the higher resistivity deeper soil layers, the addition of rods has a negligible effect on resistance and EPR.

IV. Conclusion

The introduction of geotextiles changes the earthing system behaviour by interfering into leakage current distribution into the surface and deep soil layers. The location of the earthing grid affects the results with considerable impact taking place when the earthing grid is installed above the geotextile

layer. The tolerable touch and step voltages increase proportionally to the ratio between the surface soil and geotextile resistivity where the latter is considered to change with seasonal variations and soil water content. A typical tolerable touch voltage increase of about 60 % is envisaged for native surface soil of 100 Ωm. The addition of geotextiles and associated increase in tolerable touch (and step) voltages may alleviate the need for additional high resistivity finish materials. Earthing system behaviour in the presence of geotextiles depends on whether the textile covers the grid area completely or partially. The greatest impact on earthing system impedance and surface voltage distribution is expected for new substation installations where geotextile covers the grid completely. With partial coverage such as substation extensions, the impact is negligible on overall earthing system impedance. Vertical rods penetrating the geotextile layers when the earthing grid is installed above it are effective to alleviate the increase in surface voltages due to geotextiles even with deeper soil layers having a high resistivity. Rods should be spread through the earthing grid and corners to ensure proper current dispersion into deeper soil layers away from the surface as possible.

Acknowledgement

The author would like to express grateful gratitude to Jacobs Australia Pty. for providing engineering software used in this study.

Declarations

Author contribution

M. Nazih as the contributor of this paper. Author read and approved the final paper.

Funding statement

This research did not receive any specific grant from funding agencies in the public, commercial, or not-for-profit sectors.

Conflict of interest

The author declares no conflict of interest.

Additional information

No additional information is available for this paper.

References

[1] J. He, R. Zeng, B. Zhang, *Methodology and technology for power system grounding*, John Wiley & Sons, 2013.

[2] IEC 60479-1:2018: *Effects of current on human beings and livestock - Part 1: General aspects*.

[3] *IEEE Guide for Safety in AC Substation Grounding*, in IEEE Std 80-2013 (Revision of IEEE Std 80-2000/ Incorporates IEEE Std 80-2013/Cor 1-2015), pp. 1-226, 15 May 2015.

[4] J. Liu, F. P. Dawalibi, S. Tee, "Analysis of Current Density in Soil for Resistivity Measurements and Electrical Grounding Designs," *Journal of Electrical and Electronic Engineering*, Vol. 5, No. 5, pp. 198-208, 2017.

[5] B. Alsharari, A. Olenko, H. Abuel-Naga, *Modeling of electrical resistivity of soil based on geotechnical properties*, Expert Systems with Applications, 141, 112966, available online 19 September 2019.

[6] R. A. Fayed and A. S. Ezeldin, *Simulation and optimization model for electrical substation construction. PhD diss.*, American Univeristy in Cairo, 2016.

[7] A. Ackerman, P. K. Sen, and C. Oertli, Designing safe and reliable grounding in AC substations with poor soil resistivity: An interpretation of IEEE STD. 80, Record of *Conference Papers - Annual Petroleum and Chemical Industry Conference*, 49 (4), 1883-1889, 2012.

[8] R. D. Southey, M. Siahrang, S. Fortin, and F. P. Dawalibi, "Using fall-of-potential measurements to improve deep soil resistivity estimates," *IEEE Transactions on Industry Applications*, 51(6), 5023-5029, 2015.

[9] S. C. Lim, C. Gomes, and M. Z. A. Ab Kadir, "Electrical earthing in troubled environment," *International Journal of Electrical Power and Energy Systems*, 47(1), 117-128, 2013.

[10] J. E. Edlebeck and B. Beske, "Identifying and quantifying material properties that impact aggregate resistivity of electrical substation surface material," *IEEE Transactions on Power Delivery*, 29(5), 2248-2253, 2014.

[11] C. J. F. P. Jones, J. Lamont-Black, and S. Glendinning, "Electrokinetic geosynthetics in hydraulic applications," *Geotextiles and Geomembranes*, 29(4), 381-390, 2011.

[12] A. N. Ramani, A. R. Ahmad, M. F. Sulaima, M. N. M. Nasir, and A. Ahmad, "Analysis the configuration of earthing system based on high-low and low-high soil structure," *AIP Conference Proceedings*, 1660, 2015.

[13] W. L. Lai, W. F. H. Wan Ahmad, J. Jasni, and M. Z. A. Ab Kadir, "A review on the usage of Zeolite, Perlite and Vermiculite as natural enhancement materials for grounding system installations," *IEEE Student Conference on Research and Development: Inspiring Technology for Humanity, SCOReD 2017 - Proceedings, 2018-January*, 338-343, 2018.

[14] Global Synthetics, Geofirma technical datasheet.

[15] C. Skaar, *Electrical Properties of Wood*, In: Wood-Water Relations, Springer Series in Wood Science, Springer, Berlin, Heidelberg, 1988.

[16] "*IEEE Guide for Measuring Earth Resistivity, Ground Impedance, and Earth Surface Potentials of a Grounding System*," in IEEE Std 81-2012 (Revision of IEEE Std 81-1983), pp. 1-86, 28 Dec. 2012.

[17] CDEGS RESAP Soil Resistivity Analysis Module – Safe Engineering Services & technologies ltd., Canada.

This page intentionally left blank

Journal of Mechatronics, Electrical Power, and Vehicular Technology 10 (2019) 93-101

Journal of Mechatronics, Electrical Power, and Vehicular Technology

e-ISSN: 2088-6985
p-ISSN: 2087-3379

www.mevjournal.com

Three axis deviation analysis of CNC milling machine

Dalmasius Ganjar Subagio*, Ridwan Arief Subekti, Hendri Maja Saputra, Ahmad Rajani, Kadek Heri Sanjaya

Research Centre for Electrical Power and Mechatronics, Indonesian Institute of Sciences
Komp LIPI Bandung, Gd 20, Lt 2, Bandung, West Java, 40135 Indonesia

Received 24 October 2019; accepted 18 December 2019

Abstract

The manufacturing technology has developed rapidly, especially those intended to improve the precision. Consequently, increasing precision requires greater technical capabilities in the field of measurement. A prototype of a 3-axis CNC milling machine has been designed and developed in the Research Centre for Electrical Power and Mechatronics, Indonesian Institute of Sciences (RCEPM-LIPI). The CNC milling machine is driven by a 0.4 kW servo motor with a spindle rotation of 12,000 rpm. This study aims to measure the precision of the CNC milling machine by carrying out the measurement process. It is expected that the CNC milling machine will be able to perform in an optimum precision during the manufacturing process. Accuracy level testing is done by measuring the deviations on the three axes namely X-axis, Y-axis, and Z-axis, as well as the flatness using a dial indicator and parallel plates. The measurement results show the deviation on the X-axis by 0.033 mm, the Y-axis by 0.102 mm, the Z-axis by 0.063 mm, and the flatness of the table by 0.096 mm, respectively. It is confirmed that the deviation value is within the tolerance standard limits set by ISO 2768 standard. However, the calibration is required for this CNC milling machine to achieve more accurate precision. Furthermore, the design improvement of CNC milling machine and the application of information technology in accordance with Industry 4.0 concept will enhance the precision and reliability.

Keywords: precision measurement; orthogonal axes; manufacturing machine; automation industry.

I. Introduction

Since the beginning of the industrial revolution, there has been a dramatic increase in manufacturing quality and quantity by the application of industrial mechanization, from steam powered machines to modern days automation [1]. Today, there is greater demand for higher quality and quantity products and services which consequently requires manufacturing complexity and better quality of machining which makes industrial equipment construction more complicated [2]. In developed countries, the slowing down of population growth and ageing population cause shortage in manpower for the industry. Other common problems nowadays are the depleting natural resources and shortening product life cycle [3]. All those problems are tried to be overcome by implementing the state of the art technologies in the form of Internet of Things (IoT) and Cyber-Physical System (CPS) [1][4]. Germany is the country which introduced the concept of Industry 4.0, a concept as an embodiment of those new technologies [1]. Together with Japan, Germany has been the leading country in developing manufacturing equipment such as computer numerical control (CNC) machine [5]. The concept will make the future industry more agile and flexible to meet a quickly and constantly changing market demands [6]. From the first introduction in 2011, the concept of Industry 4.0 has been gradually studied, developed and implemented not only in Europe but worldwide. The Indonesian Ministry of Industry introduced a concept of Making Indonesia 4.0 in 2019 [7]. One emphasize of Making Indonesia 4.0 is greater automation in manufacturing technology to increase competitiveness.

Recently, the development and application of manufacturing industry technology in Indonesia have been rapidly increasing, as evidenced by the increasingly modern equipment used to work on a product, such as a CNC machine which is a machine that has been equipped with a computer to facilitate the operation of the machine [8][9]. In a few examples, computer technology has been applied to machine

* Corresponding Author. Phone: +62-8122439283
E-mail address: dalmasius@yahoo.com

doi: https://dx.doi.org/10.14203/j.mev.2019.v10.93-101

Accreditation Number: (RISTEKDIKTI) 1/E/KPT/2015 (Sinta 2).

tools including lathes, milling machines, scrap machines, and drilling machines [9][10]. The operation of the CNC machine uses a program that is controlled directly by a computer [10]. Hence, the operation of CNC machine tools works by synchronizing the computer and its mechanics [9].

Nowadays many industries have begun to abandon conventional machine tools and switch to using CNC machine tools. Quality and productivity aspects are the basic reasons computer-based production machines are widely adopted in the manufacturing industry [11]. Several attributes expected from modern CNC machine include better product quality produced in higher quantity with high speed and precision [12]. The process of synchronizing movements on the axis of motion requires an interpolator system that specifically divides the movements of each axis based on global movement commands which are manifested in the form of motion command signals to the drive system [13][14]. As technology develops, the CNC milling machine conditions must be measured to have reliable performance [14][15]. Afkhamifar *et al.* conducted research on the analysis of variations for the CNC milling process with results were compared with ISO 2768, a guidelines for general geometrical tolerances and technical drawings [16]. The study underlined that the precision of the machine can be improved either by better machine design or software development.

The quality of the results of machining processes is quantified by machining performance index which includes milling accuracy and surface quality [12]. The index is affected by the integrated operations of various factors namely CAD/CAM, CNC controller, servo control, feed drive system, and mechanical bodies [12]. Another possible effector which often neglected is probe hysteresis [17] and the subsequent deformation [18]. Improving machining precision has been a widely known challenge in industry as the CNC machine is composed of various moving and rotating shafts that makes machining motion complicated [19]. With regard to milling accuracy, the vibration of the mechanical bodies, sliding motion of stick, and axial motion affect precision [12]. To solve the vibration problem, a real-time resonance signal analysis coupled with online surface quality monitoring has been proposed [20]. Another study suggested kinematic modelling as a method to improve the precision of a multi axis CNC machine [19]. Analyzing the complex CNC machine motion has been one of the most important subjects in industrial machining study [19]. Thus, when the researchers at the Research Centre for Electrical Power and Mechatronics, Indonesian Institute of Sciences (RCEPM-LIPI) developed a CNC milling machine, it is important to analyze the machine motion to measure its precision.

In a previous study, Zaynawi and Bisono calibrated the X, Y, and Z-axis of the wood CNC router machine using a dial indicator and block gauge [8]. In another study, Wijaya performed calibration of the Y-axis to the accuracy of the workpiece on a 3-Axis CNC Router Machine [21]. With regard to the Z-axis, Nayorama, and Sedyono conducted a Z-axis analysis on the calibration process and the movement of the CNC router machine [22]. Fauzi *et al.* suggested that it is necessary to carry out measurements and analysis of data in every laboratory activity to make a conclusion [23]. Therefore the analysis of measurement uncertainty becomes very important [22][24].

From the above-mentioned previous studies, we found out that the respective researchers calibrated the machine that has been calibrated by the manufacturer, whereas in this study, the measurement was performed on a self-designed CNC milling machine developed at RCEPM-LIPI. The objective of this study was to investigate the precision of the CNC milling machine developed at RCEPM-LIPI by measuring how much the deviation of the machine measurement on the X, Y, and Z-axes. The measurement of machining deviation is important in analyzing machine accuracy [25]. The results of this study will serve as the basis for the next process which is calibration, and it is expected that the CNC machine will be able to operate in optimum precision during the manufacturing process.

II. Materials and Methods

A. Straightness checking

Several predictive methods for CNC milling machine maintenance to improve reliability and prevent faults and unnecessary loss have been introduced [26]. The methods include reliability statistics method, physical model-based method, and data-driven method. Reliability statistics method is the simplest method without any mathematical model or detailed information as the method depends on historical deviation data. The physical model-based method uses a mathematical model to predict the internal working mechanism through degradation prediction. The data-driven method is the most complicated method which can be performed online. The method is very suitable for complex and expensive equipment manufacturing such as in the aircraft industry. The CNC milling machine developed in RCEPM-LIPI is a simple machine intended for an inexpensive and easy operation in small and medium enterprises. Therefore the reliability statistics method was considered the most appropriate to assess its precision.

The workpiece surface is said to be flat or straight if the results of the measurement of the plane on the surface are straight lines in three-dimensional space as measured by the tangential contact between the tool and the workpiece surface [27]. This means that there are no deviations both horizontally and vertically on the measurement results for a certain distance. Straightness of the component surface is very important in machining such as lathes, scrap machines, milling machines, and grinding machines due to the work system requires a very precise level of straightness [28]. The skills to make the surface of the workpiece completely straight are also necessary, including how to check the straightness itself [24]. In order to measure the straightness/flatness, a straightness check of the X, Y, and Z-axis, as well as

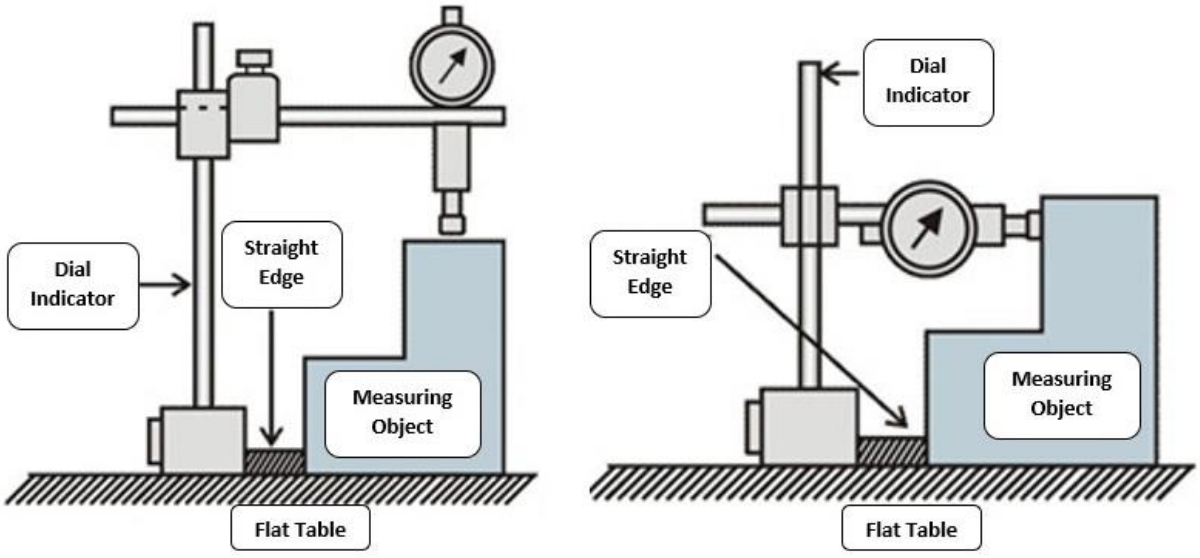

Figure 1. Straightness checking in (a) the horizontal deviation direction and (b) the vertical deviation direction

levelling checks of the machine table is performed by using a dial indicator, parallel plates, and a flat table [29].

The straightness/flatness check on the machine with a dial indicator was performed to understand the magnitude of the deviation. Any changes in the distance experienced by the dial indicator sensor will be designated by the pointer. In order to achieve accurate results, the measurements must be conducted on a flat working table [29]. It is necessary to insert a parallel plate/straight edge between the measuring plane and the dial indicator base to stabilize the dial indicator movement so that a change in the position of the sensor pressure on the measuring plane can be avoided. When placing the sensor on the measuring plane, the pointer should be set to zero. If the measuring plane is relatively long, it should be divided into several sections with the magnitude of the distance of each part being determined in advance. Between one part with another is marked by a dot or short line/strip. At each of these points, it can be described the magnitude of the deviation from the alignment of the measuring plane. Thus it can be known which parts of the measuring plane are not straight. The examples of straightness checks are shown in Figure 1. The direction of the horizontal deviation is shown in Figure 1 (a) and the direction of the vertical deviation is shown in Figure 1 (b). Figure 2 describes the deviation in the orthogonal axes, namely X-axis (X), Y-axis (Y), and Z-axis (Z). The deviation is defined as the distance between the nominal point (Pn) to the measurement point (Pm).

Measurement results and magnitude of deviations are usually illustrated in graphical form with a sign (+) for positive deviations or (-) for negative deviations. Deviations marked positive or negative are based on allowed threshold values. If the inspection result turns out to exceed the allowed threshold values, it can be said that the level of straightness of the measuring object is not good or low, regardless of whether the deviation is positive or

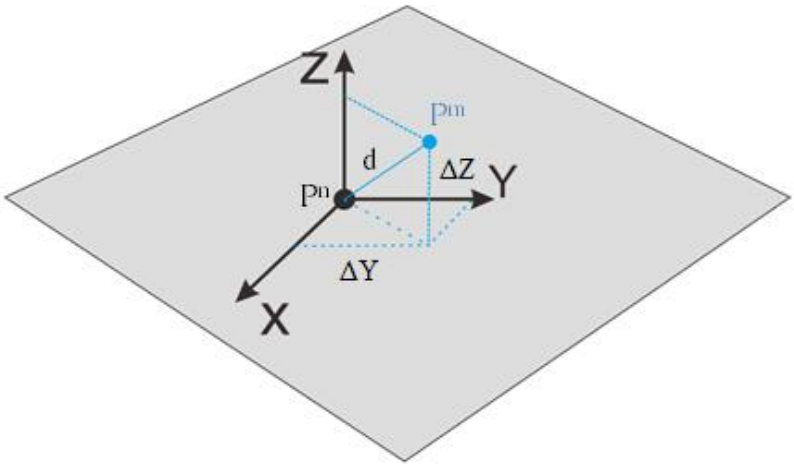

Figure 2. CNC milling machine deviation in the three axis (adapted from Werner, 2018 [25])

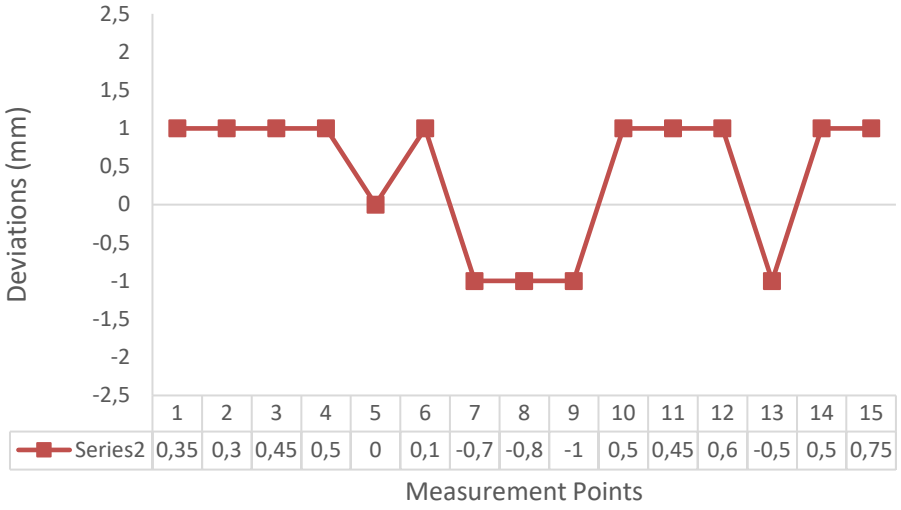

Figure 3. The results of the surface straightness check of the measurement object using the dial indicator

negative. An example of the results of the straightness checks in the form of a line graph is illustrated in Figure 3.

The above method is suitable for examining the relatively narrow side of the measuring plane and its longitudinal direction (the thick side of the measurement object). If the measuring plane is wide enough in the extended direction then the straightness check can be carried out several times in different positions according to more favourable considerations in the measurement process. Therefore, the examination is not only on one line but can be more than one line [23].

B. Object specifications, instruments, and measurement methods

The measurement object is a prototype 3-axis CNC milling machine developed by RCEPM-LIPI (Figure 4). This CNC milling machine has the following specifications:

- Maximum spindle speed = 12,000 rpm.
- Stroke of the X-axis = 180 mm, Y-axis = 160 mm and Z-axis = 200 mm.
- Servo motor power used for X, Y, and Z axes = 400 W.
- The maximum diameter of the chisel can be used on a spindle = 6 mm.
- Maximum workpiece material = aluminium.

While the equipment used in this measurement process is as follows:

- Parallel Plates or flat part of the machine on the horizontal and vertical sides.
- Clamping.
- Dial Indicator with a level of accuracy of 0.05 mm.

Dial indicator or dial gauge is used to measure bending, run out, slackness, end play, backlash, and flatness. Inside the dial indicator, there is a mechanism that can magnify the small movements. When the spindle moves along the measured surface, the movement is enlarged by a magnifying mechanism and indicated by the pointer. The procedure for using the dial indicator is as follows:

- The spindle dial indicator position must be perpendicular to the measured surface.
- The line of imagination from the measuring eye to the pointer must be perpendicular to the dial indicator surface while reading the measurement results.
- The dial indicator must be installed carefully mounted on the supporting rod, meaning that the dial indicator must not shake.
- Turn the outer ring and set it to zero. Move the spindle up and down, then check that the pointer always returns to zero after the spindle is released.
- Observe and record the changes that occur in the indicator dial pointer for each measurement point, which is every 15 mm.

Figure 4. The prototype of 3-axis CNC milling machine developed at RCEPM-LIPI

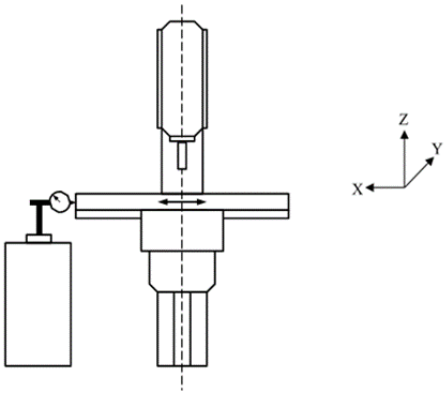

Figure 5. The deviation measurement scheme on the X-axis [10]

If the measurement has been completed up to 13 times or the last point, then return the dial indicator position to its original position by moving in the direction of the X-axis, Y-axis, or Z-axis being measured.

III. Results and Discussions

A. X-axis measurements

The measurement process on the CNC milling machine designed and developed at RCEPM-LIPI was carried out on its three axes, namely the X, Y, and Z axes. The data collection scheme on the X-axis is shown in Figure 5. X-axis measurement was carried out 3 times where each process was performed by measuring 12 measurement points. The X-axis measurement results are displayed in tabular and graphical form as shown in Table 1 and Figure 6. Table 1 and Figure 6 show that the maximum deviation on the X axis is -0.183 mm at the second test point. The smallest deviation is at the testing points 1 and 9 that are -0,017 mm. The average deviation is -0,033 mm. The minus sign means the measured area is away from the indicator needle while the positive sign means the measured field is close to the indicator needle.

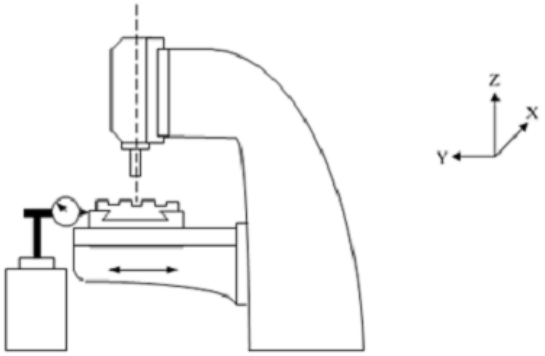

Figure 7. The deviation measurement scheme on the Y-axis [10]

Compared with previous studies, the results in this study were lower than a study by Afkhamifar *et al.* whose X-axis position error was 0.134 mm at average value [16] and within the range of acceptable deviation which a reference suggested between -0.030 mm to +0.045 mm [25]. However compared to the higher precision of CNC machine with laser measurement system, the average deviation is higher [24].

B. Y-axis measurements

The process of measuring a CNC milling machine using the indicator dial on the Y-axis is illustrated in Figure 7. Y-axis measurement was carried out 3 times where each measurement was performed on 10 points. Y-axis measurement results are shown in Table 2 and Figure 8. As described in Table 2 and Figure 8, the maximum deviation on the Y axis is -0,300 mm at the fourth test point. The smallest deviation is at the second test point of -0,033 mm. The average deviation is -0,102 mm. The minus sign means the measured area is away from the indicator needle, while the positive sign means the measured field is close to the indicator needle. The deviation in Y-axis is greater than the previous studies which reported an average deviation on Y-axis is 0.056 mm [16].

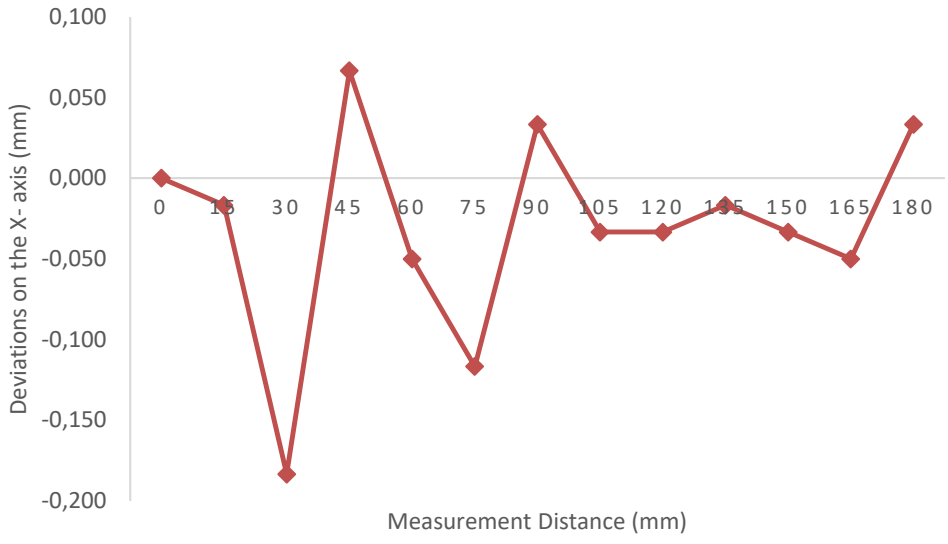

Figure 6. X-axis deviation graph

Table 1.
X-axis measurements results

NO	Measurement Distance (mm)	Deviations (mm)			Average Deviation (mm)
		1	2	3	
	0	0,00	0,00	0,00	0,000
1	15	-0,15	0,20	-0,10	-0,017
2	30	-0,30	-0,15	-0,10	-0,183
3	45	0,25	0,15	-0,20	0,067
4	60	-0,15	0,10	-0,10	-0,050
5	75	-0,10	-0,15	-0,10	-0,117
6	90	-0,15	0,10	0,15	0,033
7	105	0,10	-0,10	-0,10	-0,033
8	120	-0,10	0,15	-0,15	-0,033
9	135	-0,15	0,20	-0,10	-0,017
10	150	-0,20	0,20	-0,10	-0,033
11	165	-0,15	-0,15	0,15	-0,050
12	180	0,10	0,10	-0,10	0,033
Average					**-0,033**

Table 2.
Y-axis measurements results

NO	Measurement Distance (mm)	Deviations (mm)			Average Deviation (mm)
		1	2	3	
	0	0,00	0,00	0,00	0,000
1	15	-0,20	0,40	-0,30	-0,033
2	30	-0,20	-0,10	-0,25	-0,183
3	45	0,20	0,15	-0,15	0,067
4	60	-0,25	-0,25	-0,40	-0,300
5	75	-0,15	-0,25	-0,25	-0,217
6	90	-0,35	0,25	0,25	0,050
7	105	0,20	-0,25	-0,15	-0,067
8	120	-0,15	0,15	-0,35	-0,117
9	135	-0,35	0,20	-0,25	-0,133
10	150	-0,25	0,20	-0,20	-0,083
Average					**-0,102**

C. Z-axis measurements

The measurement scheme of the CNC milling machine on the Z-axis is illustrated in Figure 9. The measurements on the Z-axis were carried out 3 times wherein each process measurements were made of 10 points. The Z-axis measurement results are shown in Table 3 and Figure 10.

Table 3 and Figure 10 present the measurement results of the deviation on the Z-axis. The maximum deviation on the Z-axis is -0.233 mm at the sixth point test. The smallest deviation is at the ninth test point which is equal to 0 mm. The average deviation is -0,063 mm. A minus sign means the measured area is away from the indicator needle, while the positive sign means the measured field is close to the indicator needle. The average deviation of the Z-axis is larger than the previous study which resulted in a deviation on the Z-axis of -0.021 mm [16], and much larger than the previous study using laser measuring system whose largest deviation on the Z-axis is only 0.004 mm [24].

D. Flatness of the machine base table

In addition to measuring the straightness of the three working axes of the CNC milling machine designed at RCEPM-LIPI, a measurement process was also carried out on the flat table base of the machine. The scheme that shows data collection from the measurement of the flatness of the machine table is depicted in Figure 11. The measurement of the machine table flatness was also carried out 3 times with each process measuring 10 points. The CNC milling machine table measurement results are shown in Table 4 and Figure 12.

Table 4 and Figure 12 show that the maximum deviation on the X axis is -0.217 mm at the eleventh point test of 165 mm measurement distance. The smallest deviation is at the third test point at a measurement distance of 45 mm which is equal to 0.033 mm. The average deviation is -0.096 mm. A minus sign means the measured area is away from the indicator needle, while the positive sign means the measured field is close to the indicator needle.

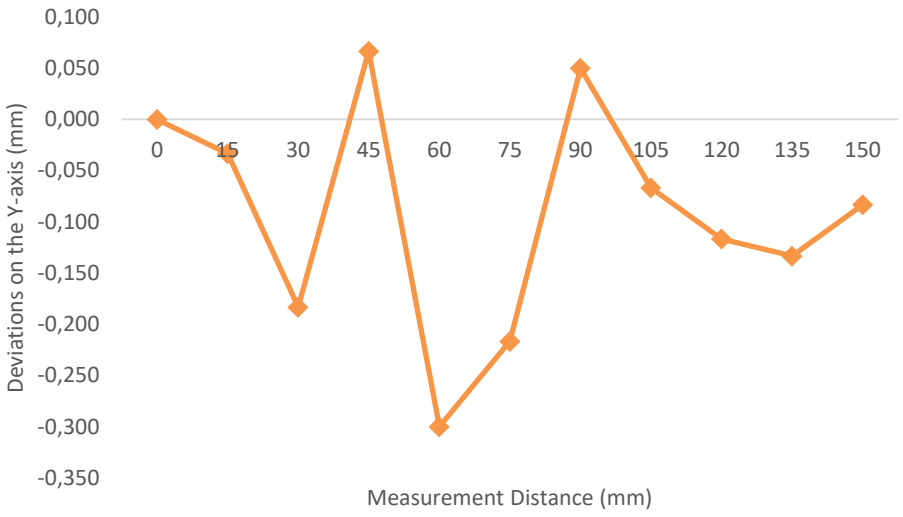

Figure 8. Y-axis deviation graph

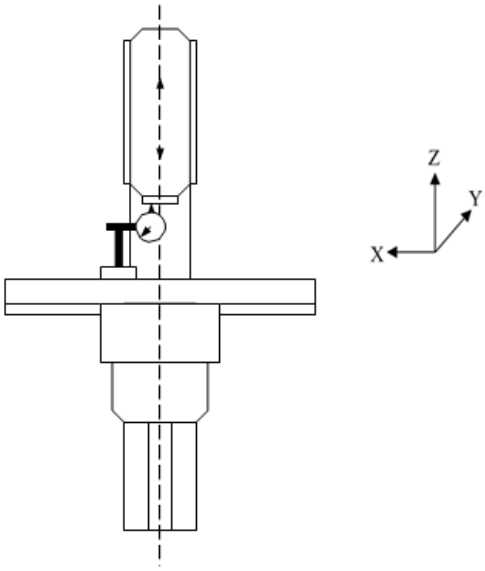

Figure 9. The deviation measurement scheme on the Z-axis [10]

Figure 11. Test scheme on the machine table

From the X, Y, Z, and flatness measurements, it is known that the deviation values: the average X axis deviation is -0.033 mm, Y -0.102 mm axis, Z -0,063 mm, and -0.096 mm flatness, respectively. The value of the deviation is still within the limits of the tolerance standard set at ISO 2768. These results are almost the same compared to previous studies conducted by Afkhamifar *et al.* where in his research it was found that the results of the X, Y, and Z axis deviations were 0.134 mm, 0.056 mm, and -0.021 mm, respectively [16].

While the results are acceptable based on ISO 2768 standard, the deviation at Y-axis and Z-axis are relatively greater than the comparable previous study which indicates an improvement for the developed CNC milling machine is necessary. There are several possible causes which resulted in inaccuracies in this study as suggested by the previous study [16]. The first possibility comes from the machine table which plays a role as a base. The second possibility comes from the upper body of the machine. The third possibility comes from the head and the last possibility comes from the interaction between the base and the workpiece. These shortcomings require a better machine design as suggested by the previous study [16]. Other solutions include a better software implementation [16][29], more complex yet reliable mathematical modelling [30], or more precise sensors such as real-time vibration monitoring [20], transducer in a kinematic probe [17], or laser measurement systems [24]. Furthermore, as a technology driven product research, the design and development phase of CNC milling machine often overlook the interdisciplinary approach, especially from industrial and human factors studies [31]. The machine design without consideration of the human factors often leads to human error and operation faults in addition to the limited technical performance of machine technology.

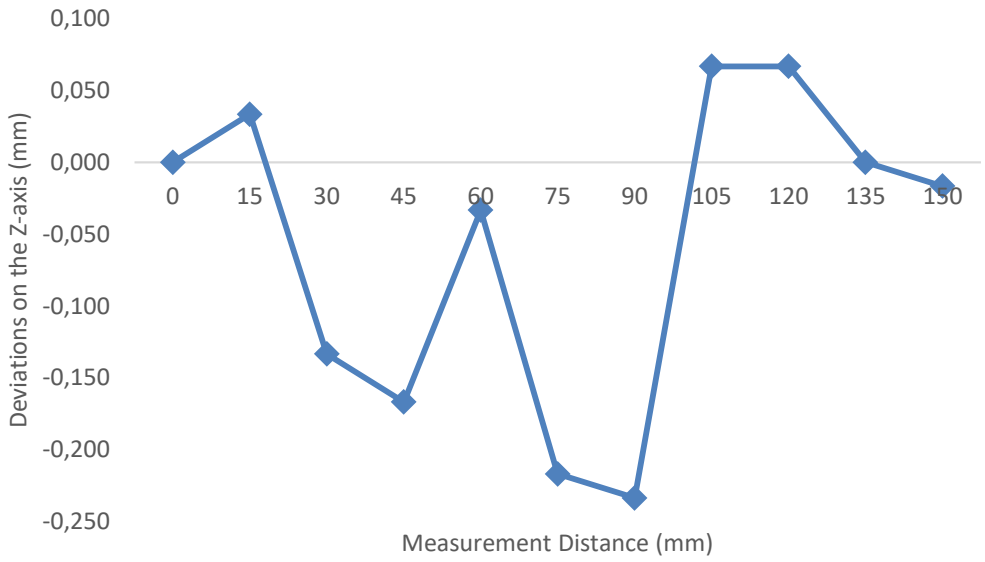

Figure 10. Z-axis deviation graph

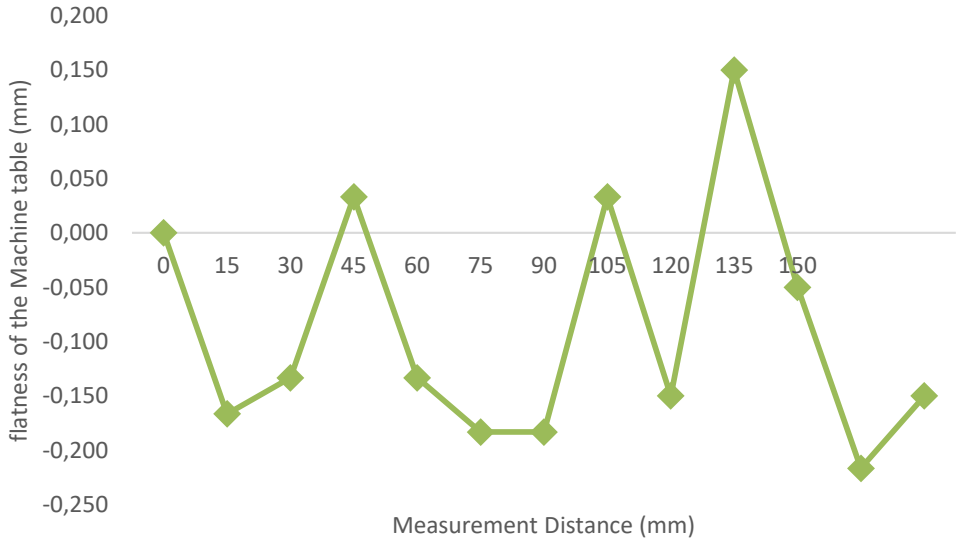

Figure 12. Machine table flatness deviation graph

Table 3.
Z-axis measurements results

NO	Measurement Distance (mm)	Deviations (mm)			Average Deviation (mm)
		1	2	3	
	0	0,00	0,00	0,00	0,000
1	20	0,15	-0,15	0,10	0,033
2	40	-0,10	-0,10	-0,20	-0,133
3	60	-0,15	-0,15	-0,20	-0,167
4	80	0,25	-0,15	-0,20	-0,033
5	100	-0,15	-0,25	-0,25	-0,217
6	120	-0,20	-0,25	-0,25	-0,233
7	140	-0,15	0,15	0,20	0,067
8	160	0,15	-0,15	0,20	0,067
9	180	0,10	0,15	-0,25	0,000
10	200	-0,15	0,25	-0,15	-0,017
Average					**-0,063**

Table 4.
Machine table flatness measurement results

NO	Measurement Distance (mm)	Deviations (mm)			Average Deviation (mm)
		1	2	3	
	0	0,00	0,00	0,00	0,000
1	20	0,15	-0,15	0,10	0,033
2	40	-0,10	-0,10	-0,20	-0,133
3	60	-0,15	-0,15	-0,20	-0,167
4	80	0,25	-0,15	-0,20	-0,033
5	100	-0,15	-0,25	-0,25	-0,217
6	120	-0,20	-0,25	-0,25	-0,233
7	140	-0,15	0,15	0,20	0,067
8	160	0,15	-0,15	0,20	0,067
9	180	0,10	0,15	-0,25	0,000
10	200	-0,15	0,25	-0,15	-0,017
Average					**-0,063**

IV. Conclusion

The measurement results of the CNC Milling machine developed at RCEPM-LIPI in Bandung show that the CNC milling machines have deviations on each axis, including the X-axis of 0.033 mm, the Y-axis of 0.102 mm, the Z-axis of 0.063 mm, and flatness of the table 0.096 mm, respectively. The results are within the acceptable performance limits required by ISO 2768. Based on these measurements, this CNC milling machine can be used for machining work processes that can move together on 3 axes namely X, Y, and Z axes where the machine can be used to make components that have tolerances above 0.1 mm. However, future manufacturing needs may require higher precision and the developed CNC milling machine still has quite high inaccuracy compared to some previous studies. The application of Industry 4.0 concept as well as more sophisticated sensors, mathematical modelling, data processing, and software are necessary for future study.

Declarations

Author contribution

All authors contributed equally as the main contributor of this paper. All authors read and approved the final paper.

Funding statement

This research did not receive any specific grant from funding agencies in the public, commercial, or not-for-profit sectors.

Conflict of interest

The authors declare no conflict of interest.

Additional information

No additional information is available for this paper.

References

[1] J. Qin, Y. Liu, and R. Grosvenor, "A categorical framework of manufacturing for industry 4.0 and beyond," in *Procedia CIRP*, vol. 52, pp. 173-178, 2016.

[2] Z. Li, Y. Wang, and K. S. Wang, "Intelligent predictive maintenance for fault diagnosis and prognosis in machine

centers: Industry 4.0 scenario," *Adv. Manuf.*, vol. 5, no. 4, pp. 377-387, 2017.
[3] L. Li, C. Li, Y. Tang, and Q. Yi, "Influence factors and operational strategies for energy efficiency improvement of CNC machining," *J. Clean. Prod.*, vol. 161, pp. 220-238, 2017.
[4] B. Bagheri, S. Yang, H. A. Kao, and J. Lee, "Cyber-physical systems architecture for self-aware machines in industry 4.0 environment," in *IFAC-PapersOnLine*, 2015, vol. 28, no. 3, pp. 1622-1627.
[5] T. K. Sung and B. Carlsson, "The evolution of a technological system: The case of CNC machine tools in Korea," *J. Evol. Econ.*, vol. 13, no. 4, pp. 435-460, 2003.
[6] A. Theorin et al., "An event-driven manufacturing information system architecture for Industry 4.0," *Int. J. Prod. Res.*, vol. 55, no. 5, pp. 1297-1311, 2017.
[7] I. M. of Industry, "Making Indonesia 4.0," 2019.
[8] Zaynawi, B. Wiro. K, and F. Bisono, "Proses Kalibrasi Sumbu X, Y, Dan Z Pada Mesin CNC Router Kayu 3 Axis Menggunakan Alat Bantu Dial Indicator dan Block Gauge " *in 1st Conference on Design and Manufacture and Its Aplication*, pp. 350-356, 2018.
[9] P. Saputra, A. Muqorobin, A. Santoso, and T. P. Purwanto, "Desain dan Implementasi Sistem Kendali CNC Router Menggunakan PC untuk Flame Cutting Machine," *J. Mechatronics, Electr. Power, Veh. Technol.*, vol. 2, no. 1, p. 41, 2012.
[10] M. Amala and S. A. Widyanto,. "Pengembangan Perangkat Lunak Sistem Operasi Mesin Milling Cnc Trainer," *J. Tek. Mesin*, vol. 2, no. 3, pp. 204-210, 2014.
[11] E. Y. Elvys and Sirama, "Peningkatan Keakurasian Gerakan Pada Protoype Mesin CNC Milling 3-Axis," *Proceeding Semin. Nas. Tah. Tek. Mesin XIV, (SNTTM XIV),* pp. 7-8, 2015.
[12] H. W. Chiu and C. H. Lee, "Prediction of machining accuracy and surface quality for CNC machine tools using data driven approach," *Adv. Eng. Softw.*, vol. 114, pp. 246-257, 2017.
[13] H. Yanuar, A. Syarief, and A. Kusairi, "Pengaruh Variasi Kecepatan Potong Dan Kedalaman Pemakanan Terhadap Kekasaran Permukaan Dengan Berbagai Media Pendingin Pada Proses Frais Konvensional," *Tek. Mesin Unlam*, vol. 03, no. 1, pp. 27-33, 2014.
[14] Syahriza, T. Firsa, and M. Ibrahim, "Rancang Bangun Mesin CNC 4 Axis Berbasis PC (Personal Computer)," J. *Tek. Mesin Unsyiah*, vol. 3, no. 2, pp. 75-79, 2015.
[15] Hendra, Sutarmadi, A. Indriani, and Hernadewita, "Jenis material pahat potong dan run out terhadap kekasaran permukaan benda kerja silinder pada proses bubut," *J. Mek.*, vol. 4, no. 2, pp. 376-385, 2013.
[16] A. Afkhamifar, D. Antonelli, and P. Chiabert, "Variational Analysis for CNC Milling Process," in *Procedia CIRP*, vol. 43, pp. 118-123, 2016.
[17] A. Wozniak and M. Jankowski, "Variable speed compensation method of errors of probes for CNC machine tools," *Precis. Eng.*, vol. 49, pp. 316–321, 2017.
[18] D. WU et al., "Machining fixture for adaptive CNC machining process of near-net-shaped jet engine blade," *Chinese J. Aeronaut.*, 2019.
[19] B. Yang, G. Zhang, Y. Ran, and H. Yu,"Kinematic modeling and machining precision analysis of multi-axis CNC machine tools based on screw theory," *Mech. Mach. Theory*, vol. 140, pp. 538-552, 2019.
[20] E. García Plaza, P. J. Núñez López, and E. M. Beamud González, "Efficiency of vibration signal feature extraction for surface finish monitoring in CNC machining," *J. Manuf. Process.*, vol. 44, pp. 145-157, 2019.
[21] F. W. Putra, "Kalibrasi Sumbu Y Terhadap Ketelitian Benda Kerja Pada Mesin Cnc Router 3 Axis," 2016.
[22] F. N. W.K, "Naskah Publikasi Analisa Sumbu Z Pada Proses Kalibrasi Dan Pergerakan Mesin CNC Router," *Universitas Muhammadiyah Surakarta (UMS)*, 2016.
[23] A. Fauzi, E. Wiyono, and S. Budiawanti, "Pengembangan Model Praktikum Fisika Berbasis Analisis Ketidakpastian Pengukuran," *J. Mater. dan Pembelajaran Fis.*, vol. 3, no. 2, pp. 27-32, ISSN: 2089-6158, 2013.
[24] S. Ekinovic, H. Prcanovic, and E. Begovic, "Calibration of machine tools by means of laser measuring systems,"" *Asian Trans. Eng.*, vol. 02, no. 06, pp. 17-21, 2013.
[25] A. Werner, "Improving the accuracy of free-form surface machining on CNC milling machines," *Mechanik*, vol. 91, no. 12, pp. 1100–1103, 2018.
[26] C. Ahilan, S. Kumanan, N. Sivakumaran, and J. Edwin Raja Dhas, "Modeling and prediction of machining quality in CNC turning process using intelligent hybrid decision making tools," *Appl. Soft Comput. J.*, vol. 13, no. 3, pp. 1543–1551, 2013.
[27] G. L. Samuel and M. S. Shunmugam, "Evaluation of Straightness and Flatness Error Using Computational Geometric Techniques," *Comput. Des.*, vol. 31, pp. 829–843, 1999.
[28] V. P. Astakhov, "Machining of hard materials - Definitions and industrial applications," in *Machining of Hard Materials*, London: Springer, pp. 1–32, 2011.
[29] J.-S. Chen, "Computer-aided accuracy enhancement," *Int. J. Mach. Tools Manuf.*, vol. 35, no. 4, pp. 593-605, 1995.
[30] L. Mironova and L. Kondratenko, "Mathematical modeling of the processing of holes on CNC machines," in *Materials Today: Proceedings*, vol. 19, pp. 2354-2357, 2019.
[31] X. Yang, X. Zhou, and K. Cheng, "Research on Morphology and Semantics of Industrial Design for CNC Machine Tools," in *Procedia Manufacturing*, vol. 17, pp. 379-386, 2018.

e-ISSN 2088-6985
p-ISSN 2087-3379

Journal of Mechatronics, Electrical Power, and Vehicular Technology

Volume 10, 2019

AUTHORS INDEX

The articles in this volume were authored/co-authored by 40 authors from Australia, Indonesia, Taiwan, Italy, Japan, and United Kingdom.

Achmad Praptijanto, "Vehicular networking and computer vision-based distance estimation for VANET application using Raspberry Pi 3," 10(1):7-16

Ahmad Rajani, "Three axis deviation analysis of CNC milling machine," 10(2):93-101

Anik Nur Handayani, "Smart grid photovoltaic system pilot scale using sunlight intensity and state of charge (SoC) battery based on Mamdani fuzzy logic control," 10(1):36-47

Ari Priharta, "Smart grid photovoltaic system pilot scale using sunlight intensity and state of charge (SoC) battery based on Mamdani fuzzy logic control," 10(1):36-47

Benyamin Kusumoputro, "Sensorless-BLDC motor speed control with ensemble Kalman filter and neural network," 10(1):1-6

Budi Azhari, "Quasi-flat linear PM generator optimization using simulated annealing algorithm for WEC in Indonesia," 10(1):29-35

Cecilia Stevany, "The effect of lightning impulse characteristics and line arrester to the lightning protection performance on 150 kV overhead lines:ATP-EMTP computational approach," 10(2):49-59

Christian Asri Wicaksana, "Exhaust emissions analysis of gasoline motor fueled with corncob-based bioethanol and RON 90 fuel mixture," 10(1):24-28

Dalmasius Ganjar Subagio, "Three axis deviation analysis of CNC milling machine," 10(2):93-101

Dian Andriani, "Smart Grid communication applications: measurement equipment and networks architecture for data and energy flow," 10(2):73-84

Didik Nurhadi, "Exhaust emissions analysis of gasoline motor fueled with corncob-based bioethanol and RON 90 fuel mixture," 10(1):24-28

Febrizal, "The effect of lightning impulse characteristics and line arrester to the lightning protection performance on 150 kV overhead lines:ATP-EMTP computational approach," 10(2):49-59

Feri Yusivar, "Sensorless-BLDC motor speed control with ensemble Kalman filter and neural network," 10(1):1-6

Firdaus, "The effect of lightning impulse characteristics and line arrester to the lightning protection performance on 150 kV overhead lines:ATP-EMTP computational approach," 10(2):49-59

Francisco Danang Wijaya, "Quasi-flat linear PM generator optimization using simulated annealing algorithm for WEC in Indonesia," 10(1):29-35

Fri Murdiya, "The effect of lightning impulse characteristics and line arrester to the lightning protection performance on 150 kV overhead lines:ATP-EMTP computational approach," 10(2):49-59

Giambattista Gruosso, "Vehicular networking and computer vision-based distance estimation for VANET application using Raspberry Pi 3," 10(1):7-16

Havel Alindo Sano, "The effect of lightning impulse characteristics and line arrester to the lightning protection performance on 150 kV overhead lines:ATP-EMTP computational approach," 10(2):49-59

Hendri Maja Saputra, "Three axis deviation analysis of CNC milling machine," 10(2):93-101

Kadek Heri Sanjaya, "Three axis deviation analysis of CNC milling machine," 10(2):93-101

Kamil Faqih, "Smart grid photovoltaic system pilot scale using sunlight intensity and state of charge (SoC) battery based on Mamdani fuzzy logic control," 10(1):36-47

Ketut Wirtayasa, "Load characteristic analysis of a double-side internal coreless stator axial flux PMG," 10(1):17-23

Kohei Arai, "Smart grid photovoltaic system pilot scale using sunlight intensity and state of charge (SoC) battery based on Mamdani fuzzy logic control," 10(1):36-47

Kriya Mateeke Moses, "Exhaust emissions analysis of gasoline motor fueled with corncob-based bioethanol and RON 90 fuel mixture," 10(1):24-28

Mikecon Cenit, "Design and development of the sEMG-based exoskeleton strength enhancer for the legs," 10(2):61-71

Mostafa Nazih, "Safety assessment of high voltage substation earthing systems with synthetic geotextile membrane," 10(2):85-91

Muhammad Alfian Mizar, "Exhaust emissions analysis of gasoline motor fueled with corncob-based bioethanol and RON 90 fuel mixture," 10(1):24-28

Muhammad Fathul Hikmawan, "Load characteristic analysis of a double-side internal coreless stator axial flux PMG," 10(1):17-23

Muhammad Kasim, "Load characteristic analysis of a double-side internal coreless stator axial flux PMG," 10(1):17-23

Muhammad Rif'an, "Sensorless-BLDC motor speed control with ensemble Kalman filter and neural network," 10(1):1-6

Mulia Pratama, "Vehicular networking and computer vision-based distance estimation for VANET application using Raspberry Pi 3," 10(1):7-16

Pudji Irasari, "Load characteristic analysis of a double-side internal coreless stator axial flux PMG," 10(1):17-23

Puji Widiyanto, "Load characteristic analysis of a double-side internal coreless stator axial flux PMG," 10(1):17-23

Ridwan Arief Subekti, "Three axis deviation analysis of CNC milling machine," 10(2):93-101

Rudi Darussalam, "Smart Grid communication applications: measurement equipment and networks architecture for data and energy flow," 10(2):73-84

Tinton Dwi Atmaja, "Smart Grid communication applications: measurement equipment and networks architecture for data and energy flow," 10(2):73-84

Vaibhav Gandhi, "Design and development of the sEMG-based exoskeleton strength enhancer for the legs," 10(2):61-71

Wahyu Primadi, "Smart grid photovoltaic system pilot scale using sunlight intensity and state of charge (SoC) battery based on Mamdani fuzzy logic control," 10(1):36-47

Widiyanti, "Exhaust emissions analysis of gasoline motor fueled with corncob-based bioethanol and RON 90 fuel mixture," 10(1):24-28

Widodo Budi Santoso, "Vehicular networking and computer vision-based distance estimation for VANET application using Raspberry Pi 3," 10(1):7-16

e-ISSN 2088-6985
p-ISSN 2087-3379

Journal of Mechatronics, Electrical Power, and Vehicular Technology

Volume 10, 2019

AFFILIATION INDEX

Bachelor Program, Department of Mechanical Engineering, State University of Malang, Malang, INDONESIA	24
Building, Infrastructure and Advanced Facilities, Jacobs, Melbourne, AUSTRALIA	85
Department of Design Engineering and Mathematics, Middlesex University London, London, UNITED KINGDOM	61
Department of Electrical Engineering and Information Technology, Engineering Faculty, Universitas Gadjah Mada, D.I. Yogyakarta, INDONESIA	29
Department of Electrical Engineering, Faculty of Engineering, Universitas Riau, Pekanbaru, INDONESIA	49
Department of Electrical Engineering, National Taiwan University of Science and Technology, Taipei, TAIWAN	17
Department of Electrical Engineering, Universitas Indonesia, Depok, INDONESIA	1
Department of Electrical Engineering, Universitas Negeri Jakarta, Jakarta, INDONESIA	1
Department of Electronics, Informatics and Bioengineering, Politecnico di Milano, Milano, ITALY	7
Department of Information Science, Saga University, Saga, JAPAN	36
Department of Mechanical Engineering, State University of Malang, Malang, INDONESIA	24
Electrical Engineering Postgraduate, Electrical engineering Department, Universitas Negeri Malang, Malang, INDONESIA	36
Graduate school of technological and vocational education, National Yunlin University of Science and Technology, Yunlin, TAIWAN	24
Research Centre for Electrical Power and Mechatronics, Indonesian Institute of Sciences (LIPI), Bandung, INDONESIA	7, 17, 29, 73, 93
Research Unit for Clean Technology, Indonesian Institute of Science (LIPI), Bandung, INDONESIA	73
School of Electrical Engineering and Telecommunications, University of New South Wales, New South Wales, AUSTRALIA	17

e-ISSN 2088-6985
p-ISSN 2087-3379

Journal of Mechatronics, Electrical Power, and Vehicular Technology

INTERNATIONAL PEER REVIEWERS ACKNOWLEDGEMENT

The Editor of MEV would like to thank the wisdom and advice of many individuals who dedicated their considerable time and expertise in safeguarding the quality and high standard of academic integrity of the journal.

We are greatly indebted to the expertise, dedication, and expeditious response of the following individuals for reviewing at least one and, in some cases, many manuscripts for the journal from early 2010 until today.

Prof. Ir. Jamasri, Ph.D.
Department of Mechanical and Industrial Engineering, Gadjah Mada University
Jl. Grafika No. 2, Yogyakarta, 55281, INDONESIA

Prof. Dr. Ir. Suhono H Supangkat, M.Eng., CGEIT.
School of Electrical Engineering and Informatics, Institut Teknologi Bandung
Jl. Ganesha No. 10, Bandung 40135, INDONESIA

Prof. Dr. Ir. Zainal Abidin
Mechanical and Aerospace Engineering, Institut Teknologi Bandung
Jl. Ganesha No. 10, Bandung 40135, INDONESIA

Prof. Dr. Ir. R. Danardono Agus Sumarsono, DEA., PE.
Department of Mechanical Engineering, University of Indonesia
Kampus UI Depok 16424
Depok, Jawa Barat, INDONESIA

Prof. Sasongko Pramono Hadi
Department of Electrical Engineering, Gadjah Mada University
Jl. Grafika No. 2, Yogyakarta 55281, INDONESIA

Ocktaeck Lim, Ph.D.
School of Mechanical Engineering
University of Ulsan
Daehakro 93, Nam-gu
44610 Ulsan,
KOREA, REPUBLIC OF

Prof. Juan Carlos Alvarez
Dept. Electrical Engineering,
University of Oviedo
Calle San Francisco, 1, 33003
Oviedo, Asturias, SPAIN

Prof. Dr. Murat Lüy
Department of Electrical and Electronic Engineering, Kirikkale Universitesi
Kırıkkale Üniversitesi, Ankara Yolu 7. Km, 71450
Yahşihan/Kırıkkale, TURKEY

Dr. Ir. Iman K Reksowardojo
Mechanical and Aerospace Engineering, Institut Teknologi Bandung
Jl. Ganesha No. 10, Bandung 40135, INDONESIA

Dr. Yuliadi Erdani
Politeknik Manufaktur Bandung
Jl. Kanayakan No. 21 Dago,
Bandung – 40135, INDONESIA

Dr. Larissa Lorenz
Bauhaus Luftfahrt e.V,
Lyonel-Feininger-Str. 28, 80807
Munchen, GERMANY

Dr. Si Steve Li
Electromechanical System Development, General Electric Global Research Centre
610 London Square Drive, Clifton Park, NY12065, UNITED STATES

Ir. Arko Djajadi, Ph.D.
Swiss German University
EduTown BSD City – Tangerang
15339, INDONESIA

Prof. István Patkó
Óbuda University, Budapest,
6. Doberdó str., Budapest H-1034
HUNGARY

Ahmad Agus Setiawan, S.T., M.Sc., Ph.D.
Department of Engineering Physics, Faculty of Engineering, Gadjah Mada University
Jl. Grafika No.2, Yogyakarta 55281, INDONESIA

Dr. Ir. Edi Leksono, M.Eng.
Engineering Physics, Institut Teknologi Bandung
Jl. Ganesha No. 10, Bandung 40135, INDONESIA

Dr. Irhan Febijanto
The Agency for the Assesment and Application of Technology
Kawasan Puspiptek Serpong
Tangerang Selatan, INDONESIA

Ir. Endra Joelianto, Ph.D.
Engineering Physics, Institut Teknologi Bandung
Jl. Ganesha No. 10, Bandung 40135, INDONESIA

Dr. Narankhuu Jamsran
Thomas Air LLC, Mongolia
"Tushig" center 204, Seoul Street-23, 4th Khoroo, Sukhbaatar district, Ulaanbaatar, MONGOLIA

Aji Prasetya Wibawa, Ph.D.
Dept of Electrical Engineering,
State University of Malang
Jl. Semarang No. 5, Malang, Jawa Timur, INDONESIA

e-ISSN 2088-6985
p-ISSN 2087-3379

PUBLICATION ETHICS AND MALPRACTICE STATEMENT

Journal of Mechatronics, Electrical Power, and Vehicular Technology (hence MEV) is a journal aims to be a leading international peer-reviewed platform and an authoritative source of information. We publish original research papers, review articles and case studies focused on mechatronics, electrical power, and vehicular technology as well as related topics that has neither been published elsewhere in any language, nor is it under review for publication anywhere. This following statement clarifies ethical behavior of all parties involved in the act of publishing an article in this journal, including the author, the editor, the reviewer, and the publisher (Research Centre for Electrical Power and Mechatronics – Indonesian Institute of Sciences). This statement is based on COPE's Best Practice Guidelines for Journal Editors.

DUTIES OF AUTHORS

1. **Reporting Standards:** Authors should present an accurate account of the original research performed as well as an objective discussion of its significance. Researchers should present their results honestly and without fabrication, falsification or inappropriate data manipulation. A manuscript should contain sufficient detail and references to permit others to replicate the work. Fraudulent or knowingly inaccurate statements constitute unethical behavior and are unacceptable. Manuscripts should follow the submission guidelines of the journal.
2. **Originality and Plagiarism:** Authors must ensure that they have written entirely original work. The manuscript should not be submitted concurrently to more than one publication unless the editors have agreed to co-publication. Relevant previous work and publications, both by other researchers and the authors' own, should be properly acknowledged and referenced. The primary literature should be cited where possible. Original wording taken directly from publications by other researchers should appear in quotation marks with the appropriate citations.
3. **Multiple, Redundant, or Concurrent Publications:** Author should not in general submit the same manuscript to more than one journal concurrently. It is also expected that the author will not publish redundant manuscripts or manuscripts describing same research in more than one journal. Submitting the same manuscript to more than one journal concurrently constitutes unethical publishing behavior and is unacceptable. Multiple publications arising from a single research project should be clearly identified as such and the primary publication should be referenced
4. **Acknowledgement of Sources:** Authors should acknowledge all sources of data used in the research and cite publications that have been influential in influential in determining the nature of the reported work. Proper acknowledgment of the work of others must always be given.
5. **Authorship of the Paper:** The authorship of research publications should accurately reflect individuals' contributions to the work and its reporting. Authorship should be limited to those who have made a significant contribution to conception, design, execution or interpretation of the reported study. Others who have made significant contribution must be listed as co-authors. In cases where major contributors are listed as authors while those who made less substantial, or purely technical, contributions to the research or to the publication are listed in an acknowledgement section. Authors also ensure that all the authors have seen and agreed to the submitted version of the manuscript and their inclusion of names as co-authors.
6. **Disclosure and Conflicts of Interest:** All authors should clearly disclose in their manuscript any financial or other substantive conflict of interest that might be construed to influence the results or interpretation of their manuscript. All sources of financial support for the project should be disclosed.
7. **Fundamental Errors in Published Works:** If the author discovers a significant error or inaccuracy in the submitted manuscript, then the author should promptly notify the journal editor or publisher and cooperate with the editor to retract or correct the paper.
8. **Hazards and Human or Animal Subjects:** The author should clearly identify in the manuscript if the work involves chemicals, procedures or equipment that have any unusual hazards inherent in their use.

DUTIES OF EDITOR

1. **Publication Decisions:** Based on the review report of the editorial board, the editor can accept, reject, or request modifications to the manuscript. The validation of the work in question and its importance to researchers and readers must always drive such decisions. The editors may be guided by the policies of the journal's editorial board and constrained by such legal requirements as shall then be in force regarding libel, copyright infringement and plagiarism. The editors may confer with other editors or reviewers in making this decision. Editors have to take responsibility for everything they publish and should have procedures

and policies in place to ensure the quality of the material they publish and maintain the integrity of the published record.

2. **Review of Manuscripts:** Editor must ensure that each manuscript is initially evaluated by the editor for originality. The editor should organize and use peer review fairly and wisely. Editors should explain their peer review processes in the information for authors and also indicate which parts of the journal are peer reviewed. Editor should use appropriate peer reviewers for papers that are considered for publication by selecting people with sufficient expertise and avoiding those with conflicts of interest.
3. **Fair Play:** The editor must ensure that each manuscript received by the Journal is reviewed for its intellectual content without regard to sex, gender, race, religion, citizenship, etc. of the authors. An important part of the responsibility to make fair and unbiased decisions is the upholding of the principle of editorial independence and integrity. Editors are in a powerful position by making decisions on publications, which makes it very important that this process is as fair and unbiased as possible.
4. **Confidentiality:** The editor must ensure that information regarding manuscripts submitted by the authors is kept confidential. Editors should critically assess any potential breaches of data protection and patient confidentiality. This includes requiring properly informed consent for the actual research presented, consent for publication where applicable.
5. **Disclosure and Conflicts of Interest:** The editor of the Journal will not use unpublished materials disclosed in a submitted manuscript for his own research without written consent of the author. Editors should not be involved in decisions about papers in which they have a conflict of interest

DUTIES OF REVIEWERS

1. **Confidentiality:** Information regarding manuscripts submitted by authors should be kept confidential and be treated as privileged information. They must not be shown to or discussed with others except as authorized by the editor.
2. **Acknowledgement of Sources:** Manuscript reviewers must ensure that authors have acknowledged all sources of data used in the research. Reviewers should identify relevant published work that has not been cited by the authors. Any statement that an observation, derivation, or argument had been previously reported should be accompanied by the relevant citation. The reviewers should notify the journal immediately if they come across any irregularities, have concerns about ethical aspects of the work, are aware of substantial similarity between the manuscript and a concurrent submission to another journal or a published article, or suspect that misconduct may have occurred during either the research or the writing and submission of the manuscript; reviewers should, however, keep their concerns confidential and not personally investigate further unless the journal asks for further information or advice.
3. **Standards of Objectivity:** Review of submitted manuscripts must be done objectively and the reviewers should express their views clearly with supporting arguments. The reviewers should follow journals′ instructions on the specific feedback that is required of them and, unless there are good reasons not to. The reviewers should be constructive in their reviews and provide feedback that will help the authors to improve their manuscript. The reviewer should make clear which suggested additional investigations are essential to support claims made in the manuscript under consideration and which will just strengthen or extend the work
4. **Disclosure and Conflict of Interest:** Privileged information or ideas obtained through peer review must be kept confidential and not used for personal advantage. Reviewers should not consider manuscripts in which they have conflicts of interest resulting from competitive, collaborative, or other relationships or connections with any of the authors, companies, or institutions connected to the papers. In the case of double-blind review, if they suspect the identity of the author(s) notify the journal if this knowledge raises any potential conflict of interest.
5. **Promptness:** The reviewers should respond in a reasonable time-frame. The reviewers only agree to review a manuscript if they are fairly confident they can return a review within the proposed or mutually agreed time-frame, informing the journal promptly if they require an extension. In the event that a reviewer feels it is not possible for him/her to complete review of manuscript within stipulated time then this information must be communicated to the editor, so that the manuscript could be sent to another reviewer.

CROSSMARK POLICY PAGE

All articles published in MEV receive a DOI and are permanently published. This applies regardless of the outcome of the peer review that follows after publication. All content, including articles that have not (yet) passed peer review, is permanently archived in Portico. All versions of all articles that have passed peer review will be archived in PubMed and elsewhere.

Authors can revise, change and update their articles by publishing new versions, which are added to the article's history; however, the individual versions, once published, cannot be altered or withdrawn and are permanently available on the MEV website. MEV participates in the CrossMark scheme, a multi-publisher initiative that has developed a standard way for readers to locate the current version of an article. By applying the CrossMark policies, MEV is committed to maintaining the content it publishes and to alerting readers to changes if and when they occur.

Clicking on the CrossMark logo (at the top of each MEV article) will give you the current status of an article and direct you to the latest published version; it may also give you additional information such as new referee reports. In order to maintain the integrity and completeness of the scholarly record, the following policies will be applied when published content needs to be corrected; these policies take into account current best practice in the scholarly publishing and library communities:

CORRECTION TO AN ARTICLE

In traditional journals, where articles are peer reviewed before publication, Corrections (or Errata) are published to alert readers to errors in the article that became apparent following the publication of the final article. By contrast, articles in MEV undergo peer review post publication and publication is not 'final' as new versions can be added at any stage. Possible mistakes that come to light during the peer review process may be highlighted in the published referee reports, which are part of the article. Authors can publish revised versions, and any errors that become apparent during peer review or later can be corrected through the publication of new versions. Corrections and changes relative to the previous version are always summarized in the 'Amendments' section at the start of a new version.

RETRACTION

Articles may be retracted for several reasons, including:

- honest errors reported by the authors (for example, errors due to the mixing up of samples or use of a scientific tool or equipment that is found subsequently to be faulty)
- research misconduct (data fabrication)
- duplicate or overlapping publication
- fraudulent use of data
- clear plagiarism
- unethical research

For any retracted article, the reason for retraction and who is instigating the retraction will be clearly stated in the Retraction notice. The retraction notice will be linked to the retracted article (which usually remains on the site) and the article will be clearly marked as retracted (including the PDF).

An article is usually only retracted at the authors' request or by the publisher in response to an institutional investigation. It is important to note in the context of MEV's publication model, that - as in traditional journals - a retracted article is not 'unpublished' or 'withdrawn' in order for it to be published elsewhere. The reasons for retraction are usually so serious that the whole study, or large parts of it, are not appropriate for inclusion in the scientific literature anywhere.

The content of a retracted article would only be removed where legal limitations have been placed upon the publisher, copyright holder or author(s), for example, if the article is clearly defamatory or infringes others' legal rights, or if the article is the subject of a court order. In such cases, the bibliographic information for the article will be retained on the site along with information regarding the circumstances that led to the removal of the content.

Under rare circumstances, for example, if false or inaccurate data have been published that, if acted upon, pose a serious health risk, the original incorrect version(s) may be removed and a corrected version published. The reason for this partial removal would be clearly stated on the latest version.

PREPARING THE MANUSCRIPT

FORMATTING REQUIREMENTS

Please use the author submission template available online at MEV Journal website. To use the template, kindly 'Save As' the MS Word file to your document, then copy and paste your document. To copy and paste the text into the template, please use 'Special Paste' and choose 'Unformatted Text'. Papers not prepared in accordance with author guidelines and manuscripts with number of mistakes will have to be pre-rejected by Editor.

Download the 'Author Submission Template' DOCX
http://www.mevjournal.com/mevfiles/MEV_author_submission_template_17.1.docx

If your article includes any Videos and/or other Supplementary material, this should be included in your supplementary file at initial submission for peer review purposes.

Word Processing Software

The manuscript should contain at least 2.000 words and should not exceed 25 pages including embedded figures and tables, contain no appendix, and the file should be in Microsoft Office (.doc/.docx) or Open Office (.odt) format. The paper should be prepared in A4 paper (210 mm x 297 mm) using 25 mm for left margin and 2 mm for the top, bottom, and right margin. No need to alter page number in this template as the page number will be reordered at preprinting process. The whole manuscript body should be in one column, using font type Times New Roman (TNR), font size 12, first line indent 5 mm, and 1.5 line spacing.

Please make sure that you use as much as possible normal fonts in your documents. Special fonts, such as fonts used in the Far East (Japanese, Chinese, Korean, etc.) may cause problems during processing. To avoid unnecessary errors, you are strongly advised to use the 'spellchecker' function of MS Word.

Section Headings

Divide your article into clearly defined and numbered sections. The abstract is not included in section numbering. Use this numbering also for internal cross-referencing: do not just refer to 'the text'. Any subsection may be given a brief heading. Each heading should appear on its own separate line.

Heading should be made in four levels. Level five cannot be accepted.

- *Heading Level 1;* Heading 1 should be written in title case, left aligned, bold, 14 TNR, and Roman numbered followed by a dot.
- *Heading Level 2;* Heading 2 should be written title case, left aligned, bold, 12 TNR, Capital Arabic numbered followed by a dot.
- *Heading Level 3;* Heading 3 should be written title case, left aligned, italic, 12 TNR, numbered by Arabic number followed by closed bracket
- *Heading level 4;* Heading 4 is not recommended, however, it could still be accepted with the format of sentence case, left indent 5 mm, hanging indent 5 mm, italic, 12 TNR, numbered by small cap followed by a closed bracket.
- *Heading Level 5;* Heading Level 5 cannot be accepted in the manuscript.

ARTICLE STRUCTURE

The manuscript should begin with title, abstract, and keyword(s) followed by the main text. The main text should consist of at least IMRaD structure, except for the review article: Introduction, Method/Material, Result and Discussion, and Conclusion; followed by acknowledgement and References.

Introduction

State the objectives of the work and provide an adequate background, state of the art, and should be avoiding a detailed literature survey or a summary of the results. Explain how you addressed the problem and clearly state the aims of your study.

Material and methods

Provide sufficient details to allow the work to be reproduced by an independent researcher. Methods that are already published should be summarized and indicated by a reference. If quoting directly from a previously published method, use quotation marks and also cite the source. Any modifications to existing methods should also be described. A Theory section (if necessarily added) should extend, not repeat, the background to the article already dealt with in the Introduction and lays the foundation for further work. A Calculation section represents a practical development from a theoretical basis.

Results and discussion

Results should be clear and concise. Discussion should explore the significance of the results of the work, not repeat them. Avoid extensive citations and discussion of published literature. The following components should be covered in the discussion section: How do your results relate to the original question or objectives outlined in the Introduction section (what)? Do you provide interpretation scientifically for each of your results or findings

e-ISSN 2088-6985
p-ISSN 2087-3379

presented (why)? Are your results consistent with what other investigators have reported (what else)? Or are there any differences?

Conclusions

The main conclusions of the study may be presented in a short Conclusions section, which may stand alone or form a subsection of a Discussion or Results and Discussion section. The conclusion section should lead the reader to the important matter of the paper. Suggestion or recommendation related to further research can also be added but not to confuse the research with an uncompleted work.

Acknowledgements

Collate acknowledgements in a separate section at the end of the article before the references and do not, therefore, include them on the title page, as a footnote to the title or otherwise. List here those individuals who provided help during the research (e.g., providing language help, writing assistance or proof reading the article, etc.).

Appendices

It is not recommended to use appendices in MEV Journal submission.

ESSENTIAL TITLE PAGE INFORMATION

Title

The title of the manuscript should be concise and informative, less than 15 words, title case, centered, bold. Titles are often used in information-retrieval systems. The title should be accurate, unambiguous, specific, and completely identify the main issue of the paper. Avoid abbreviations and formulae where possible.

Author names and affiliations

Author names should not contain academic title, official rank, or professional position. Please clearly indicate the given name(s) and last/family name(s) -full name if possible- of each author and check that all names are accurately spelled. Present the authors' affiliation addresses (where the actual work was done) below the names. Write clear affiliation of all Authors. Affiliation includes name of department/unit, (faculty), the name of university/institution, complete postal address, and country. All contributing author should be shown in contribution order.

Corresponding author

Clearly indicate the corresponding author clearly for handling all stages of pre-publication, refereeing, and post-publication. This responsibility includes answering any future queries about Methodology and Materials. Ensure that the e-mail address is given and that contact details are kept up to date by the corresponding author.

Present/permanent address

If an author has moved since the work described in the article was done, or was visiting at the time, a 'Present address' (or 'Permanent address') may be indicated as a footnote to that author's name. The address at which the author actually did the work must be retained as the main, affiliation address. Superscript Arabic numerals are used for such footnotes.

ABSTRACT AND KEYWORDS

Abstract

Abstract should be concise and factual, contains neither pictures nor tables, and should not exceed 250 words. The abstract should state briefly the purpose of the research, reserch methods, the principal results, and major conclusions. An abstract is often presented separately from the article, so it must be able to stand alone. For this reason, References should be avoided, but if essential, then cite the author(s) and year(s). Also, non-standard or uncommon abbreviations should be avoided, but if essential they must be defined at their first mention in the abstract itself.

Graphical abstract

A graphical abstract is optional. Its use is encouraged as it draws more attention to the online article. The graphical abstract should summarize the contents of the article in a concise, pictorial form designed to capture the attention of a wide readership. Graphical abstracts should be submitted as a supplementary file in the online submission system. Image size: Please provide an image with a minimum of 531 × 1328 pixels (h × w) or proportionally more. The image should be readable at a size of 5 × 13 cm using a regular screen resolution of 96 dpi. Preferred file types: TIFF, EPS, PDF or MS Office files. You can view Example Graphical Abstracts on our information site.

Keywords

The keywords should be avoiding general and plural terms and multiple concepts. Be sparing with abbreviations: only abbreviations firmly established in the field may be eligible. These keywords will be used for indexing purposes.

INSTRUMENTS

Abbreviations, Acronyms, and Units

Define abbreviations and acronyms at the first time they are used in the text, even after they have been defined in the abstract. Abbreviations such as IEEE, SI, MKS, CGS, sc, dc, and rms do not have to be defined. Do not use abbreviations in the title or heads unless they are unavoidable. Use either SI (MKS) or CGS as primary units. (SI units are encouraged.) English units may be used as secondary units (in parentheses). An exception would be the use of English units as identifiers in trade, such as "3.5-inch disk drive."Avoid combining SI and CGS units, such as current in amperes and magnetic field in oersteds. This often leads to confusion because equations do not balance dimensionally. If you must use mixed units, clearly state the units for each quantity that you use in an equation.

Do not mix complete spellings and abbreviations of units: "Wb/m^2" or "webers per square meter," not "webers/m^2." Spell units when they appear in text: "...a few henries," not "...a few H." Use a zero before decimal points: "0.25," not ".25." Use "cm3," not "cc".

Math formulae

Mathematical equation should be clearly written, numbered orderly, and should be an editable text prepared using MS Equation Editor (not in image format) and should also be separated from the surrounding text. Be sure that the symbols in your equation have been defined before or immediately following the equation. Use "(1)," not "Eq. (1)" or "equation (1)," except at the beginning of a sentence: "Equation (1) is ...". Italicize Roman symbols for quantities and variables, but not Greek symbols. Use a long dash rather than a hyphen for a minus sign.

Header-footer and hyperlink

Header and footer including page number must not be used. All hypertext links and section bookmarks will be removed from papers. If you need to refer to an Internet email address or URL in your paper, you must type out the address or URL fully in Regular font.

Footnotes

Footnotes should be avoided if possible. Necessary footnotes should be denoted in the text by consecutive superscript letters. The footnotes should be typed at the foot of the page in which they are mentioned, and separated from the main text by a short line extending at the foot of the column.

FIGURE AND TABLE

Figure should be in grayscale, and if it made in color, it should be readable (if it later printed in grayscale). A caption should be sequentially numbered with Arabic numerals and comprise a brief title (not on the figure itself) and a description of the illustration. Keep text in the illustrations themselves to a minimum but explain all symbols and abbreviations used. The lettering on the artwork should be clearly readable and in a proportional measure and should have a finished, printed size of 8 pt for normal text and no smaller than 6 pt for subscript and superscript characters. Use words rather than symbols or abbreviations when writing Figure axis labels to avoid confusing the reader. As an example, write the quantity "Magnetization," or "Magnetization, M," not just "M." If including units in the label, present them within parentheses. Do not label axes only with units. In the example, write "Magnetization (A/m)" or "Magnetization (A (m(1)," not just "A/m." Do not label axes with a ratio of quantities and units. For example, write "Temperature (K)," not "Temperature/K."

Figures should have a brief description in the main body of the manuscript. Insert figures and tables after they are cited in the text. For layouting purpose, please provide high resolution figure (≥300dpi) in .tif/.jpg/.jpeg. Low-quality scans are not acceptable. Figures and tables should be embedded and not supplied separately. Moreover, kindly avoid mentioning the position of figure/table e.g. "figure below" or "table as follow" because the position will be rearranged in layouting process. DO NOT put boxes around your figures to enclose them.

We suggest that you use a text box to insert a graphic (which is ideally at least 300 dpi resolution TIFF or EPS file with all fonts embedded) because this method is somewhat more stable than directly inserting a picture. To have non-visible rules on your frame, use the MSWord "Format" pull-down menu, select Text Box > Colors and Lines to choose No Fill and No Line.

Electronic artwork

General points:

- Make sure you use uniform lettering and sizing of your original artwork.
- Preferred fonts: Arial (or Helvetica), Times New Roman (or Times), Symbol, Courier.
- Number the illustrations according to their sequence in the text.
- Use a logical naming convention for your artwork files.

Formats

Regardless of the application used, when your electronic artwork is finalized, please 'save as' or convert the images to one of the following formats (note the resolution requirements for line drawings, halftones, and line/halftone combinations given below):

e-ISSN 2088-6985
p-ISSN 2087-3379

- EPS (or PDF): Vector drawings. Embed the font or save the text as 'graphics'.
- TIFF (or JPG): Color or grayscale photographs (halftones): always use a minimum of 300 dpi.
- TIFF (or JPG): Bitmapped line drawings: use a minimum of 1000 dpi.
- TIFF (or JPG): Combinations bitmapped line/half-tone (color or grayscale): a minimum of 500 dpi is required.

Please do not:
- Supply files that are optimized for screen use (e.g., GIF, BMP, PICT, WPG); the resolution is too low.
- Supply files that are too low in resolution.
- Submit graphics that are disproportionately large for the content.

Figure captions

Ensure that each illustration has a caption. A caption should comprise a brief title (not on the figure itself) and a description of the illustration. Keep text in the illustrations themselves to a minimum but explain all symbols and abbreviations used. figure caption of a single line must be centered whereas multi-line captions must be justified

Tables

Please submit tables as editable text and not as images. Number tables consecutively with Arabic numerals in accordance with their appearance in the text. Place footnotes below the table body and indicate them with superscript lowercase letters. Be sparing in the use of tables and ensure that the data presented in them do not duplicate results described elsewhere in the article. Please avoid using vertical rules and shading in table cells.

CONSTRUCTION OF REFERENCES

References are recommended using IEEE referencing style. Please ensure that every reference cited in the text is also present in the reference list (and vice versa). References should be listed at the end of the paper and numbered in the order of their appearance in the text. The template will number citations consecutively within brackets [1]. The sentence punctuation follows the bracket [2]. Refer simply to the reference number, as in [3]—do not use "Ref. [3]" or "reference [3]" except at the beginning of a sentence: "Reference [3] was the first ..."

Unpublished results and personal communications are not recommended in the reference list but may be mentioned in the text. If these references are included in the reference list, they should follow the standard reference style of the journal and should include a substitution of the publication date with either 'Unpublished results' or 'Personal communication'. Citation of a reference as 'in press' implies that the item has been accepted for publication. Wikipedia, personal blog, or non-scientific website is not allowed to be taken into account. Primary references should be at least 80% from at least fifteen references. References should be taken from the late ten years.

Avoid bulk references such as [1–9]. Avoid excessive self-citations (no more than 20%). If possible, article's DOI should be given for each reference list.

Reference formatting

There are two types of references, i.e., electronics sources and nonelectronics sources. Sample of correct formats for various types of references are as follows
- *Book*: Author, *Title*. edition, editor , City, State or Country: Publisher, year, Pages.
- *Part of book*: Author, "Title", in *Book*, edition, editor, City, State or Country: Publisher, year, Pages.
- *Periodical*: Author, "Title", *Journal*, *volume (issue)*, pages, month, year.
- *Proceeding:* Author, "Title", in *Proceeding*, year, pages.
- *Unpublished paper*: Author, "Title", presented at Conference/ event title, City, State or Country, year.
- *Paten/Standart*: Author, "Title", patent number, month day, year.
- *Technical report*: Author, "Title", Company, City, State or Country, Tech. Rep. Number, month, year.

Three pieces of information are required to complete each reference from electronics sources: 1) protocol or service; 2) location where the item is to be found; and 3) item to be retrieved. Sample of correct formats for electronics source references are as follows:
- *Book*: Author. (year, month day). *Title*. (edition) [Type of medium]. *volume (issue)*. Available: site/path/file.
- *Periodical*: Author. (year, month). Title. *Journal*. [Type of medium]. *volume (issue)*, pages. Available: site/path/file.
- *Papers presented at conferences*: Author. (year, month). Title. Presented at Conference title. [Type of Medium]. Available: site/path/file.
- *Reports and handbooks*: Author. (year, month). Title. Company. City, State or Country. [Type of Medium]. Available: site/path/file.

Reference management software

Every article submitted to MEV Journal shall use reference management software that supports Citation Style Language styles, such as Mendeley and Zotero, as well as EndNote®.

Journal of Mechatronics, Electrical Power, and Vehicular Technology, Volume 10, Issue 2, 2019

Secretariat
Research Centre for Electrical Power and Mechatronics
Indonesian Institute of Sciences
Komp LIPI Jl. Sangkuriang, Building 20, 2nd Floor, R 209
Bandung, West Java, 40135 Indonesia
Telp: +62-022-2503055 / 2504770
Fax: +62-22-2504773
e-mail: sekretariat@mevjournal.com
Homepage: www.mevjournal.com

ISSN 2087-3379